LUND UNIVERSITY

Vibrations in a Built Environment

Prediction and Reduction

Persson, Peter

2016

Document Version:
Förlagets slutgiltiga version

Link to publication

Citation for published version (APA):
Persson, P. (2016). *Vibrations in a Built Environment: Prediction and Reduction*.

Total number of authors:
1

VIBRATIONS IN A BUILT ENVIRONMENT

Prediction and Reduction

PETER PERSSON

VIBRATIONS IN A BUILT ENVIRONMENT

Prediction and Reduction

PETER PERSSON

Acknowledgements

First, I would like to thank my supervisors, Prof. Kent Persson and Prof. Göran Sandberg, for all the work they have put in to finalise this thesis. I am thankful for the fruitful discussions we have had during my years at the Division of Structural Mechanics at Lund University. I would also like to thank my supervisors for giving me the opportunity to be a PhD candidate. I gratefully acknowledge the financial support from Silent Spaces, a project that formed part of the EU program Interreg IVA, and from the MAX IV Laboratory.

Furthermore, I am grateful to my fellow PhD candidates, Ola Flóden and Juan Negreira. They have not only improved the quality of the thesis, but have also increased the quality of my life. I will forever be grateful for that. I am indebted to the staff at the Division of Structural Mechanics for giving me an easy and fun time at work, and for their assistance with various tasks. I am especially grateful to Håkan Hansson, Bo Zadig and Artur Grabowski.

Finally, many thanks are directed to my family and friends for their decisive support in both good and bad times throughout my life – and in particular to my brother Ola Persson, my mother Inger Nordeng and my father Ronny Persson.

Lund, April 2016
Peter Persson

Abstract

Vibrations in a built environment can exceed the requirements for sensitive equipment in a building or can cause annoyance to residents. Hence, there is often a need for reducing such vibrations. The vibrations can originate from ambient sources such as motorway traffic, or from internal sources such as people walking inside the building. Disturbing vibrations can be reduced by reduction measures. Vibration-reduction measures can be evaluated numerically, with for instance the finite element method, to avoid construction of expensive mock-ups. In the thesis, large finite element models involving several physical domains (e.g. road, soil, bedrock, and building parts) were developed to study the effect of vibration-reduction measures.

Ground vibrations can be reduced by installing a wave barrier between an external source and a receiver. As concluded in the thesis, an empty barrier (i.e. a trench) installed in the soil has the ability to reduce the ground-vibration level by approximately 60%. If the barrier contains a solid material, however, the level of reduction is reduced to approximately 30%. At long distances, at around 500 m and longer, from the vibration source, an amplification in vibration is observed. At such distances, moreover, the ground motion follows the motion of the bedrock. Another example of a wave obstacle that is studied in the thesis involves shaping the landscape surrounding a building. The topsoil that is usually transported from the construction site can be used to construct hills and valleys that constitute the shaped landscape. However, this can result in anything from an appreciable reduction to an appreciable amplification in the ground-vibration levels, depending on how the landscape is formed. If constructed properly, the reduction in the level of vibration can reach approximately 35%. Vibrations from both external and internal sources can be reduced by modifying the properties of the concrete slabs and the soil underneath. The soil properties can be improved by mixing the soil with a binder, in order to stiffen the soil. Is is shown in the thesis that by using stabilised soil underneath a concrete slab, vibrations originating from motorway traffic can be reduced by almost 60%, and up to 80% for an internal pedestrian load.

By using a time-efficient numerical model developed in the thesis, the effect by using different positions for the supports of a water-pipe system on vibrations transmitted to other parts of buildings was studied. Because frequency peaks can be avoided, a marked change of vibration characteristics can be achieved. A reduction of more than 60% in the transmitted vibrations was observed.

The general methods and measures presented in the thesis are exemplified by the conceptual design process of the MAX IV Laboratory, a vibration-sensitive research facility. This laboratory exhibited the phenomena needed for selecting it as a comprehensive example case.

Populärvetenskaplig sammanfattning

Att minska störande vibrationer i en byggnad när den är färdigställd kan resultera i dyra åtgärder i jämförelse med att konstruera byggnaden så att störande vibrationer undviks. I avhandlingen beskrivs hur man med hjälp av datorberäkningar kan uppskatta effekter av olika åtgärder för att minska vibrationsnivåer på mark eller i byggnader som genereras utanför eller inne i byggnaden.

Alla typer av konstruktioner är utsatta för vibrationer av varierande storlek, i allt från vibrationer på molekylnivå till vibrerande mark på grund av jordbävningar. Men störande vibrationer är samtidigt ett ökande problem i många städer på grund av dess förtätning. Genom förtätning av städer byggs hus närmare exempelvis motorvägar och järnvägar, vilket dessutom kräver ny infrastruktur såsom spårtrafik och bilväg. Avhandlingen är inriktad på vibrationer i byggd miljö, i mark och i byggnader. Storleken på vibrationerna är viktig vid bedömning av hur stor negativ påverkan de kan ha. Men även hur ofta de förekommer är av betydelse. På ett kontor, till exempel, kan man kanske tillåta att störas av vibrationer från gående personer då och då, men knappast en gång per minut. De vibrationer som inte är kännbara för människan kan fortfarande störa känslig utrustning såsom en ögonlaser eller ett avancerat mikroskop.

Vibrationsreducerande åtgärder kan vara att grundläggningen görs styvare eller att man bygger en barriär mellan en motorväg och byggnaden som ska skyddas. Det är viktigt att kunna uppskatta effekten av eventuella åtgärder med datormodeller för att undvika dyra tester med prototyper. De utvecklade datormodellerna behöver inkludera olika delar såsom berg, jord och byggnad, och blir därför stora och tar lång tid att beräkna. Då är det även viktigt att datormodellerna kan göras effektiva, det vill säga att beräkningstiden är kort samtidigt som beräkningarna är korrekta genom att modellen hanterar de olika vibrationsfenomen som förekommer. För att datormodellerna ska ge resultat av tillräcklig noggrannhet behöver materialens egenskaper vara korrekta i modellen. Jord har en stor variation i materialparametrar, vilket innebär att olika typer mätningar och undersökningar av marken vid det aktuella området behöver utföras innan tillförlitliga datormodeller kan skapas.

I avhandlingen undersöks främst tre olika metoder för att minska störande vibrationer. i) Anlägga ett dike mellan vibrationskälla och mottagare (exempelvis en byggnad), antingen öppet eller fyllt med något material. ii) Forma landskapet mellan vibrationskälla och mottagare med vågformade kullar och dalar. iii) Göra grundläggningen för en byggnad styvare genom att exempelvis blanda jorden under byggnaden med cement. De två förstnämnda metoderna avser att minska vibrationer från externa laster såsom spår- och biltrafik. Den tredje metoden avser att reducera vibrationer från både trafik och interna laster såsom gående personer i en byggnad.

Contents

Paper A
Numerical study of reduction in ground vibrations by using barriers.
P. Persson, K. Persson, G. Sandberg.
Engineering Structures, 115 (2016) 18–27.

Paper B
Reduction in ground vibrations by using shaped landscapes.
P. Persson, K. Persson, G. Sandberg.
Soil Dynamics and Earthquake Engineering, 60 (2014) 31–43.

Paper C
Numerical study on reducing building vibrations by foundation improvement.
P. Persson, K. Persson, G. Sandberg.
Submitted to Engineering Structures.

Paper D
Reduced order modelling of liquid-filled pipe systems.
P. Persson, K. Persson, G. Sandberg.
Journal of Fluids and Structures, 61 (2016) 205–217.

Part I

Introduction and overview

1 Introduction

1.1 BACKGROUND

Vibrations occurring in built environments may cause annoyance for residents or disturb machines. As the population size increases, an increase in facilities is needed in turn, such as dwellings, subway stations, and industrial buildings. This results in that unbuilt spaces both within cities and in areas nearby motorways and railways will be used for construction. The decrease of unbuilt spaces within cities is usually referred to as 'densification'. The establishment of new buildings close to vibration sources such as motorways, railways and tramways increases the risk of disturbing vibrations. These vibrations can affect residents and sensitive equipment, for instance by limiting the effectiveness of sensitive equipment such as microscopes and machines for eye surgery. Similarly, establishment of new vibration sources close to existing buildings can result in disturbing vibrations as well.

It is thus important do develop efficient methods for reducing ground vibrations, especially in cases where these vibrations are problematic. Vibration-reduction measures can be evaluated numerically in order to avoid expensive and time-consuming mock-ups. In order to develop such measures, it is necessary to employ numerical models that can predict the vibration phenomena occurring in built environments.

1.2 AIM AND OBJECTIVE

The aim of this research is to develop strategies for reducing vibration levels in buildings with advanced equipment, such as hospitals and research facilities, and in buildings where these vibrations affect the comfort of residents. The objective is to suggest and investigate vibration-reduction measures that can be used by the building industry, as well as to develop methods for analysing and predicting vibrations in a built environment. Accurate numerical models that can visualise propagating waves were developed such that vibration phenomena can be studied. By understanding how vibration waves are propagated, efficient vibration-reduction measures can be developed. Efficient and accurate numerical models also reduce the need

to study the effects of vibration-reduction measures with mock-ups, which are expensive and time-consuming. The time-efficiency of the models allows for a large number of analyses to be carried out, such that the problem at hand can be investigated comprehensively.

The research presented in the thesis will increase the knowledge within the field of predicting and reducing vibrations in a built environment, and it will mitigate the challenges regarding densifications of cities. By developing vibration-reduction measures, the need for densifying cities can be met, thus enabling facilities to be built closer to disturbing vibration sources, and new vibration sources to be built closer to existing facilities. The vibration-reduction measures also allow more sensitive equipment to be used in hospitals and research facilities, for example.

1.3 LIMITATIONS AND ASSUMPTIONS APPLIED

The limitations and assumptions applied in the thesis are as follows:

- Environmental loads such as wind and earthquakes are not considered.

- Loads are assumed to be of low magnitude. Thus, only linear elastic material response has to be considered.

- Long wavelengths in relation to heterogeneities in the materials is assumed. Hence, homogeneous material models are sufficient.

In addition, the finite element method was used for the numerical analyses presented in the thesis. Moreover, qualitative, comparative and conceptual studies were the key issue and concern of the thesis.

1.4 OUTLINE

The thesis includes two main parts. In the first part, an introduction and overview of the work are given in six chapters:

- Chapter 1 gives an introduction to the work presented in the thesis.

- Chapter 2 describes vibrations in built environments in general terms.

- Chapter 3 discusses theories commonly applied in the research area.

- Chapter 4 describes the numerical modelling of physical domains in built environments.

- Chapter 5 discusses, in general terms, various vibration-reduction measures.

- Chapter 6 presents the concluding remarks of the thesis.

In the second part of the thesis, the appended papers are presented.

1.5 ABSTRACTS FROM THE APPENDED PAPERS

1.5.1 Paper A

Reduction in traffic-induced ground vibrations by the use of barriers is investigated here. The traffic load characteristics were measured for motorway traffic. The effects of parameters on various types of barriers were examined by the use of a finite element model that was calibrated to green-field measurements. The depth of a trench and the elastic modulus of a solid back-fill material were found to be the most important parameters to consider. In investigation of the effects of infiltration of water into an open trench, a coupled finite element formulation of the water and the soil was applied. Infiltration of water was found to decrease the achieved reduction. At long distances from the vibration source, of around 500 m and longer, amplification in vibration levels can be seen when a trench has been installed. It was also found, at long distances, that the motion of the ground surface follows the motion of the bedrock.

1.5.2 Paper B

Reduction in traffic-induced ground vibrations by use of shaped landscapes is investigated here by shaping the landscape surrounding a high-tech facility, using the landscape thus produced as a wave obstacle. The effects of the geometric parameters of a shaped landscape were examined in parametric studies. An architectural landscape design was also investigated in terms of its effectiveness in reducing traffic-induced ground vibrations. Finite element models, analysed in the frequency domain, were employed. The models involve a layer of soil and the underlying bedrock. It was found that anywhere from an appreciable reduction to an appreciable amplification of the vibrations produced can occur, depending upon the geometric parameters

of the shaped landscape involved. The most effective shape was found for a topography that acted as a waveguide that reduced the level of vibration by approximately 35%.

1.5.3 Paper C

Numerical study on reducing building vibrations by foundation improvement.
P. Persson, K. Persson, G. Sandberg.
Submitted to Engineering Structures.

Vibration disturbances in buildings may stem from ambient sources, such as motorway traffic, or from internal sources such as people walking inside the building itself. Vibrations may exceed requirements for sensitive equipment or cause annoyance to humans and therefore the vibrations may need to be reduced. Vibrations from both external and internal sources can be reduced by modifying the properties of concrete slabs and of the soil underneath. Soil can be improved by being mixed with a binder in order to increase its stiffness. In this study, parametric finite element analyses were conducted on the achieved vibration reduction from improving the properties of a concrete slab on soil or of the soil underneath. The size, elastic modulus, and depth of the stabilised soil were found to markedly affect the level of reduction obtained. The soil stabilisation at a vibration-sensitive facility was used as an example case. The developed finite element model was calibrated to green-field measurements carried out on-site. Frequency spectra of both road traffic loads and internal pedestrian loads were considered in the model. The validated finite element model predicted reductions of almost 60% for the road traffic and 80% for the pedestrian load.

1.5.4 Paper D

Reduced order modelling of liquid-filled pipe systems.
P. Persson, K. Persson, G. Sandberg.
Journal of Fluids and Structures, 61 (2016) 205–217.

In the design of vibration-sensitive structures, large three-dimensional numerical models are frequently used, those occasionally being too large to be simulated in a practical manner. More specifically, the analyses of vibrating complex water-pipe systems require efficient model order reduction strategies. In the paper, a numerical procedure for model order reduction of a water-pipe system housed in a vibration-sensitive research facility is presented. The finite element model employed includes a water-pipe system where fluid-structure interaction effects are accounted for. The reduced model is developed using component mode synthesis and a reduction of the interface degrees of freedom, enabling time-efficient dynamic analyses. The model was proven to be time-efficient and to generate output of high accuracy.

1.5.5 Contributions by Peter Persson

Peter Persson contributed to the work by taking the main responsibility for the research presented in the papers (viz. Papers A–D). This included planning and developing the research tasks and writing the papers as the main author. He performed the calculations and developed the numerical strategies and the finite-element models employed. Moreover, he contributed to the vibration measurements presented in Paper C. The results and conclusions of the papers have been discussed with the co-authors.

1.6 PUBLICATIONS NOT INCLUDED IN THE THESIS

Licentiate dissertation

- Persson, P. (2013). Reduction in ground vibrations by the use of wave obstacles. Licentiate Dissertation, Report TVSM-3072, Lund University.

Conference papers

- Persson P, Persson K, Sandberg G. (2015). Numerical study of reduction in vibrations induced by water-pipe system. In: Dynamics of Civil Structures, vol. 2, 2015. Springer.

- Persson P, Persson K, Sandberg G. (2014). Fluid-structure interaction analysis of vibration reduction in pipe systems. In: Dynamics of Civil Structures, vol. 4, 2014. Springer.

- Persson P, Persson K, Jørstad P, Sandberg G. (2012). Reduction of ground vibrations by landscape shaping. In: 25th Nordic Seminar on Computational Mechanics, Lund, Sweden, Oct 25–26, 2012. Persson, K., Revstedt, J., Sandberg, G. & Wallin, M. eds.

- Persson P, Persson K, Jørstad P, Sandberg G.. (2012). Vibration reduction by landscape shaping at high-tech facility. In: 10th World Congress on Computational Mechanics, Sao Paulo, Brazil, July 8–13, 2012.

- Persson P, Persson K, Sandberg G. (2011). Reduction of traffic-induced vibrations at high-tech facility using trenches. In: 24th Nordic Seminar on Computational Mechanics, Helsinki, Finland, Nov 3–4, 2011. Freund, J. & Kouhia, R. eds.

- Persson P, Persson K. (2010). Analysis of dynamic soil-structure interaction at high-tech facility. In: 23rd Nordic Seminar on Computational Mechanics, Stockholm, Sweden, Oct 21–22, 2010. Eriksson, A. & Tibert, G. eds.

- Bard D, Persson P, Negreira J, Persson K, Austrell PE, Sandberg G. (2010). Vibration Analysis in high-tech facility: A swedish light synchroton. In: International Conference of Sound and Vibration 17, Cairo, Egypt, July 18–22, 2010.

Conference abstracts

- Persson P, Persson K, Sandberg G. (2016). Mitigation of building vibrations by foundation improvement. In: A Conference and Exposition on Structural Dynamics, IMAC-XXXIV, Orlando, FL, USA, Jan 25–28, 2016.

- Persson P, Persson K, Sandberg G. (2015). Efficient numerical procedure for predicting vibrations induced by pipe systems. In: 5th International Conference on Computational Methods in Structural Dynamics and Earthquake Engineering, Crete Island, Greece, May 25–27, 2015.

- Persson P, Persson K, Sandberg G. (2015). Reduced order modelling in vibration analysis of water-pipe system. In: VI International Conference on Coupled Problems in Science and Engineering, Venice, Italy, May 18–20, 2015.

- Persson P, Persson K, Sandberg G. (2014). Dynamic fluid-structure interaction analysis of water-pipe systems. In: 11th World Congress on Computational Mechanics, Barcelona, Spain, June 20–25, 2014.

- Persson P, Persson K, Sandberg G. (2013). Fluid-Structure Interaction Analysis of Vibrations in Water Pipe System at High-Tech Facility. In: V International Conference on Coupled Problems in Science and Engineering, Ibiza, Spain, June 17–19, 2013.

- Persson P, Persson K, Sandberg G. (2011). Dynamic analysis of soil-structure at high-tech facility. In: 3rd ECCOMAS Thematic Conference on Computational Methods in Structural Dynamics and Earthquake Engineering, Corfu, Greece, May 25–28, 2011.

- Persson P, Persson K, Bard D, Austrell PE, Sandberg G. (2010). Analysis of vibrations in high-tech facility. In: European Conference on Computational Mechanics, Paris, France, May 16–21, 2010.

2 Vibrations in a built environment

2.1 VIBRATION TRANSMISSION

Vibrations in built environments can be divided into: the *source* generating the vibrations, the *medium* in which the vibrations propagate, and the *receiver* that is to be protected. This is shown schematically in Figure 2.1. In order to predict vibration levels and to suggest reduction measures, it is important to understand how these three parts influence vibrations. Moreover, it is important to understand how vibration-reduction measures can be implemented and evaluated.

In a densified built environment, each of the three parts (viz. the source, medium, and receiver) can change such that the risk of disturbing vibrations will increase. For example, vibrations stemming from railway traffic are intensified by faster and more frequent trains (the source). Communities that are densified will have shorter distances between the source and the receiver
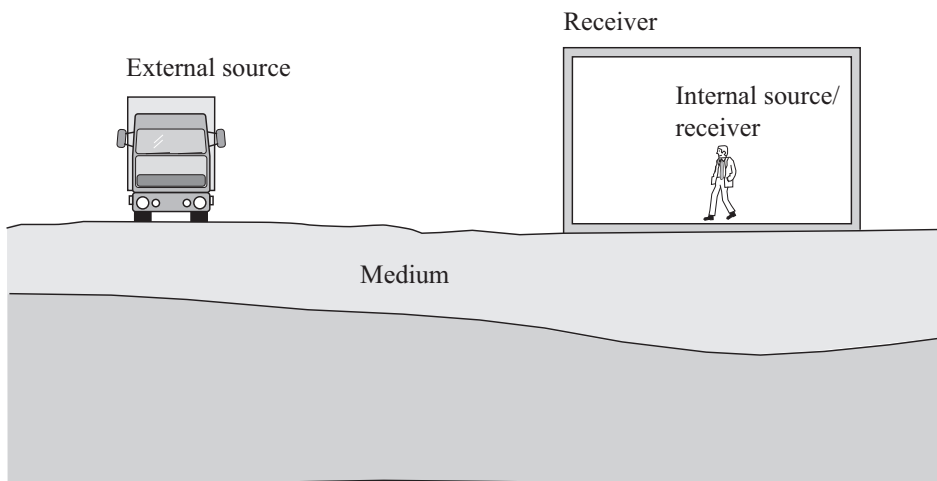
Figure 2.1: Sketch of the vibration-transmission process.

(the medium). Hospitals with vibration-sensitive equipment are vulnerable from the general tendency in the building industry to have longer slabs (the receiver).

2.1.1 Source

Numerous sources can generate disturbing vibrations in a built environment. The sources can be divided into 'external sources' and 'internal sources'. External sources are those located outside of a building needing protection, and internal sources are located inside the building. Common external sources include traffic-induced ground vibrations stemming from cars, trucks, trains, or trams. Such vibrations can propagate to facilities nearby, and they can disturb residents or exceed the vibration requirements of sensitive equipment. Traffic-induced vibrations can originate from irregularities in the asphalt layer, the roughness of rails, or traffic entering and exiting a bridge [1, 2]. Externally induced vibrations increase as public transport systems are extended and as trains and trucks become heavier and faster. Common internal sources include vibrating machinery such as water-pipe systems and pumps, as well as the effects from walking and other human activities. Vibrations from pedestrians stem from the impact of the footfall. The amplitude of vibrations varies with the frequency, thus the frequencies of interest can vary extensively. The highest energy content in a pedestrian footfall is below 5 Hz [3, 4]. For railway traffic, the highest energy content is usually below 20 Hz [5, 6]. For motorway traffic the highest frequency of interest is usually less than 25 Hz [7, 8]. For trams, the frequencies of interest are higher, up to approximately 60 Hz [9].

2.1.2 Medium

The medium in which the generated vibrations propagate can differ significantly in its dynamic properties. For the internal load in buildings, the media often constitute structural parts such as supports or slabs, resulting in structure-borne vibrations. For loads outside a building, the ground becomes the propagating medium. The properties of the soil layers markedly affect the ground response. Moreover, the bedrock is of interest, depending on the wavelengths and the distance between the source and the receiver. At long distances from the source, the parameters of the underlying bedrock is a significant contributor to ground-vibration levels, because it transports waves further than the soil, owing to a lower attenuation in the bedrock. Waves attenuate due to geometrical damping, material damping, and other energy losses from the reflection and refraction of the propagating waves.

2.1.3 Receiver

The receiver refers to an object, e.g. a building, that has limitations in terms of the allowed vibration level. Requirements can be set due to sensitive equipment such that a surgical micro-

scope, for example, can achieve its full potential. Requirements can also be set due to humans, with a threshold established where vibrations cause annoyance.

A structure is most sensitive to vibrations at its natural frequencies (see Section 3.2.1 for a detailed description). The structure can refer to the building as a whole or to parts of it, e.g. a slab. The natural frequencies depend on the distribution of mass and stiffness throughout a structure. Hence, the design of the building's structure influences the resulting vibration level. Buildings with a lightweight structure, e.g. steel- or wood-framed buildings, are more sensitive to vibrations due to their low mass. By contrast, buildings with a pre-cast concrete structure provide relative higher resistance to vibrations, due to a higher mass. The so-called footprint of a building affects the vibration response. Depending on the dimensions of the foundation, the response will differ when the foundation is excited by a short wavelength as compared to a long wavelength. Long wavelengths will move the entire foundation up and down uniformly, whereas short wavelengths introduce a bend to the foundation. A critical situation for a building affected by ambient vibrations is when the natural frequencies of the building or its parts, usually a slab, coincide with the resonance frequency of the ground. Of course, this requires that the frequency content of the excitation covers that specific frequency. Critical frequencies for a building can range from below 1 Hz to over 50 Hz. Skyscrapers tend to have their first natural frequency, so-called fundamental frequency, below 1 Hz. Long-span floor (and ceiling) structures tend to have their fundamental frequency as low as approximately 2 Hz, whereas short-span floors tend to have their fundamental frequency at 20–30 Hz or higher. Walls and windows usually have their fundamental frequency at approximately 40 Hz and higher [10].

2.2 IMPACT OF VIBRATIONS

In general, there are three main ways in which vibrations can cause problems. Vibrations can cause structural damage, annoyance for residents and disturb sensitive equipment.

2.2.1 Structural damage

Damage to the building itself can occur from high vibration levels. In the case of vibrations produced by sources such as rail- and tramways, the level of vibration is at such a level that damage to the building's structure is uncommon. According to [6], it is unlikely that railway-induced vibrations result in structural damage to a building. However, cosmetic damage can nevertheless occur in extreme cases. Therefore, structural and cosmetic damage from road traffic or other sources, e.g. pedestrians, is even less likely to occur. Sensitive buildings such as historic masonry structures founded on poor soil can develop small cracks (i.e. cosmetic damage) from vibrations [6]. Even though these structures are usually much heavier than wood-framed buildings, for example, they can be more sensitive to vibration damage [5]. It is

not the vibrations themselves that cause these cracks. However, the vibrations can aggravate already existing cracks. Several other factors can contribute to cosmetic damage of masonry structures. Such factors include movements in the masonry due to temperature or moisture variation and time-dependent settlements. It is for these reasons that it is difficult to determine which of these factors contributes to the cosmetic damage of a building.

2.2.2 Human perception

The effect of vibrations on humans depends on several physical quantities, such as vibration amplitude, frequency content, and the duration of the vibration [11]. Other factors affect the perception of vibrations, including gender, age, body position and expectation of vibration level, as well as whether a person is lying down or standing up, for example, [12]. A person who is lying down is more sensitive to horizontal vibrations than vertical ones. Moreover, people are more annoyed with vibrations when noise is perceived at the same time. The noise can be direct from the source itself, i.e. air-borne noise. Or, it can be indirect, e.g. from the rattling of glasses on a shelf, i.e. structure-borne noise, excited by the vibrations stemming from the same source. Therefore, it is desirable to implement noise-reduction measures alongside vibration-reduction measures to reduce annoyance.

Government agencies in Sweden have determined guideline values for rail-traffic-induced vibrations in buildings [13]. These values should be interpreted as recommendations or target values. The value is calculated as the root mean square (RMS) values in the frequency range of 1–80 Hz and is set to 0.4 mm/s or, in acceleration, 14 mm/s^2. The perception threshold for humans varies with the frequency. That is, humans differ in their sensitivity to different frequencies, see Figure 2.2. According to the international standard, ISO 2631 [14], the perception threshold is assumed to be constant between 8–80 Hz. Below 8 Hz, the perception
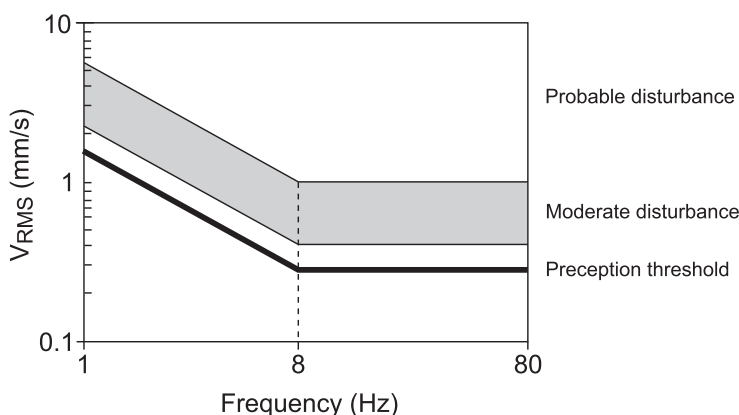
Figure 2.2: *Perception threshold, as well as the range of moderate and probable disturbance, respectively.*
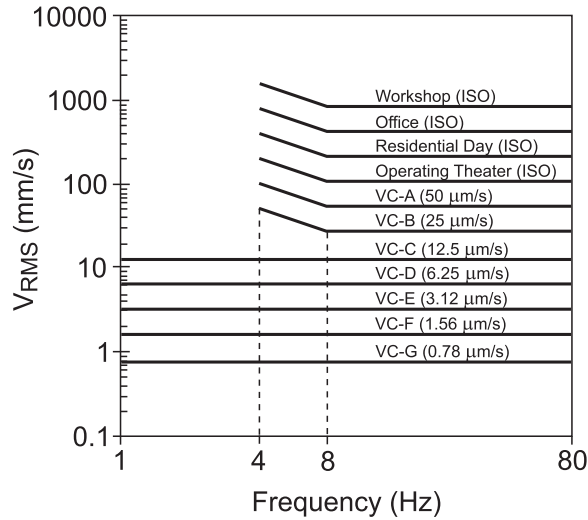
Figure 2.3: *Vibration requirements. ISO guidelines and VC curves. The RMS velocities are de-termined as 1/3 octave band frequencies.*

threshold increases, indicating that humans are more sensitive to vibration frequencies there. According to the Swedish standard, SS 4604861 [15], two additional ranges are provided based on the probability of disturbance from vibrations. The annoyance from vibrations depends on the person's activity. In Figure 2.3, the guidelines given in ISO 2631 [14] are shown for build-ings of various types. Indeed, long-term effects related to vibration include sleeping disorders, degraded concentration, and fatigue [13].

2.2.3 Sensitive equipment

It is not only residential buildings that must be isolated from disturbing vibrations. Strict vibrational limits are specified for sensitive equipment in hospitals and high-tech facilities such as synchrotrons. The manufacturers of sensitive equipment usually specify vibrational limits. When these are not provided in advance, velocity curves of vibration criteria (VC-curves) can be used [16]. The curves are listed as VC-A to VC-G, where VC-G has the most strict requirements, see Figure 2.3. VC-A and VC-B are constant in the frequency range of 8–100 Hz. Below 8 Hz, the curves are constant in acceleration. The stricter VC-curves are constant throughout the entire frequency range. For some equipment, the requirements are set in displacements. More specifically, for a research facility, this can refer to the relative displacement between an electron gun and its target of interest.

2.3 PREDICTION AND REDUCTION

In general, models that predict vibrations in built environments are developed for two major reasons. First, a model can be used to predict the vibration levels of a future construction site, in order to determine whether it is a suitable site. Second, a more detailed model can be used for determining vibrations that are occurring and for predicting the effectiveness of vibration-reduction measures.

Predictions of vibration levels at a new construction site must be based on measurements at that site or at a site with similar geotechnical conditions. For railway-induced vibrations, several semi-empirical models have been developed [6, 17]. These models include parameters such as the train type, soil type, distance between the railway track and receiver, as well as the structural design of the building. Such models may offer precise predictions of the vibration levels. For a detailed investigation of the vibrations, numerical models are suitable. These involve several physical domains and the interaction between them. The physical domains can be a motorway, the ground and a building. In such investigations, large numerical models are required. Hence, computationally efficient models are desirable. One disadvantage to using numerical prediction models in relation to semi-empirical models is that they tend to be time-consuming. However, these models can be time-efficient by using various methods, including reduced dimensions and model order reduction, for example. Moreover, computing power increases rapidly over time, allowing for larger and more complex models to be analysed. With a time-efficient numerical model, the effects of various vibration-reduction measures can be studied extensively. A numerical model developed in a desirable manner can predict vibration phenomena, vibration levels, and the effectiveness of vibration-reduction measures. These models can be more precise than semi-empirical models and are applicable to a wide range of problems. Moreover, numerical models are faster than the construction and measurement of mock-ups, and they are cheaper and more versatile. Therefore, a numerical investigation can be preferable.

In order to study the feasibility of vibration reduction, the source, medium, and receiver must be quantified and predicted. Several measures have been developed to reduce disturbing vibrations and protect the receiver. The main part of this thesis focuses on predicting the reduction in vibration as a result of a vibration-reduction measure. A reduction in vibration levels can be carried out by modifying the source, medium, or receiver. To reduce disturbing vibrations stemming from a motorway, for instance a new asphalt layer can be applied to reduce the vibrations at the source, a wave barrier can be installed in the ground medium to reduce incident vibrations and a thicker slab-on-grade can be employed to reduce vibrations at the receiver. In Chapter 5, vibration-reduction measures are discussed in detail.

3 Governing theory

In this chapter, an overview of theories applied in the research presented in the thesis, as well as commonly applied in the research area, are given.

3.1 WAVE PROPAGATION

In this section, of wave propagation in ground materials are described. For a more detailed description see [2, 18, 19].

3.1.1 Material modelling

Ground materials, such as the soil and bedrock, are heterogeneous materials with variations in granularity and strata. However, when modelling these materials it is convenient to regard them as homogeneous. In the case of wave propagation, local variations in the material can be neglected when they are small in comparison to the wavelengths. This can be illustrated by the following example: the common speed of Rayleigh waves in clay tills is around 200 m/s. This means that Rayleigh waves at a frequency of 50 Hz have a wavelength of 4 m. In stiffer clay tills and in bedrock, the wavelengths become longer. When comparing the wavelengths with the typical size of the heterogeneities, a homogeneous material is applicable. Heterogeneities can be accounted for by increasing the material damping. In many areas of civil engineering, soil is not considered a linear elastic material. This is true in the case of earthquake-caused vibrations where strains are of such a high magnitude that nonlinearities must be considered. In the case of human-made vibrations from sources such as motorways and pedestrians, however, the strains are usually at a level such that the assumption of linear elasticity applies. This assumption is also valid for common building materials such as concrete and steel.

(a) Pressure wave (P-wave).

(b) Shear wave (S-wave).

(c) Rayleigh wave.
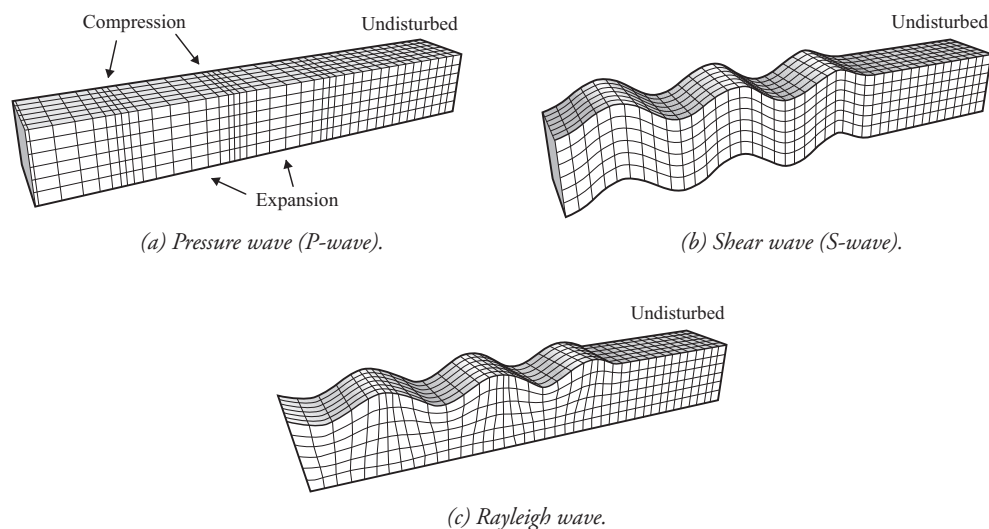
Figure 3.1: *Different wave types commonly occurring in soil.*

3.1.2 Wave types

In linear elastic materials, there are two types of waves that occur in response to dynamic loading: body and surface waves. Body waves are primarily pressure (P) and shear (S) waves. P-waves are body waves that travel throughout the volume of the material and have the highest wave-speeds among different wave types. Such waves are therefore referred to as primary waves. P-waves are pressure (i.e. compression) waves, as such, they travel through both solids and fluids. See Figure 3.1(a) for the particle motion for P-waves. S-waves are the secondary waves that involve particle motion in shearing. Like P-waves, S-waves travel within the volume at hand, although at a wave speed that is only about half that of P-waves. S-waves appear in an elastic medium when subjected to periodic shear deformation. Hence, S-waves cannot propagate in fluids. The elastic deformation involved, i.e. changes in shape without a change in volume, occurs perpendicular to the direction of the motion of the wave. See Figure 3.1(b) for the particle motion for S-waves. By contrast, surface waves travel along a free surface and primarily comprise Love waves and Rayleigh waves. Love waves are the faster of the two and occur perpendicular to the direction of propagation, i.e. the transverse direction, hence it has no vertical component. Since vertical displacement amplitudes are of main interest in the thesis, Love waves are not hereafter discussed. Rayleigh waves travel close to the ground surface and represent a mixture of changes in both pressure and shear, and the particles move in elliptical paths. See Figure 3.1(c) for the particle motion for Rayleigh waves. The relationship between the three different wave types (viz. P-waves, S-waves, and Rayleigh waves) in terms of wave speed are is discussed in the subsequent section.

3.1.3 Wave speed

The wave speed for P-waves and S-waves in a linearly elastic homogeneous isotropic medium is given by

$$c_P = \sqrt{\frac{\lambda_L + 2\mu}{\rho}}; \qquad c_S = \sqrt{\frac{\mu}{\rho}} \qquad (3.1)$$

where λ_L and μ are known as the first and second Lamé constant, respectively, and ρ is the mass density [2]. The Lamé constants are related to the engineering constants as

$$\lambda_L = \frac{\nu E}{(1 + \nu)(1 - \nu)}; \qquad \mu = \frac{E}{2(1 + \nu)} \qquad (3.2)$$

where ν is the Poisson's ratio, and E is the elastic modulus. The second Lamé constant, μ, is identified as the shear modulus, which is often referred to as G.

The wave speed of S-waves, c_S, is slower than that of the P-waves, c_P. The relationship between the two depends on the Poisson ratio, see Table 3.1. The difference in wave speed between the two wave types increases with an increase in the Poisson's ratio.

Rayleigh waves are slightly slower in speed than shear waves. The wave-speed relationship between the two depends on the Poisson's ratio, see Table 3.2. The difference in wave speed increases with an increase in Poisson's ratio. The wave speed of Rayleigh waves, c_R, can be determined on the basis of

$$V^6 - 8V^4 - (16\alpha^2 - 24)V^2 - 16(1 - \alpha^2) = 0 \qquad (3.3)$$

where $V = c_R/c_S$ and α can be found in Table 3.1 [2].

Table 3.1: Shear wave speed in relation to pressure wave-speed: $\alpha = c_S/c_P$.

ν	α
0.20	0.61
0.30	0.53
0.40	0.41
0.49	0.14

Table 3.2: Rayleigh wave speed in relation to shear wave-speed: $V = c_R/c_S$.

ν	V
0.20	0.91
0.30	0.93
0.40	0.94
0.49	0.95

The relationship between the wave speed, c, and the wavelength, λ_w is given by

$$\lambda_w = 2\pi \frac{c}{\omega} = \frac{c}{f} \tag{3.4}$$

where ω is the angular frequency, and f is the frequency.

3.2 STRUCTURAL DYNAMICS

For detailed information regarding structural dynamics see [20–23]. The easiest way to describe a dynamic system is by using a single degree of freedom (sdof) system. An sdof system involves only one degree of freedom (dof). Thus, only one dof is needed in order to describe the exact position of a given object (mass). The system shown in Figure 3.2 consists of the mass, m, a damper, c, and a spring, k. The load f is time-dependent. The damper and the spring are regarded as massless. The force equilibrium involved and Newton's second law gives

$$f - c\dot{u} - ku = m\ddot{u} \tag{3.5}$$

which, if rewritten, gives the equation of motion for an sdof system

$$m\ddot{u} + c\dot{u} + ku = f. \tag{3.6}$$

In order to describe the motion of a more complex structure, a multi-degree of freedom (mdof) system is needed. In general, the greater number of dofs that are used to describe the system, the more accurate the results. The equation of motion of a body, assuming small deformations, can be described with the differential equation

$$\tilde{\boldsymbol{\nabla}}^T \boldsymbol{\sigma} + \mathbf{b} = \rho \frac{\partial^2 \mathbf{u}}{\partial t^2} \tag{3.7}$$

in which $\tilde{\boldsymbol{\nabla}}$ is a differential operator matrix, $\boldsymbol{\sigma}$ denotes the stress vector, $\mathbf{b}$ is the body force vector, ρ is the mass density, $\mathbf{u}$ is the displacement vector, and t denotes time. The equation of motion for a dynamic problem, as derived from Equation 3.7, can be written as (cf. Equation 3.6)

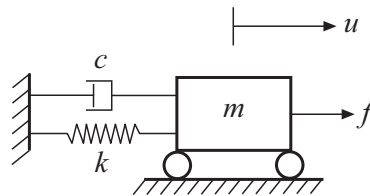$$\mathbf{M\ddot{u} + C\dot{u} + Ku = f} \tag{3.8}$$

Figure 3.2: Mass-spring-damper system, involving a friction-free surface.

where $\mathbf{M}$ is the mass matrix, $\mathbf{C}$ is the damping matrix, $\mathbf{K}$ is the stiffness matrix, $\mathbf{f}$ denotes the load vector, and $\mathbf{u}$ denotes the nodal displacement vector.

The response of a system under harmonic loading is common in structural dynamics. Understanding a system's response to harmonic loading provides insight into how the system responds to other types of excitations [21]. In harmonic loading, steady-state vibration occurs. The load and the corresponding displacements can be expressed as complex harmonic functions

$$\mathbf{f} = \hat{\mathbf{f}}e^{i\omega t}; \qquad \mathbf{u} = \hat{\mathbf{u}}e^{i\omega t} \tag{3.9}$$

where $\hat{\mathbf{f}}$ and $\hat{\mathbf{u}}$ denote the complex load amplitude and the complex displacement amplitude, respectively, i is the complex number, and ω is the angular frequency. Inserting Equation 3.9 into Equation 3.8 results in the equation of motion in the frequency domain,

$$\mathbf{D}(\omega)\hat{\mathbf{u}} = \hat{\mathbf{f}} \tag{3.10}$$

where $\mathbf{D}$ is the frequency-dependent dynamic stiffness matrix, expressed as

$$\mathbf{D}(\omega) = -\omega^2\mathbf{M} + i\omega\mathbf{C} + \mathbf{K}. \tag{3.11}$$

For the transient analyses conducted in this thesis, an implicit solver was used. One potential drawback to an implicit solver in contrast to an explicit solver is that the system matrix must be inverted at every time step. However, in linear analyses this is unnecessary, because the system matrices do not depend on strain or time. Moreover, an implicit solver is also unconditionally stable for linear problems, unlike an explicit solver. Indeed, different integration schemes have been developed, such as the Euler method and the Crank-Nicolson method. The time-integration scheme by Hilber-Hughes-Taylor (referred to as the HHT-α method) was used in the numerical integrations in time [24].

In order to convert time series to the frequency domain, the Fast Fourier Transform (FFT) can be used [25]. To convert from the frequency domain to the time domain, the inverse FFT can be used. Figure 3.3 shows a plot in the time domain and its representation in the frequency domain obtained by using FFT.

Resonance

A structure has an unlimited number of natural frequencies, also known as resonance frequencies. In a numerical model, a structure is discretised into dofs. In a linear system, the number of natural frequencies is equal to the number of dofs. Hereafter, the calculated natural frequencies are referred to as eigenfrequencies. If a structure is excited by a load with a frequency content close to a natural frequency, the amplitude of the vibrations produced increases significantly, a phenomenon referred to as resonance. The displacement amplitude of a steady-state response to the harmonic force of an undamped sdof system can be written as

$$u(\omega) = \frac{f}{k}\frac{1}{1 - (\omega/\omega_n)^2} \tag{3.12}$$
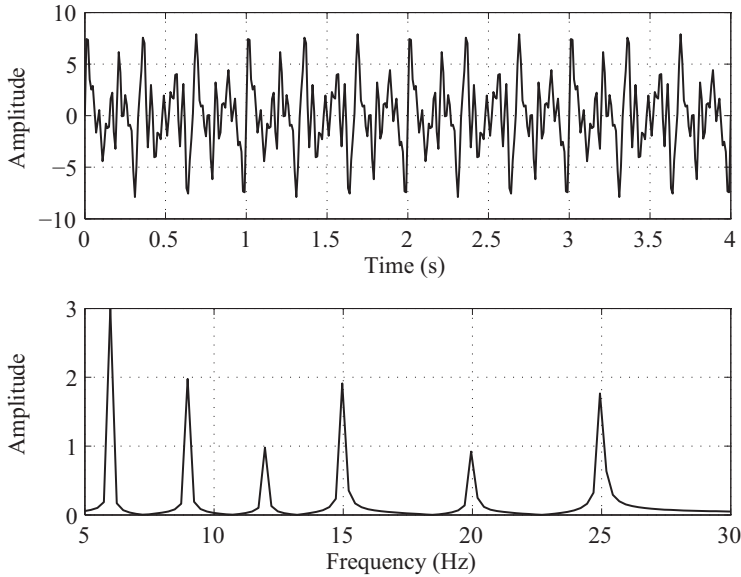
Figure 3.3: *Time series (upper plot) and its representation in the frequency domain (lower plot).*

where ω_n is the angular eigenfrequency of the system. If the exciting frequency, ω, is equal to the eigenfrequency, ω_n, the response amplitude, u, is infinite. Because damping is always present in any given structure, however, the response can never be infinite. See subsequent section for an elaborated discussion about damping. For any given eigenfrequency, there is a corresponding deformation shape of the structure, referred to as an eigenmode of the structure. When examining how the eigenfrequencies and the corresponding eigenmodes can be determined from an mdof system, an undamped system will be considered. The equation of motion of such a system in the case of **f**=0 is

$$\mathbf{M\ddot{u}} + \mathbf{Ku} = 0. \tag{3.13}$$

The solution, $\mathbf{u}(t)$, then needs to satisfy the initial conditions at t=0:

$$\mathbf{u} = \mathbf{u}(0); \qquad\qquad \dot{\mathbf{u}} = \dot{\mathbf{u}}(0). \tag{3.14}$$

The free vibration of an undamped system in a given eigenmode can be written as

$$\mathbf{u}(t) = q_n(t)\phi_n \tag{3.15}$$

where $q_n(t)$ is time-dependent and can be described by the harmonic function

$$q_n(t) = A_n \cos \omega_n t + B_n \sin \omega_n t \tag{3.16}$$

where ϕ_n, which denotes the eigenmodes, does not vary over time. If $q_n(t)$=0, there is no motion to the system, since this implies that $\mathbf{u}(t)$=$\mathbf{0}$. Under such conditions, both ϕ_n and ω_n must satisfy the eigenvalue problem

$$(-\omega_n^2 \mathbf{M} + \mathbf{K})\phi_n = 0. \tag{3.17}$$

In line with the previous argument, if ϕ_n=0, there is no motion in the system. The solution then results in the eigenfrequencies $\omega_1, ..., \omega_n$, where n denotes the number of dofs. When the eigenfrequencies are known, the eigenmodes ϕ_n can be calculated by solving the eigenvalue problem, as given in Equation 3.17. The eigenfrequencies and eigenmodes are thus a property of the structure, and they depend on the value and distribution of the mass and on the stiffness of the structure.

Because modelling a semi-infinite ground medium involves far-field conditions, the eigenfrequenies of a ground medium cannot be calculated in the same manner as for a structure. However, in soil dynamics it is common to consider resonance, which occurs at frequencies where the ground has a large response to the dynamic load. Analytical expressions can be derived for resonances in ground medium. For example, the analytical expression [26]

$$f_n = \frac{c_s(2n + 1)}{4h} \tag{3.18}$$

where f_n are the frequencies of a standing wave in a soil layer covering a stiff bedrock, c_s is the shear-wave speed and h is the thickness of the soil layer. In complex situations involving different types of waves and layering, however, it is preferable to make predictions with numerical steady-state analyses of the frequencies where the ground has its largest response.

3.3 DAMPING

Geometrical attenuation, also known as geometric damping, is a feature of the geometry of the medium in which the waves propagate. It is, however, different for point sources and line sources. In the case of a homogeneous halfspace, body waves originating from a point source propagate as a hemispherical wave front with an area of $4\pi r^2$. Because the same energy must be present independently of the distance to the wave source, the geometric attenuation of the body waves is proportional to $1/r$. Rayleigh surface waves propagate radially as a cylindrical wave front with a surface area of $2\pi r$. Hence, the geometric attenuation of the Rayleigh waves is proportional to $1/\sqrt{r}$. In cases with an applied line source, the geometric damping of body waves is proportional to $1/\sqrt{r}$, and the Rayleigh surface waves do not attenuate due to geometric damping. Thus, at a relatively large distance from a vibration source, it is the Rayleigh waves that are more likely to be the dominant wave form. In analyses involving both soil and underlying bedrock, which differ significantly in their damping properties and stiffness, the wave propagation is nonetheless more complex than outlined here.

Damping refers to an energy-loss effect that reduces the level of vibration in a medium. Damping is always present, and it arises from such sources as internal material damping or friction that occurs in cracks and joints. It can have an appreciable effect on the response of a structure exposed to a dynamic load. Because the damping properties of a given material cannot be calculated directly, they need to be determined on the basis of measurement data obtained from similar structures. Damping involves, in general, non-linear effects. However, in cases with small strains and slight damping, linear damping models are sufficient [27].

In order to introduce rate-independent linear damping into a system, a loss factor can be employed. It is defined as

$$\eta = \frac{1}{2\pi} \frac{E_D}{E_S} \tag{3.19}$$

where E_D denotes the energy dissipated per unit volume in the form of a viscous damping of a given cycle of harmonic vibrations, and E_S denotes the strain energy [21]. Here, E_D and E_S can be written respectively as

$$E_D = \pi c \omega u^2 \tag{3.20}$$

where c is the damping constant, and u is the amplitude of the motion involved, and

$$E_S = k u^2 / 2. \tag{3.21}$$

By inserting Equation 3.20 and Equation 3.21 into Equation 3.19, gives the loss factor

$$\eta = \frac{\omega c}{k}. \tag{3.22}$$

In generalising this to a mdof system, Equation 3.22 can be written as

$$\mathbf{K}\eta = \omega \mathbf{C}. \tag{3.23}$$

Inserting Equation 3.23 into Equation 3.11 results in

$$\mathbf{D}(\omega) = -\omega^2 \mathbf{M} + (1 + i\eta)\mathbf{K}. \tag{3.24}$$

The imaginary part of the stiffness matrix is referred to as the structural damping matrix [20]. A limitation to the assumed damping model is that it cannot be used in the time domain. In order to do so, rate-dependent Rayleigh damping can be applied. For a narrow range of frequency, however, the frequency-dependence of the Rayleigh damping can be neglected.

Rayleigh damping, which can be used in both transient and steady-state analyses, is a procedure for determining the classical damping matrix by using damping ratios. Classical damping is an appropriate idealisation, provided that the mass and the stiffness are distributed evenly throughout the structure. It consists of two parts, one that is mass-proportional and another that is stiffness-proportional, such that

$$\mathbf{C} = \alpha \mathbf{M} + \beta \mathbf{K}. \tag{3.25}$$
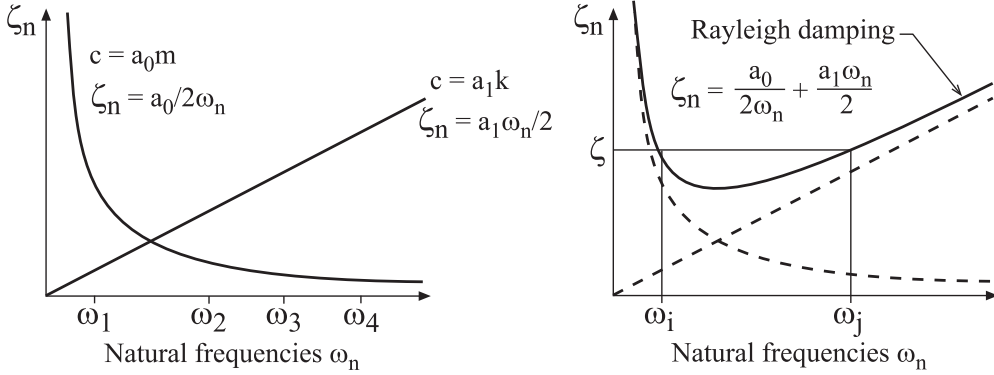
Figure 3.4: Rayleigh damping.

Rayleigh damping is affected by the mass at the lower frequencies and by the stiffness at the higher frequencies, see Figure 3.4.

Although it has no physical basis, Rayleigh damping has been shown to provide a good approximation [21]. The damping ratio for the n-th mode is written as

$$\zeta_n = \frac{\alpha}{2} \frac{1}{\omega_n} + \frac{\beta}{2} \omega_n. \tag{3.26}$$

The damping ratio is dimensionless, and it refers to the ratio of the damping constant, c, to the critical damping coefficient, c_{cr}, according to

$$\zeta = \frac{c}{c_{cr}} \tag{3.27}$$

where $c_{cr} = 2m\omega_n$. In buildings, the damping ratio is normally around a few percent, which means that the system is underdamped. If the damping ratio is 1, the system is critically damped, whereas damping ratios of greater than 1 refer to a system that is overdamped. If the damping ratios ζ_i and ζ_j, for the i-th and j-th modes, respectively, are assumed to have the same value, the coefficients α and β can be written as

$$\alpha = \zeta \frac{2\omega_i \omega_j}{\omega_i + \omega_j}; \qquad \beta = \zeta \frac{2}{\omega_i + \omega_j} \tag{3.28}$$

where ω_i and ω_j determine the frequency range in which the damping ratio is valid.

The relationship between structural damping and Rayleigh damping can be expressed in steady-state analysis as

$$\eta = \frac{1}{2\pi} \frac{E_D}{E_S} = 2\zeta \frac{\omega}{\omega_n}, \tag{3.29}$$

and, when the exciting frequency is equal to the eigenfrequency, it can be expressed as

$$\eta = 2\zeta. \tag{3.30}$$
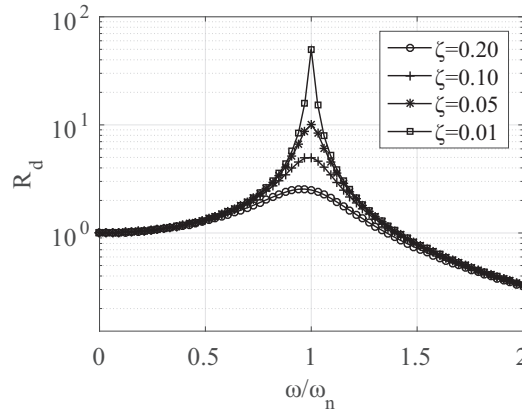
Figure 3.5: *The amplitude response R_d (ratio of the dynamic to the static deformation) versus the ratio of the excitation frequency to the natural frequency, for a resonant structure.*

As mentioned in the previous section, if the exciting frequency of an undamped system were equal to one of the system's eigenfrequencies, the response amplitude (i.e. Equation 3.12) would be infinite. Because damping is always present, however, the response amplitude is never infinite. See Figure 3.5 for the influence of damping on the vibration response. When damping is considered in terms of a loss factor, Equation 3.12 can be written as

$$u(\omega) = \frac{f}{k} \frac{1}{\sqrt{[1 - (\omega/\omega_n)^2]^2 + \zeta^2}}. \tag{3.31}$$

The additional term containing ζ prevents the occurrence of an infinite response amplitude. In the previous section, it was noted that in an undamped system, the eigenfrequencies depend on both the mass and the stiffness of the structure. The eigenfrequencies of a damped system also depend upon damping properties, such as the damping ratio ζ, in accordance to

$$\omega_D = \omega_n \sqrt{1 - \zeta^2}. \tag{3.32}$$

3.4 NUMERICAL METHODS

3.4.1 Finite element method

Partial differential equations (PDEs) are used to describe various physical problems. Numerical methods can be used to solve PDEs that are too complicated to be solved analytically. The finite element (FE) method is such a tool. It is used in a large number of engineering disciplines related to physics and mathematics to solve PDEs with arbitrary geometries and materials.

The development of the FE method took off in the early 1960s, and it is currently one of the most effective methods available. In order to solve differential equations with the FE method, the body is divided into small elements, termed finite elements. Rather than approximating the region in question as a whole through use of higher-order functions, simpler functions such as linear or quadratic polynomials can be used for each element. An FE solution requires that the boundary conditions for all the boundaries are known. That is, it is a boundary-value problem. Because there are often tens of thousands, or even millions, of finite elements in the element mesh, the system of equations cannot be solved without computer calculations. Extensive work on the FE method is presented in [22, 23].

FE formulation for linear elasticity

In this subsection, the FE method is described through the use of a dynamic equilibrium situation for a linear elastic continuum body. Its differential equation is given as

$$\tilde{\nabla}^T \sigma + \mathbf{b} = \rho \frac{\partial^2 \mathbf{u}}{\partial t^2} \tag{3.33}$$

where $\tilde{\nabla}$ is a matrix differential operator, σ is a vector composed of all the stress components involved, and $\mathbf{b}$ is a body force vector containing the body forces present per unit volume, such that

$$\tilde{\nabla}^T = \begin{bmatrix} \frac{\partial}{\partial x} & 0 & 0 & \frac{\partial}{\partial y} & \frac{\partial}{\partial z} & 0 \\ 0 & \frac{\partial}{\partial y} & 0 & \frac{\partial}{\partial x} & 0 & \frac{\partial}{\partial z} \\ 0 & 0 & \frac{\partial}{\partial z} & 0 & \frac{\partial}{\partial x} & \frac{\partial}{\partial z} \end{bmatrix}; \quad \sigma = \begin{bmatrix} \sigma_{xx} \\ \sigma_{yy} \\ \sigma_{zz} \\ \sigma_{xy} \\ \sigma_{xz} \\ \sigma_{yz} \end{bmatrix}; \quad \mathbf{b} = \begin{bmatrix} b_x \\ b_y \\ b_z \end{bmatrix}; \quad \mathbf{u} = \begin{bmatrix} u_x \\ u_y \\ u_z \end{bmatrix}. \tag{3.34}$$

Whereas the body force vector, $\mathbf{b}$, acts on the body-per-unit volume, the traction vector acts on the surface of the body, as a force-per-unit area. Insofar as it is present on the surface, the traction vector, $\mathbf{t}$, must fulfil the boundary conditions

$$\mathbf{t} = \mathbf{Sn} \tag{3.35}$$

where $\mathbf{n}$ is the stress tensor, and $\mathbf{n}$ is the unit normal vector.

In order to derive the weak formulation, the arbitrary vector $\mathbf{v}$ is introduced as

$$\mathbf{v} = \begin{bmatrix} v_x \\ v_y \\ v_z \end{bmatrix}. \tag{3.36}$$

Multiplying Equation 3.33 with Equation 3.36 and integrating the expressions over the volume, V, results in

$$\int_V \mathbf{v}^T (\tilde{\nabla}^T \sigma + \mathbf{b} - \rho \frac{\partial^2 \mathbf{u}}{\partial t^2}) dV = 0. \tag{3.37}$$

This is followed by integration by parts using the Green-Gauss theorem on the first term in Equation 3.37 and the components of the traction vector emerge as

$$\int_V \mathbf{v}^T \tilde{\boldsymbol{\nabla}}^T \boldsymbol{\sigma} \mathrm{d}V = \int_S \mathbf{v}^T \mathbf{t} \mathrm{d}S - \int_V \left(\tilde{\boldsymbol{\nabla}} \mathbf{v}\right)^T \boldsymbol{\sigma} \mathrm{d}V. \tag{3.38}$$

Finally, the terms are added together, resulting in the weak formulation

$$\int_V \mathbf{v}^T \rho \frac{\partial^2 \mathbf{u}}{\partial t^2} \mathrm{d}V + \int_V \left(\tilde{\boldsymbol{\nabla}} \mathbf{v}\right)^T \boldsymbol{\sigma} \mathrm{d}V = \int_S \mathbf{v}^T \mathbf{t} \mathrm{d}S + \int_V \mathbf{v}^T \mathbf{b} \mathrm{d}V. \tag{3.39}$$

In order to utilise this in the FE formulation, the displacement vector, $\mathbf{u}$, is approximated by

$$\mathbf{u} = \mathbf{N}\mathbf{a} \tag{3.40}$$

where $\mathbf{N}$ contains the global shape functions, and $\mathbf{a}$ contains the displacements. The use of the Galerkin method implies that

$$\mathbf{v} = \mathbf{N}\mathbf{c} \tag{3.41}$$

where $\mathbf{c}$ is a vector with arbitrary constants. Accordingly,

$$\tilde{\boldsymbol{\nabla}} \mathbf{u} = \boldsymbol{\varepsilon} = \mathbf{B}\mathbf{a} \tag{3.42}$$

and

$$\tilde{\boldsymbol{\nabla}} \mathbf{v} = \mathbf{B}\mathbf{c} \tag{3.43}$$

where $\mathbf{B} = \tilde{\boldsymbol{\nabla}} \mathbf{N}$. Inserting Equation 3.41 and Equation 3.43 into the weak formulation shown in Equation 3.39 allows for the extraction and elimination of $\mathbf{c}$. Introducing the behaviour of linear elastic material through use of the constitutive matrix $\mathbf{D}$ results in

$$\boldsymbol{\sigma} = \mathbf{D}\boldsymbol{\varepsilon}. \tag{3.44}$$

Through use of the kinematic relationship for elastic strains derived with Equation 3.42, Equation 3.44 can be written as

$$\boldsymbol{\sigma} = \mathbf{D}\mathbf{B}\mathbf{a}. \tag{3.45}$$

The FE formulation for a linear elastic case can then be rewritten as

$$\int_V \mathbf{N}^T \rho \mathbf{N} \mathrm{d}V \ddot{\mathbf{a}} + \int_V \mathbf{B}^T \mathbf{D}\mathbf{B} \mathrm{d}V \mathbf{a} = \int_S \mathbf{N}^T \mathbf{t} \mathrm{d}S + \int_V \mathbf{N}^T \mathbf{b} \mathrm{d}V. \tag{3.46}$$

The boundary conditions involved can be stated either as the essential boundary condition, i.e. prescribed displacements $\mathbf{u}$, or as the natural boundary condition, i.e. prescribed traction vector $\mathbf{t}$.

To obtain a more compact formulation, matrices and vectors are defined as

$$\mathbf{M} = \int_V \mathbf{N}^T \rho \mathbf{N} \mathrm{d}V; \quad \mathbf{K} = \int_V \mathbf{B}^T \mathbf{D}\mathbf{B} \mathrm{d}V; \quad \mathbf{f} = \int_S \mathbf{N}^T \mathbf{t} \mathrm{d}S + \int_V \mathbf{N}^T \mathbf{b} \mathrm{d}V \tag{3.47}$$
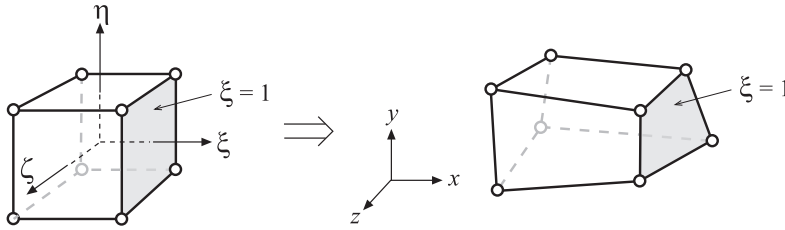
Figure 3.6: *Isoparametric element with its coordinate axis.*

such that

$$\mathbf{M\ddot{a} + Ka = f}. \tag{3.48}$$

where $\mathbf{M}$ is the mass matrix, $\mathbf{K}$ is the stiffness matrix, $\mathbf{f}$ is the force vector.

A two-dimensional form that is valid in plane strain, plane stress or axisymmetric cases can be found by integrating the expressions in Equation 3.48 over the thickness or circumferential direction.

Isoparametric elements

The use of isoparametric finite elements allows the sides of quadrilateral elements to be non-parallel to the coordinate axes, while still behaving in a compatible manner. This is needed when modelling structures with an arbitrary geometry.

Consider a cubic domain bounded by a $\xi\eta\zeta$-coordinate system (parent domain), in which $\xi = \pm 1$, $\eta = \pm 1$, and $\zeta = \pm 1$ (see Figure 3.6). The process by which the parent domain is transformed into another and more complicated region is called mapping. Mapping transforms the parental domain into a global Cartesian xyz-coordinate system as follows:

$$x = x(\xi,\eta,\zeta); \qquad y = y(\xi,\eta,\zeta); \qquad z = z(\xi,\eta,\zeta). \tag{3.49}$$

This relationship is unambiguous, since for every point given by $\xi\eta\zeta$-coordinates in the parent domain, there exists a unique point given by xyz-coordinates in the global domain. By differentiating Equation 3.49 and using the chain rule, an expression is derived that allows for the transformation between the two domains:

$$\begin{bmatrix} dx \\ dy \\ dz \end{bmatrix} = \begin{bmatrix} \frac{\partial x}{\partial \xi} & \frac{\partial x}{\partial \eta} & \frac{\partial x}{\partial \zeta} \\ \frac{\partial y}{\partial \xi} & \frac{\partial y}{\partial \eta} & \frac{\partial x}{\partial \zeta} \\ \frac{\partial z}{\partial \xi} & \frac{\partial z}{\partial \eta} & \frac{\partial z}{\partial \zeta} \end{bmatrix} \begin{bmatrix} d\xi \\ d\eta \\ d\zeta \end{bmatrix} \tag{3.50}$$

where the Jacobian matrix $\mathbf{J}$ can be written as

$$\mathbf{J} = \begin{bmatrix} \frac{\partial x}{\partial \xi} & \frac{\partial x}{\partial \eta} & \frac{\partial x}{\partial \zeta} \\ \frac{\partial y}{\partial \xi} & \frac{\partial y}{\partial \eta} & \frac{\partial x}{\partial \zeta} \\ \frac{\partial z}{\partial \xi} & \frac{\partial z}{\partial \eta} & \frac{\partial z}{\partial \zeta} \end{bmatrix}. \tag{3.51}$$

If the values in the parental domain are the target values, Equation 3.50 can be written as

$$
\begin{bmatrix} d\xi \\ d\eta \\ d\zeta \end{bmatrix} = \mathbf{J}^{-1} \begin{bmatrix} dx \\ dy \\ dz \end{bmatrix}
\tag{3.52}
$$

which obviously requires that $det\mathbf{J} \neq 0$. If an element behaves in a conforming manner in the parent domain, its isoparametric version also behaves in a conforming manner, and no mismatch between adjacent elements exists. The completeness criterion is satisfied if and only if

$$
\sum_{i=1}^{n} \mathbf{N}_i^e = 1.
\tag{3.53}
$$

If the compatibility and completeness requirements are fulfilled individually, then the element fulfils the convergence criterion and, thus, converge towards the exact solution. Mapping an element entails that the vertex-nodes in the parent domain are also located on the boundary following the transformation.

Viscous absorbing boundaries

One effective way to reduce the size of FE models of semi-infinite media is to introduce viscous absorbing boundaries (VABs). Finite elements can be used for the region of interest, with infinite elements introducing VABs to represent the far-field region. In Figure 3.7, an example of a mesh involving both finite and infinite elements is shown. The material responses at the VABs are assumed to be linear elastic. A popular method used by the commercial FE software, Abaqus, was proposed by Lysmer and Kuhlemeyer in 1969 [28]. They used boundary conditions in terms of dashpots to absorb incident waves, hence providing non-reflecting boundaries through a damping matrix. Owing to the suppression of the element stiffness matrix, the elements provide no contribution to the eigenmodes. Nevertheless, rigid body motions can occur. However, these are usually of no significance to engineering problems. The VABs are completely effective for orthogonally impinging plane body waves, assuming a linear-elastic material model. For waves that are not propagating normally to the boundary, and for surface waves such as Rayleigh waves, boundary damping is still sufficient from an engineering perspective [29]. Owing to the fact that the VABs do not transmit all waves exactly, they are advantageously placed at some distance from the region of interest.

In order to demonstrate how VABs are derived, the following derivation considering plane longitudinal waves is made. The stress-strain relation is given by

$$
\sigma_{xx} = 2\mu\epsilon_{xx} + \lambda_L(\epsilon_{xx} + \epsilon_{yy} + \epsilon_{zz})
\tag{3.54}
$$

where λ_L and μ are known as the first and second Lamé constant, respectively, see Equation 3.2. The incoming wave can be written as

$$
u_x = f_1(x - c_p t)
\tag{3.55}
$$

and the reflected wave as

$$u_x = f_2(x + c_p t). \tag{3.56}$$

Hence, the total displacement can be written as $f_1 + f_2$. The idea is to introduce distributed damping constants, d, such that

$$\sigma_{xx} = -d_p \dot{u}_x. \tag{3.57}$$

By assuming small strains and inserting Equation 3.57 into Equation 3.54, results in

$$(2\mu + \lambda)(f_1' + f_2') = -d_p c_p (f_2' - f_1'). \tag{3.58}$$

By setting $f_2'=0$ in order to ensure that $f_2=0$, the damping constant results in

$$d_p = \rho c_p \tag{3.59}$$

and analogously for shear waves

$$d_s = \rho c_s. \tag{3.60}$$

3.4.2 Other numerical methods

The field of numerical analysis includes many different methods. Here, some additional methods for solving PDEs are briefly summarised. For detailed information, see e.g. [30–33]. The finite difference (FD) method uses a grid of points at which the variable in the PDE is approximated. The partial derivatives in the PDE are approximated at these points using finite differences. Compared to the FE method, the FD method does not work well with complex geometries, because a square pattern of lines is used to discretise the PDE. In the finite volume (FV) method, values are calculated at discrete places on a meshed geometry in the same manner as the FD and FE methods. A finite volume refers to the small volume surrounding each node point on a mesh. In the FV method, volume integrals in the PDE are converted to surface integrals. These terms are then evaluated as fluxes at the surface of each finite volume. The FV
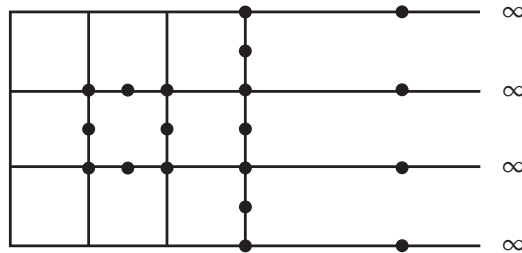
Figure 3.7: *Example of a mesh involving nine finite and three infinite elements under plane strain conditions using quadric approximation. The element nodes are shown for one finite element and for the three infinite elements.*

method can be applied to complex geometries. Because the FV method is easily employed for unstructured meshes, it is often used for computational fluid dynamics.

Similar to the FE method, the boundary element (BE) method numerically solves partial differential equations for several engineering problems. The BE method is especially advantageous over the FE method for problems with large domains, e.g. with infinite or semi-infinite boundaries, as exemplified in ground vibration or acoustic problems. The BE method reduces the dimensions of the problem by one dimension. The BE method approximates the solution of a PDE using the solution to it on the boundary in order to find the solution for the interior domain. The main advantage to the BE method is that only the boundary is discretised. By contrast, the FE method discretises the entire domain. The BE method usually results in fully populated system matrices, unlike FE matrices, which are typically banded. This leads to the need for increased memory and computation time. However, BE matrices have fewer unknowns. The FE method is a more versatile approach to handling heterogeneous materials, non-linear problems and complex geometries that are difficult to solve with the BE method. In ground-vibration problems involving the visualisation of the wave propagation, the displacements for the interior domain must be solved. In such cases, the computation benefit of the BE method decreases. However, the BE method can be coupled with the FE method, resulting in a coupled FE-BE method. As such, the advantages from both methods can be exploited.

3.5 COMPUTATIONAL STRATEGIES

In this section, the strategies undertaken when modelling with the FE method are described in terms of the coupling and interaction between domains. Moreover, strategies for developing time-efficient numerical models is described in this section.

3.5.1 Coupled problems

Soil-structure interaction

When the response of the soil influences the response of the structure, and vice-versa, an interaction between the soil and the structure occurs. Extensive work on soil-structure interaction can be found in [34]. The loads might originate from the deadweight of the structure, resulting in settlements, or from vibrations originating from a motorway that generates vibrations in a building. By considering soil-structure interaction, as opposed to the use of fixed displacement boundary conditions of the building, the structure is more flexible, changing the dynamic behaviour by increasing the eigenfrequency of the structure. Furthermore, resonant frequencies of the soil affects the response, and this is of great importance to structures affected by ground vibrations. It can also be important for internal loads. Furthermore, a building can affect the response in the soil in terms of being a wave obstacle, for example. The soil can be coupled

with the structure in different ways. One common method is to assume considerable friction wherein the structure and the soil can be fully tied. This prevents relative motion to the parts at their interface. Other methods involve slip and viscous behaviour between the structure and the soil by non-linear contact analysis.

Fluid-structure interaction

Fluid-structure interaction (FSI) occurs between a structure and a fluid. The analysis of this interaction is used to consider how the fluid affects the behaviour of the structure, and vice-versa. For detailed information about FSI see [22, 23, 35].

The indices s and f are here used to denote the properties of the structural and the fluid domains, respectively. Two governing equations can be employed to describe an acoustic fluid, which is assumed to be inviscid, irrotational, and compressible, and which is further assumed to undergo small pressure changes. The equation of motion, when the volumetric drag is neglected, can be written as

$$\rho \frac{\partial^2 \mathbf{u}_f}{\partial t^2} + \boldsymbol{\nabla} p = 0 \tag{3.61}$$

where ρ is the static density, $\boldsymbol{\nabla}$ is the gradient of a given variable, and p is the dynamic pressure, under the assumption that the density has only negligible variation in space. In the absence of an added fluid mass inflow, the constitutive equation can be written as

$$p = -c^2 \rho \boldsymbol{\nabla} \mathbf{u}_f \tag{3.62}$$

with the speed of sound, c, related to the density on the basis of the bulk modulus, K, where

$$c = \sqrt{\frac{K}{\rho}}. \tag{3.63}$$

With use of Equations 3.61 and 3.62, the wave equation for the acoustic fluid, in which the pressure serves as the field variable, can be written as

$$\frac{\partial^2 p}{\partial t^2} - c^2 \boldsymbol{\nabla}^2 p = 0. \tag{3.64}$$

The pressure can be expressed as the complex harmonic function

$$p = \hat{p} e^{i\omega t} \tag{3.65}$$

where $\hat{p}$ denotes the complex pressure amplitude. Inserting Equation 3.65 into Equation 3.64 results in the wave equation for the frequency domain

$$\boldsymbol{\nabla}^2 \hat{p}_d + \frac{\omega^2}{c^2} \hat{p}_d = 0. \tag{3.66}$$

Equation 3.66 can be formulated in terms of the FE method, with the pressure serving as the approximated nodal field variable, as

$$\mathbf{M}_f \ddot{\mathbf{p}}_f + \mathbf{K}_f \mathbf{p}_f = \mathbf{f}_{f,p} \tag{3.67}$$

where $\mathbf{M}_f$ and $\mathbf{K}_f$ are matrices, $\mathbf{p}_f$ is the pressure vector, and $\mathbf{f}_{f,p}$ is the boundary vector.

The coupling of the structure and the fluid at their common boundary, S, is made through static and kinematic boundary conditions. The force vector $\mathbf{f}$ in Equation 3.8 can be divided into three parts:

$$\mathbf{f} = \mathbf{f}_b + \mathbf{f}_l + \mathbf{f}_{s,p} \tag{3.68}$$

where $\mathbf{f}_b$ is the body force vector, $\mathbf{f}_l$ is the boundary force vector, and $\mathbf{f}_{s,p}$ corresponds to the acoustic fluid pressure that acts on the structure at S. The continuity of the fluid displacements and the structural displacements is assumed in the normal direction to their common boundary S. By introducing a normal vector, $\mathbf{n}$, the kinematic boundary condition can be formulated as

$$\mathbf{u}_s \cdot \mathbf{n}|_S = \mathbf{u}_f \cdot \mathbf{n}|_S. \tag{3.69}$$

Owing to the continuity in pressure at S, the static boundary condition for the coupling can be formulated as

$$\sigma_{s,n}|_S = -p_f \tag{3.70}$$

where $\sigma_{s,n}$ denotes the stresses at S in the normal direction, and p_f is the acoustic fluid pressure.

By introducing a coupling matrix, $\mathbf{H}$, the complete fluid-structure system of equations can be written as

$$\begin{bmatrix} \mathbf{M}_s & \mathbf{0} \\ \rho\mathbf{H}_{sf}^T & \mathbf{M}_f \end{bmatrix} \begin{bmatrix} \ddot{\mathbf{u}} \\ \ddot{\mathbf{p}} \end{bmatrix} + \begin{bmatrix} \mathbf{K}_s & -\mathbf{H}_{sf} \\ \mathbf{0} & \mathbf{K}_f \end{bmatrix} \begin{bmatrix} \mathbf{u} \\ \mathbf{p} \end{bmatrix} = \begin{bmatrix} \mathbf{f}_s \\ \mathbf{f}_f \end{bmatrix}. \tag{3.71}$$

3.5.2 Model order reduction

To develop time-efficient numerical models, model order reduction is a common strategy. In this section, the use of substructuring is described.

Substructuring involves dividing a structure into smaller parts called substructures, each of which is described by the equation of motion [20]. Because the damping is low in the reduced parts, it is assumed to have a negligible influence on their corresponding eigenmodes and eigenfrequencies. Hence, the damping matrix can be constructed in the reduced system. Therefore, the damping matrix is left out in the following derivations. The size of a substructure is reduced by transforming the displacement vector $\mathbf{u}$. The equation of motion for the reduced system can then be written as

$$\mathbf{M}_R \ddot{\mathbf{u}}_R + \mathbf{K}_R \mathbf{u}_R = \mathbf{f}_R \tag{3.72}$$

with

$$\mathbf{M}_R = \mathbf{T}^T \mathbf{M} \mathbf{T}; \quad \mathbf{K}_R = \mathbf{T}^T \mathbf{K} \mathbf{T}; \quad \mathbf{f}_R = \mathbf{T}^T \mathbf{f} \tag{3.73}$$

where $\mathbf{M}_R$ and $\mathbf{K}_R$ are the reduced mass and stiffness matrices, respectively, $\mathbf{f}_R$ is the reduced load vector, $\mathbf{u}_R$ is the reduced state vector, and $\mathbf{T}$ is the transformation matrix. Introducing master (index m) and slave (index s) dofs in the state vector allows the matrices in Equation 3.72 to be partitioned as

$$\begin{bmatrix} \mathbf{M}_{mm} & \mathbf{M}_{ms} \\ \mathbf{M}_{sm} & \mathbf{M}_{ss} \end{bmatrix} \begin{bmatrix} \ddot{\mathbf{u}}_m \\ \ddot{\mathbf{u}}_s \end{bmatrix} + \begin{bmatrix} \mathbf{K}_{mm} & \mathbf{K}_{ms} \\ \mathbf{K}_{sm} & \mathbf{K}_{ss} \end{bmatrix} \begin{bmatrix} \mathbf{u}_m \\ \mathbf{u}_s \end{bmatrix} = \begin{bmatrix} \mathbf{f}_m \\ \mathbf{f}_s \end{bmatrix}. \tag{3.74}$$

Component mode synthesis

Several substructuring methods exist (see e.g. [36]), but the substructuring process used in this thesis is the component mode synthesis by Craig–Bampton (hereafter denoted by CMS). CMS is currently the most common method used for substructuring in structural dynamics problems [37]. With CMS, the neglected inertia terms in condensation methods, e.g. in Guyan reduction [38], are compensated by considering the eigenmodes of the substructures that are obtained with fixed-interface dofs, $\mathbf{u}_m = \mathbf{0}$. Therefore, a set of generalised coordinates $\boldsymbol{\xi}$ is used. These coordinates represent the amplitudes of the eigenmodes. Assuming unloaded slave dofs, $\mathbf{f}_s = \mathbf{0}$, as well as a harmonic solution, the following eigenvalue problem is obtained from Equation 3.74

$$\mathbf{K}_{ss} \boldsymbol{\Phi} = \lambda \mathbf{M}_{ss} \boldsymbol{\Phi} \tag{3.75}$$

where λ denotes the eigenvalues, $\boldsymbol{\Phi}$ denotes the eigenmodes. The eigenmodes are selected as additional basis vectors for the approximation of slave dofs, resulting in

$$\mathbf{u}_s = -\mathbf{K}_{ss}^{-1} \mathbf{K}_{sm} \mathbf{u}_m + \sum \boldsymbol{\Phi}_i \xi_i = \boldsymbol{\Psi} \mathbf{u}_m + \boldsymbol{\Phi} \boldsymbol{\xi}. \tag{3.76}$$

The transformation matrix, $\mathbf{T}_{\mathrm{CMS}}$, can be defined by

$$\begin{bmatrix} \mathbf{u}_m \\ \mathbf{u}_s \end{bmatrix} = \begin{bmatrix} \mathbf{I} & \mathbf{0} \\ \boldsymbol{\Psi} & \boldsymbol{\Phi} \end{bmatrix} \begin{bmatrix} \mathbf{u}_m \\ \boldsymbol{\xi} \end{bmatrix} = \mathbf{T}_{\mathrm{CMS}} \begin{bmatrix} \mathbf{u}_m \\ \boldsymbol{\xi} \end{bmatrix}. \tag{3.77}$$

The accuracy of the solution depends both on the selection of the master dofs, which affects the eigenmodes of the substructure, as well as on the selection of the retained eigenmodes.

Interface reduction

Because the computational efficiency of CMS depends on the number of retained dofs, they determine the bandwidth of the system matrices, it is advantageous to reduce these dofs. It is usually the interface dofs that are retained. A condensation node, with three translational and three rotational dofs, can be introduced for each interface surface of the substructure. This is done with the intention of representing the motion of the interface in question, i.e. the dofs at

the interface are coupled with the condensation node. The coupling can be realised with rigid coupling or distributed coupling.

With rigid coupling, the interface is assumed to undergo rigid body motions that are then described with the six dofs from the condensation node. The coupling between the interface nodes and the condensation node is given by

$$\mathbf{u}_i = \mathbf{u}_c + \mathbf{\Theta}_c \times \mathbf{r}_{ci} \tag{3.78}$$

where $\mathbf{u}_i$ is the displacement vector of the i-th interface node, $\mathbf{u}_c$ is the displacement vector for the condensation node, $\mathbf{\Theta}_c$ is a vector containing the rotations of the condensation node, and the vector $\mathbf{r}_{ci}$ contains the distances from the condensation node to node i.

With distributed coupling, on the other hand, the weighted average motion of the interface surface is used to describe the motion of the condensation node. The forces and moments acting on the condensation node are coupled with the interface nodes [39] as

$$\mathbf{f}_i = \hat{v}_i \left(\mathbf{f}_c + \left(\mathbf{P}^{-1} \left(\mathbf{m}_c + \mathbf{r}_c \times \mathbf{f}_c \right) \right) \times \mathbf{r}_i \right) \tag{3.79}$$

where

$$\mathbf{P} = \sum_i \hat{v}_i \left(\left(\mathbf{r}_i^T \mathbf{r}_i \right) \mathbf{I} - \left(\mathbf{r}_i \mathbf{r}_i^T \right) \right). \tag{3.80}$$

The forces acting on the interface node i are denoted by $\mathbf{f}_i$; the forces and the moments acting on the condensation node are denoted by $\mathbf{f}_c$ and $\mathbf{m}_c$, respectively; the vectors $\mathbf{r}_c$ and $\mathbf{r}_i$ contain the distances from the weighted centre of the interface, $\bar{\mathbf{x}}$, to the condensation node and to node i, respectively. These are given by

$$\mathbf{r}_i = \mathbf{x}_i - \bar{\mathbf{x}}; \qquad \mathbf{r}_c = \mathbf{x}_c - \bar{\mathbf{x}} \tag{3.81}$$

where

$$\bar{\mathbf{x}} = \sum_i \hat{v}_i \mathbf{x}_i; \qquad \hat{v}_i = \frac{v_i}{\sum_i v_i}. \tag{3.82}$$

The vectors $\mathbf{x}_i$ and $\mathbf{x}_c$ contain the coordinates of the interface node i and the condensation node, respectively, and the weight factor assigned to interface node i is denoted by v_i. This type of coupling results in the displacements of the condensation node corresponding to the weighted averages of the displacements of the interface, such that

$$\mathbf{u}_c = \sum_i \hat{v}_i \mathbf{u}_i \tag{3.83}$$

$$\mathbf{\Theta}_c = \sum_i \hat{v}_i \frac{\mathbf{r}_{ci}}{|\mathbf{r}_{ci}|^2} \times \mathbf{u}_i. \tag{3.84}$$

The weight factors can be selected arbitrarily, resulting in an infinite number of ways to define the coupling. The simplest approach is uniform weighting, where the loads are distributed equally to the condensation node by

$$v_i = 1. \tag{3.85}$$

Other common methods involve polynomials to describe the decreasing influence of the interface forces with the increasing distance to the condensation node, for example by linearly and quadratically decreasing the weight as

$$v_i = 1 - \frac{|\mathbf{r}_{ci}|}{|\mathbf{r}_{c0}|}; \qquad v_i = 1 - \left(\frac{|\mathbf{r}_{ci}|}{|\mathbf{r}_{c0}|}\right)^2 \qquad (3.86)$$

where $\mathbf{r}_{c0}$ is the distance from the condensation node to the farthest interface node.

3.6 EVALUATION OF VIBRATIONS

Vibration levels

Root mean square (RMS) values are commonly used to measure the magnitude of vibrations. RMS values for the complex magnitude of the vertical displacements from a steady-state analysis can be determined with two different equations: Equations 3.87 and 3.88. The RMS value in Equation 3.87 is used to achieve one graph for an evaluation point pattern, defined as

$$u_{RMS}^I(f) = \frac{1}{n}\sqrt{\sum_{i=1}^{n} u_i^2} \qquad (3.87)$$

where u_i is the magnitude of the displacement at node i, and n is the number of evaluation nodes. A different RMS value can be used to determine one value for the frequency-dependent RMS value in Equation 3.87 and is here defined as

$$u_{RMS}^{II} = \frac{1}{m}\sqrt{\sum_{j=1}^{m} u_{RMS}^I(f_j)^2} \qquad (3.88)$$

where $u_{RMS}^I(f_j)$ is the magnitude of the displacement at frequency step j, and m is the number of frequency steps considered.

Level of reduction

The level of reduction can be used to evaluate the effectiveness of a vibration-reduction measure. The displacement-reduction factor, U_{red}, pertains to the relationship of the displacement amplitude after a reduction measure has been introduced (i.e. post-obstacle), U_{post}, to the amplitude prior to its introduction (i.e. pre-obstacle), U_{pre}, in accordance with Equation 3.88. The displacement-reduction factor is expressed as

$$U_{red} = \frac{U_{pre} - U_{post}}{U_{pre}}. \qquad (3.89)$$

Eigenmodes

The modal assurance criterion (MAC) can be used to compare eigenmodes, which can be obtained both from FE models and from measurements [40]. This criterion provides a measure of the consistency between two eigenmode vectors, were a MAC value of 1 is obtained in the case of two identical vectors. The MAC value for the i-th eigenmode of model A, Φ_i^A, as compared with the j-th eigenmode of model B, Φ_j^B, is defined as

$$\text{MAC} = \frac{\left|(\Phi_i^A)^T (\Phi_j^B)\right|^2}{(\Phi_i^A)^T (\Phi_i^A)(\Phi_j^B)^T (\Phi_j^B)}. \tag{3.90}$$

Eigenfrequencies

The normalised relative frequency difference (NRFD) can be used to compare eigenfrequencies determined from different models. It is defined, as a percentage, for the i-th eigenmode as

$$\text{NRFD} = 100 \frac{\left|f_i^A - f_i^B\right|}{f_i^B} \tag{3.91}$$

where f_i^A is the i-th eigenfrequency from model A, and f_i^B is the i-th eigenfrequency from model B.

Action value

In order to evaluate the vibration energy present at different sections in the ground, the action value was used, defined as

$$Action = \int_\omega E(\omega)d\omega \tag{3.92}$$

where the total energy, E, is calculated as

$$E = E_{kinetic} + E_{strain} \tag{3.93}$$

using the cyclic mean value of the kinetic energy and of the strain energy, and ω is the angular frequency. The kinetic energy and the strain energy, defined as

$$E_{kinetic} = \int_V \frac{1}{2}\rho\mathbf{v} \cdot \mathbf{v}dV \tag{3.94}$$

$$E_{strain} = \int_V \frac{1}{2}\boldsymbol{\sigma} : \boldsymbol{\epsilon}dV \tag{3.95}$$

where ρ is the density, $\mathbf{v}$ is the velocity, $\boldsymbol{\sigma}$ is the stresses and $\boldsymbol{\epsilon}$ is the strains, were evaluated from the FE analyses.

4 Modelling of vibrations in a built environment

In modelling vibrations in a built environment, several physical domains have to be considered. The numerical models often need to include both the ground and the building, and account for realistic loads such as motorway traffic or pedestrians. To describe modelling of a built environment the conceptual design of research facility, MAX IV Laboratory, is used as an example case in this chapter. Modelling of vibrations at the facility required various physically interacting domains to be considered involving various vibration phenomena to serve as a comprehensive example case. It should be noted that the methods and strategies presented in the thesis are general, and they can be used in several other cases.

4.1 THE MAX IV LABORATORY

To design the vibration-sensitive research facility MAX IV Laboratory (hereafter denoted as 'Max IV'), a group of vibration specialists was selected. The author belonged to that group, together with colleagues from Lund University and members of the construction industry. The main goal of the group was to ensure that vibration requirements could be fulfilled. Conceptual studies were performed to specify and verify design solutions aimed at minimising the vibration levels in sensitive areas. Detailed information regarding Max IV is provided in [41].

Max IV (the Microtron Accelerator for X-rays) is a Swedish national laboratory for research based on synchrotron radiation. It is located in the outskirts of the city of Lund and is jointly operated by the Swedish Research Council and Lund University. An architectural rendering of the facility is shown in Figure 4.1. A new storage ring was built to facilitate research in different areas, including material science, medicine, and biology. Max IV consists of a 3 GeV storage ring with a circumference of 528 m, used for the production of both soft and hard x-rays. It also includes a linear accelerator (Linac), located in a 400 m long underground tunnel next to the main ring. In the Linac, the electron beam is pre-accelerated almost to the speed of light. The electrons then enter the storage ring, where a large number of strong magnets

Figure 4.1: *Max IV rendered by the architecture firms, Fojab and Snøhetta [42,43]. The motorway E22 is located on the far side of the main building.*
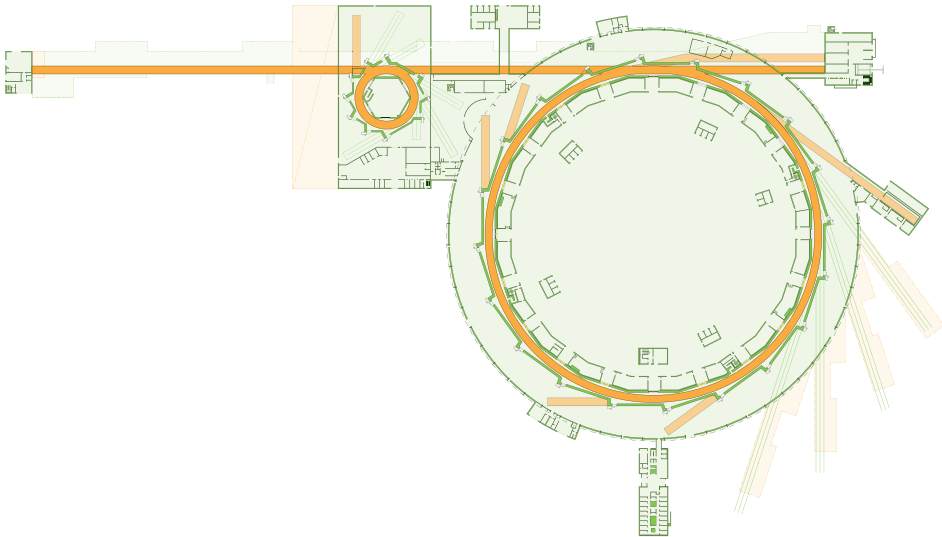
Figure 4.2: *Floor plan for the buildings at Max IV.*

distributed along the ring controls their position. The electrons that are accelerated along the ring emit electromagnetic radiation, called synchrotron light. The storage ring has space for 20 experimental stations distributed around the storage ring, where synchrotron light is led out tangentially in beamlines for measurement purposes. Figure 4.2 provides a 2D plan of the Max IV area, showing the main storage ring (the large ring-shaped building) and the Linac (the straight tunnel). The Linac tunnel consists mainly of concrete, as does the floor of the main building. The ring-shaped building has an outer diameter of approximately 200 m, and its roof extends to a height of approximately 12 m.

Of major concern is the fact that vibrations will result in changes to the position of the magnets, which in turn leads to a ten-fold increase in the positional change of the electron beam. The quality of the experimental results that will be performed in Max IV depend on the precision of the synchrotron light. Thus, very strict requirements concerning the vibration levels of the magnet foundations are specified. In particular, strict requirements are placed on the mean vertical vibration level. The aim is for the displacements to be less than 20–30 nm RMS per second within the frequency span of 5–100 Hz. An active beam-positioning system is employed for the magnets. Because of this, and because of the wavelengths being very long at frequencies of less than 5 Hz, vibrations with frequencies of less than 5 Hz will not affect the relative displacements of the magnets in relation to one another to any appreciable extent. Vibrations at frequencies higher than 100 Hz are easily damped out in the soil and in the structure, and is assumed to be negligible.

4.2 VIBRATION SOURCES

Buildings are often exposed to both internal and external vibration sources. Several different externally located vibration sources can affect a building, such as temporary construction sites, as well as, traffic from trains, trams and trucks. Several indoor sources affect the building as well, such as water-pipe systems, pumps, pedestrians and transportation of goods inside the building. The main disturbing vibrations from external sources at Max IV are the motorway E22, which passes 100 m from the main ring-shaped building (see Figure 4.1). The pedestrians are the internal source of primary interest since the other internal sources can often be controlled at the source itself. Hence, road traffic and pedestrians are discussed in the follow subsections.

4.2.1 Road traffic

Vibrations stemming from traffic occur, on the one hand, due to the stress field of the static deformation moving with the speed of the vehicle and, on the other hand, due to imperfections and irregularities. The latter includes defects to the vehicle itself (e.g. poor suspension) or to the ground (e.g. irregular ground surfaces, or defects in the asphalt), other important factors being the speed and weight of the vehicle [2]. For traffic-induced ground vibrations, the strains involved are usually at a level such that the assumption of linear elasticity is applicable both to soil and bedrock. In order to account for traffic loads in an FE model, the frequency content of the load was measured on the road or roads in question. If linearity is assumed, the frequency spectrum can be employed to scale the load or the calculated displacements, provided that a harmonic unit load is employed. Although absolute values for the displacements obtained cannot be achieved in this manner, relative differences can be obtained in terms of a reduction in the level of vibration.
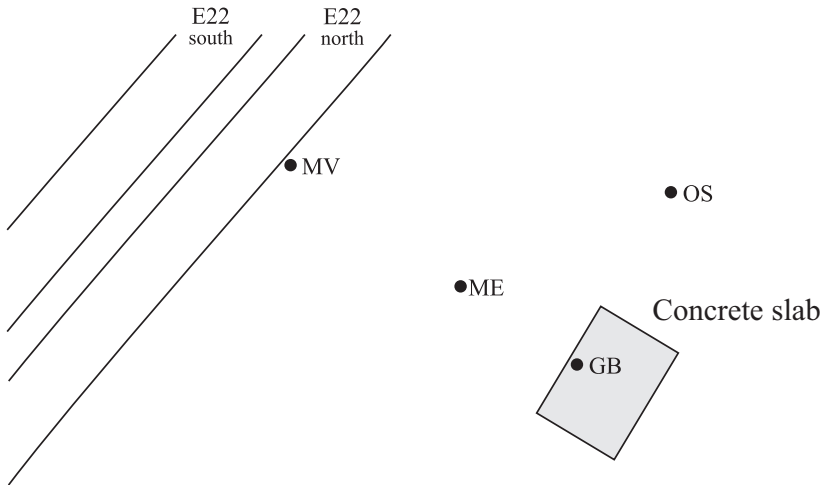
Figure 4.3: *Schematic plan of the measurement setup.*

The frequency content of the traffic load on the motorway near Max IV was assessed on the basis of green-field in-situ measurements (see Figure 4.3) for a schematic plan of the measurement setup). The measurements were setup according to [44]. Four seismometers was placed on granite plates on the ground-level surface. The seismometers were used to sample the velocity over time. In the figure, one of the seismometers (*MV*) was placed at the top of the motorway embankment. A second seismometer (*ME*) was placed 40 m away, perpendicular to the motorway. A third (*GB*) was placed on a concrete slab located on a mock-up with stabilised soil about 70 m away. The fourth (*OS*) was likewise placed about 70 m from the motorway, yet at some distance from the area with stabilised soil, so as to avoid the effects on the measurement data regarding the stabilisation of the soil. Full velocity-time series were measured on the embankment (*MV*) as vehicles passed by, with the aim of evaluating the frequency content of the traffic load. See Figure 4.4 for a schematic drawing of the measurement setup for the evaluation point that was located on the embankment. It is evident from Figure 4.5 that trucks generated the highest velocities. The peak velocity amplitudes were approximately six times higher for trucks than for cars. Of the ten events resulting in the highest velocity amplitudes during a one-hour period, all of them involved heavy trucks. An FFT of the time series was performed in order to obtain a velocity spectrum so that the frequency content of the
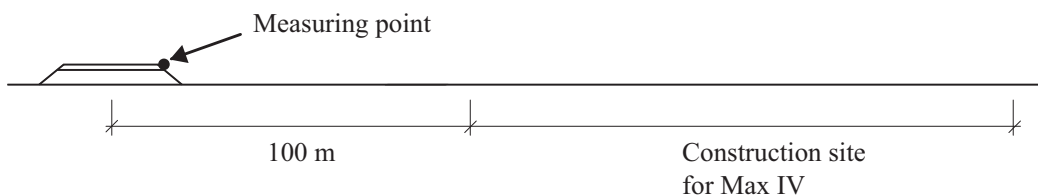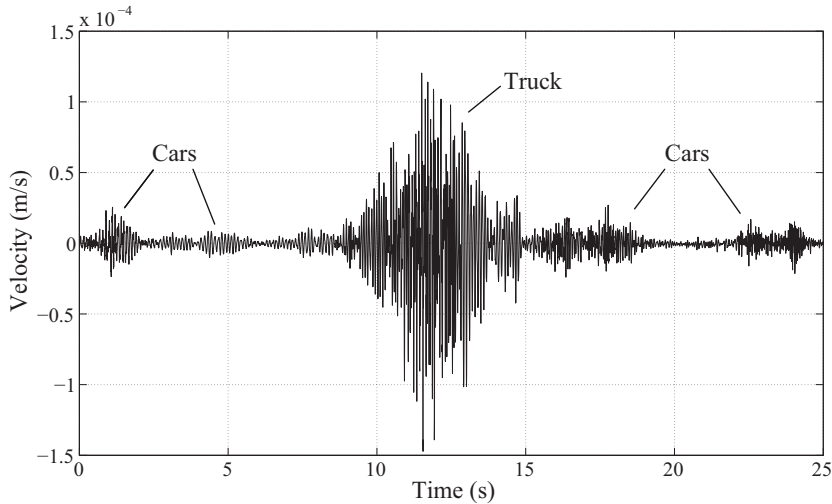

**Figure 4.4:** *Schematic measurement setup.*

Figure 4.5: *Measured vertical velocities over time for the responses at the E22 motorway adjacent to Max IV.*

traffic load could be determined. A displacement spectrum was then obtained by dividing the velocity spectrum by $i\omega$. In order to account for the frequency content of the traffic load in the numerical analyses, the median value (50% quantile) of the measured data was calculated for each frequency and used to scale the frequency response function (FRF) obtained from the FE analyses. Figure 4.6 shows the magnitude spectrum of displacements obtained from the measured data.

4.2.2 Pedestrians

The impact of pedestrians should be described as a dynamic load and considered as a load case when designing buildings where vibrations can disturb humans or sensitive equipment. Vibrations induced by pedestrians depend on the number of pedestrians and whether they are walking in pace (known as the crowd effect). According to the international standard, ISO 10137 [3], the crowd effect can be accounted for by multiplying the obtained level of vibration by the square root of the number of persons walking. In comparative studies, however, a single pedestrian is usually considered. The pedestrian load can be modelled with time-varying force amplitudes (see Figure 4.7 for an example). The weight of the person, the stride length, and the walking rate do not appreciably affect the shape of the forcing function, however, they do affect the peak force amplitude [45]. The load can also be described in the frequency domain with multiple harmonic functions, where the response is usually dominated by the first three or four harmonics. Hence, little energy is assumed to be present in the higher harmonics. If extreme vibration requirements must be met, however, higher harmonics may be of interest. Frequencies up to 20 Hz can then be of importance [4].
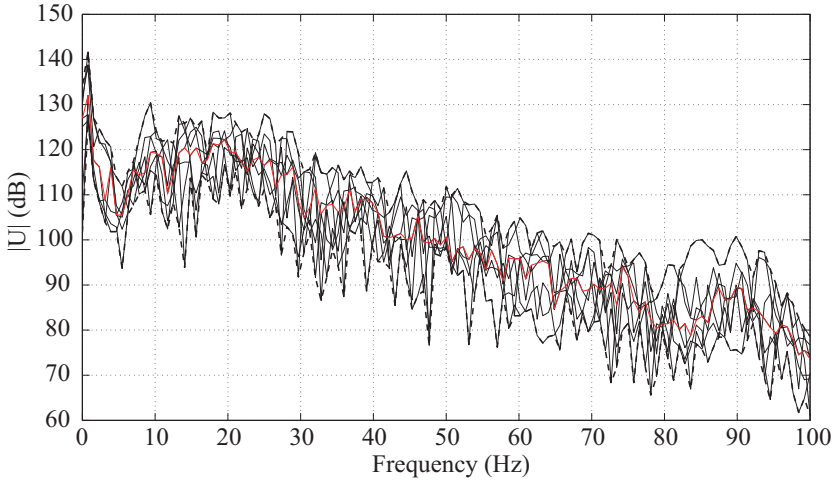
Figure 4.6: *Magnitude spectrum of displacements, U(f). The 95% and the 5% quantile curves are shown as dashed lines. The median value (50% quantile) used in the numerical analyses is shown as a solid red line. A reference displacement of 10^{-12} m is used.*

The frequency range of interest was set to 5–20 Hz since the vibration requirements at Max IV do not involve frequencies below 5 Hz. The walking rate of the pedestrians in Max IV can be assumed to be moderate, or at least not more than at an average rate, because it is an office-like environment. Hence, the walking rate was assumed to be less than 2.5 Hz. According
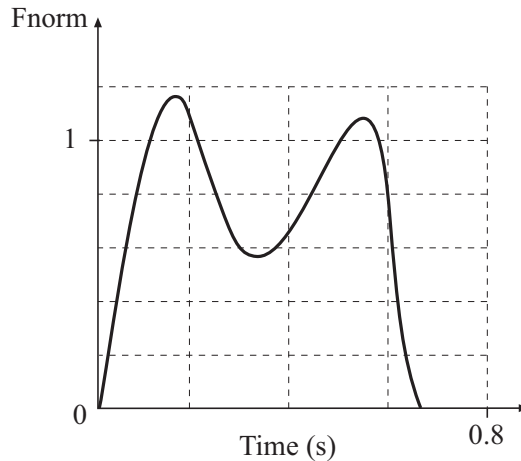
Figure 4.7: *Schematic example of vertical force against stiff ground for one step by one walking person. Based on curve found in [3]. F_{norm} is the dynamic force normalised to the static one.*

to the international standard, ISO 10137 [3], the force in the pedestrian load can be assumed to be constant for frequencies at the third harmonic and higher. Measurements presented by [4] show that the force of a 89 kg pedestrian walking at 2.4 Hz is somewhat constant in amplitude for frequencies between 5 and 20 Hz. Thus, the applied pedestrian load in numerical simulations, with Max IV as an example case, was set to be constant in amplitude in the frequency range of interest.

4.3 TRANSMISSION MEDIUM

This section describes the measurements carried out at Max IV for determining the material parameters and vibration levels. The involved ground and building materials are discussed. The damping properties of the materials are described in a separate subsection. Measurements for determining the material parameters and vibration levels are discussed. Occurring vibration phenomena in the ground are also presented.

4.3.1 Measurements

Conventional geotechnical surveys are insufficient for determining the ground-material parameters under small (or moderate) strain dynamic loading, because they provide parameters under large strain. Therefore, geophysical measurements are needed. These can also be referred to as seismic, vibrational or geodynamic measurements. In situations with human-caused vibrations (e.g. road traffic and pedestrians), small strains occur. In the example case, rate-independent engineering constants (E, ν, ρ, η) are sufficient for describing the materials. Geotechnical and geophysical measurements were carried out at the construction site in order to determine the material parameters of the ground [46]. The material parameters of both the soil and the bedrock, as well as their variations from the location at the site, are needed as inputs for the employed FE models in order for the FE simulations to provide accurate results. The measurements and evaluation of the ground material parameters were performed by Tyréns, Peab and Lund University. The author was mainly involved in the falling weight deflectometer tests (described below) and in calibrating material parameters by validating numerical analyses to measurements.

Geotechnical methods and laboratory tests

Geotechnical methods, such as auger drilling and dynamic sounding, were carried out at different locations at the construction site in order to evaluate various ground-material parameters. Soil samples were taken at the construction site and classified both on location and in a laboratory. The mass density, water content, and undrained shear strength were evaluated, and wave speeds were measured in a laboratory on cores obtained from boreholes by means of seismic velocity tests. Because soil samples are always more or less disturbed, their measurements

should be treated with caution. The advantage of laboratory tests is that the state of the test can be changed in order to simulate various conditions. This can be useful when evaluating material parameters at different strains.

Green-field measurements

Green-field measurements are advantageous over laboratory tests insofar as the ground material is not disturbed. Moreover, with green-field measurements, a large area can be covered with only one measurement setup. The latter is beneficial, because local effects, such as heterogeneities, are smeared out over a large volume. However, green-field measurements are disadvantageous insofar as the sought parameter itself is not measured. Rather, this parameter is derived from accurate empirical models.

Two different vibration sources (a sledge hammer and explosives) were used when the **surface wave seismic measurements** were carried out. The Multi-channel Analysis of Surface Waves (MASW) approach was employed for the evaluations, and the vertical velocity amplitudes were measured and recorded by geophones and seismographs, respectively. They were placed along straight lines. The obtained data was processed to obtain depth profiles of shear wave speeds. **Vertical Seismic Profiling (VSP) measurements** in cored boreholes were carried out in order to correlate these with the surface wave seismic data (obtained from MASW). A vertical shear and a pressure wave speed profile were obtained by using recording devices placed in the boreholes to record the seismic energy levels produced by vibration sources at the ground surface. **Resistivity measurements** were used to obtain plots of the resistivity distribution in the ground. Resistivity is a material property, indicating how strongly a given material opposes the flow of an electric current. To measure the resistivity, direct current (DC) was injected into the ground between two electrodes, and the voltage between two additional inner electrodes was measured to determine the electrical resistance of the material. This enables the resistivity to be evaluated. The resistivity is primarily useful for determining the location of various ground materials, such as those in the form of strata. The resistivity of different materials can differ considerably, yet different materials can also have the same resistivity. This is why additional reference drilling at the same location is needed in order to properly interpret the ground stratigraphy along the measured line. In **Falling Weight Deflectometer (FWD) tests**, a weight is dropped on the ground surface, creating an impulse load. The peak force amplitude and the frequency content of the load can be adjusted (see Figure 4.8 for the FWD test setup). Geophones were used to measure velocity, along with accelerometers to measure acceleration, and these were distributed along a straight line from the location of the FWD. The tests were used to correlate measurements with the results from numerical simulations, and to provide information concerning the attenuation properties of the ground.

Evaluation of material parameters

The mass density was evaluated mainly through soil sampling. The elastic modulus was determined from the wave speeds obtained either from soil samples or from correlations between

(a) The FWD machine that generates an impulse load.

(b) The seismic measurement station.

Figure 4.8: *Photographs of the FWD test setup at the Max IV site [46].*

the results of numerical simulations and of FWD tests, or on the basis of relationships between VSP measurements and to surface seismic data. Relating the speed of the pressure wave and of the shear wave enables Poisson's ratio to be determined. The damping (energy loss) was estimated by a combinations of several methods involving measurements on cores from bore-holes, studies of the decay of surface wave seismic measurements and of FWD tests, as well as by calibrating the results of numerical simulations such that they were consistent with the measurement data.

The aforementioned methods were used to determine the uncertainty interval of each parameter. In order to appropriately estimate each parameter used for the numerical simulations, the simulation results must be calibrated to the measurement data.

4.3.2 Materials

Ground materials

The ground materials considered in the thesis are those found at the Max IV site. Owing to its large area, around $300,000$ m^2, soil properties were found to vary throughout the site. The soil layer has a depth of 14 to 16 m and mainly consists of two layers of different clay tills, the softer layer covering the stiffer one. The bedrock consists mainly of sandstone and shale [46, 47]. The material parameters for each of the ground materials, evaluated from measurements and simulations, used in the thesis are found in Table 4.1.

Clay tills can vary considerably in their composition. This can range from a high propor-

Table 4.1: Ground-material parameters used in the thesis.

Material Parameter	Upper clay layer	Lower clay layer	Bedrock
Mass density (kg/m^3)	2100–2125	2100–2125	2500–2600
Elastic modulus (MPa)	378–500	1136–2000	8809–10,000
Poisson ratio	0.48	0.48	0.40
Loss factor	0.07–0.14	0.06–0.14	0.04

Figure 4.9: Photograph of the soil at the excavation site for the Linac tunnel [48].

tion of stones and boulders to clay tills comprised almost entirely of clay. Tills are thus a highly unsorted and coarsely graded type of soil, with highly varying properties. Therefore, the elastic modulus can vary extensively. The density of clay tills is normally between 2000 and 2200 kg/m^3. Clay tills are usually water-saturated and have low hydraulic conductively. Since water is close to incompressible, the Poisson ratio of a clay till is often near 0.5. Over-consolidated clay tills typically show an elastic response to loads of low magnitude. The soil types that cover the bedrock at the Max IV site are for the most part over-consolidated Low Baltic Clay Till and the Northeast Clay Till. Figure 4.9 shows a photograph of the soil at the excavation site for the Linac tunnel.

In principle, the formation of sedimentary rocks such as sandstone and shale begins as sediment particles on the ocean bottom. These become packed and undergo biochemical processes of various types over thousands of years. Consequently, they are transformed into hard formations in the form of sedimentary rocks. Sandstone is medium-grained, consisting mainly of sand-sized minerals such as quartz and feldspar. These are the most common minerals in the earth's crust. Sandstone is commonly yellow, red, grey, or brown. The properties of sandstone can differ, however, depending on how it was formed. Shale is fine-grained, typically comprised of variable amounts of clay minerals and grains of quartz. Shale is usually grey. If the clay in it is dominant, the shale is denoted as clay shale, which is characterised by its thin lamina structure or parallel layering.

Table 4.2: *Building material parameters used in the thesis.*

| Material Parameter	Concrete	Steel	Elastomer
Mass density (kg/m^3)	2400	7900	1000
Elastic modulus (MPa)	35,000	200,000	1
Poisson ratio	0.2	0.30	0.45
Loss factor	0.04	0.02	0.1

Building materials

The building materials employed in the studies in the thesis are described here. The main Max IV building is in general constructed by concrete and steel. The material parameters of each of the materials are provided in Table 4.2.

Concrete is a composite material that mainly consists of cement, sand, aggregate, and water. The water reacts with the cement, hardening the concrete. Different admixtures result in concrete with various properties. Hardened concrete has a density of approximately 2400 kg/m^3, approximately 2500 kg/m^3 when adding the reinforcing bars, a Poisson's ratio of around 0.2 and an elastic modulus typically in the range of 30–40 GPa.

Steel has high tensile strength, ductile failure behaviour and it can most often be modelled as isotropic and homogeneous. Steels are alloys of iron and other elements. The material parameters used in the thesis (see Table 4.2) do not change significantly among different types of steel commonly used for construction. However, the strength, corrosion resistance, and weldability can vary appreciably. There are standards that define different classes of steel. The steel components analysed in the thesis (a pipe system and its supports) were assumed to be made from stainless steel, type EN 1.4432 (European standard) or ASTM 316L (American standard).

4.3.3 Damping

Damping ratios applied to various types of ground materials and structures depend on the type of material, the type and number of connections and joints, and the load magnitude. In the case of vibrations due to human activity, such as road traffic and pedestrians, the strains are at a level where hysteric (frequency-independent) damping can be assumed. The damping ratio for a concrete structure is usually in the range 2–5%, where lower values corresponds to a well-reinforced concrete structure with few joints and slight cracking. By contrast, the damping ratio for a steel structure is usually in the range 2–7%, where lower values correspond to a structure with welded joints [21]. The damping ratio of ground materials can be anywhere from approximately 2% for bedrock to approximately 10% for soft soil, given small strains.
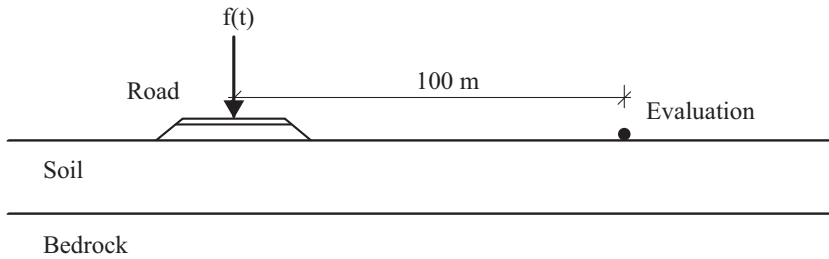
Figure 4.10: *Model of road, soil and bedrock. The soil layer is 14 m thick. The displacements were evaluated on the ground surface, 100 m from the excitation.*

At the Max IV site, the topography of both the soil and the bedrock is somewhat irregular, meaning that the horizontal layering used in FE models is merely a simplification. To appropriately take both this simplification and the heterogeneity that exists into consideration, the applied loss factor must be calibrated. Traffic-induced ground vibrations are strongly affected by the loss factor employed. To exemplify the effect of varying the loss factor on the ground vibration levels at the Max IV site, a plane strain FE model (cf. Figure 4.10) was used, employing material parameters typical for the site. The loss factor for the soil was varied between 0.05 and 0.20, whereas the other material parameters were kept constant. Figure 4.11 shows the effects of variations in the loss factor on the displacement response to a harmonic load. As
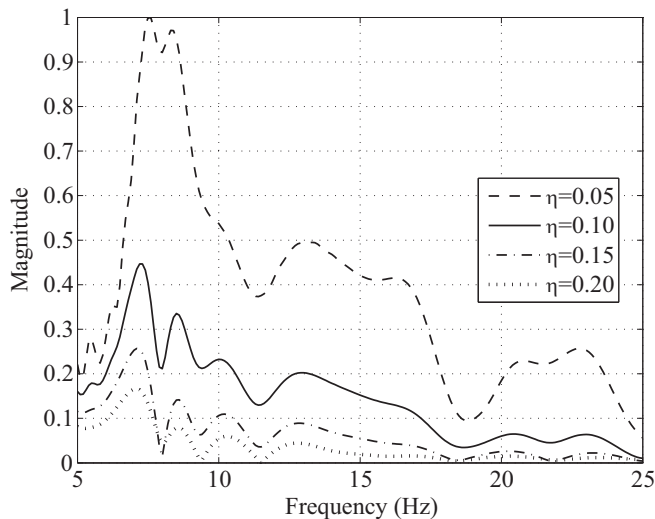
Figure 4.11: *Complex magnitude of vertical displacements versus frequency, for different loss factors of the soil. The loss factor for the bedrock was kept constant. The amplitudes were normalised with respect to the highest amplitude.*

can be seen in the figure, the value of the loss factor has a major impact on the displacement amplitude.

4.3.4 Vibration phenomena

Dispersion

Since the ground waves considered in the thesis are non-dispersive, the waves propagate at the same velocity, regardless of its frequency, in the case of an isotropic homogeneous ground medium. In practice, however, the ground is rarely isotropic homogeneous. Stratification is often present in terms of a layered soil profile and/or the presence of bedrock. Consequently, the different layers have different stiffness, and hence different wave speeds. Thus, in the layers with higher wave speeds, the wavelengths are longer than those in the softer layers with lower wave speeds, given the same frequency. This phenomenon is called dispersion. In a steady-state analysis, wave propagation can be observed for one single frequency where the shape of the wavefront changes with the phase.

Reflection and refraction

A wavefront incident to an interface between two ground layers with different material parameters experiences reflection and refraction. The waves that propagate back are *reflected*, and the waves that continue to other layers are *refracted*. In the special case of a free boundary, the waves are obviously not refracted. The direction and amplitude of the reflected and refracted waves depends in the impedance of the two adjacent layers. The impedance is in turn defined as the wave speed multiplied by the density ($Z = c\rho$).

Long distances

In the detailed investigation of various effects at long distances between the vibration source and the receiver presented in the appended Paper A, it was the vibrations can be higher in the bedrock than in the soil. In order to exemplify those effects, results from numerical calculations are visualised in Figure 4.12. The FE model employed, which involves axisymmetric conditions, was analysed in the frequency domain using a harmonic vertical unit point load. The geometry was $1000{\times}216$ m^2, involving a 16 m deep soil layer and the use of non-reflecting boundaries. The material parameters employed were typical for clay tills and sedimentary bedrock in southern Sweden. As can be seen in Figure 4.12 (lower plot) at a frequency of 12.5 Hz and at a distance of 300 m or more from the excitation point, the vertical displacement amplitudes were higher in the bedrock than in the soil. However, this was not the case at a frequency of 7.2 Hz (upper plot). Moreover, the differences in wavelength between waves in the soil and in the bedrock are clearly shown in the figure.

Another example of the effects of varying the distance between the excitation and the evaluation

16 m

16 m

300 m

700 m
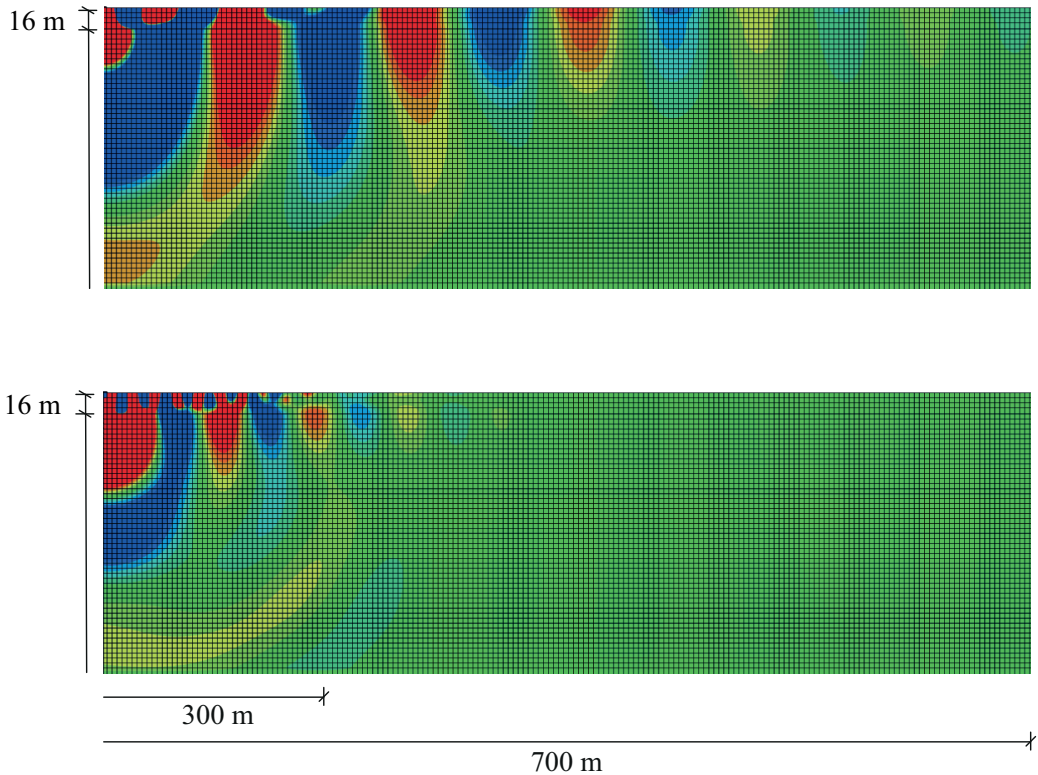
Figure 4.12: Visualisation of the vertical displacements occurring at 7.2 Hz (upper plot) and at 12.5 Hz (lower plot). The horizontal dimensions indicate the distance to the excitation point.

points can be seen in the measurements carried out at the motorway that runs adjacent to the Max IV site as discussed in Section 4.2 and shown in Figure 4.3. As can be seen in Figure 4.13, by comparing the response in (a) with that in (b), the high frequency content found at the top of the embankment was already considerably attenuated at 40 m from the motorway.

The effectiveness of a wave obstacle, such as a barrier or a shaped landscape, in terms of reducing incident ground vibrations is also affected by the distance from the load to the area where the vibration amplitudes are of interest. In Figure 4.14, vertical displacement amplitudes are shown in two separate plots: with and without considering an open barrier (i.e. a trench) in the axisymmetric FE model described above. Figure 4.14(a) concerns responses 95 m from the excitation point, whereas Figure 4.14(b) concerns responses 300 m from the excitation point. Indeed, the trench is significantly less effective at a distance 300 m from the excitation point than it is at a distance of 95 m. Figure 4.15 reveals that higher frequencies are reduced to a greater extent 300 m from the excitation point than they are at 95 m. The same tendencies and phenomena as those for vertical displacements apply to horizontal displacements.
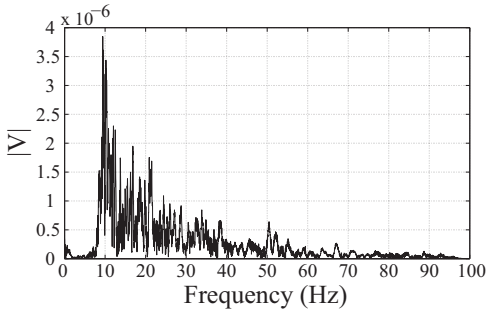
(a) Measurements made at the top of the motorway embankment.
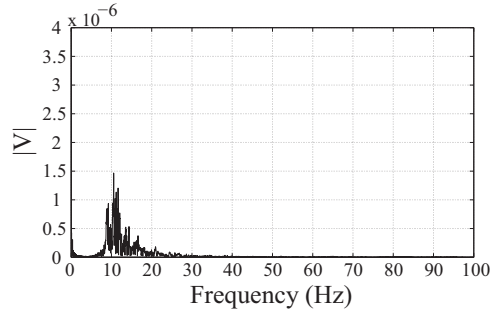
(b) Measurements made 40 m from the motorway.

Figure 4.13: *FFT of the time signal at different distances from the E22 motorway.*
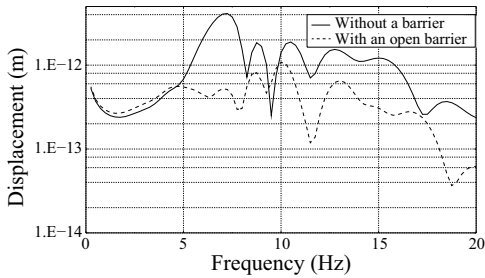
(a) Evaluated 95 m from the excitation point.
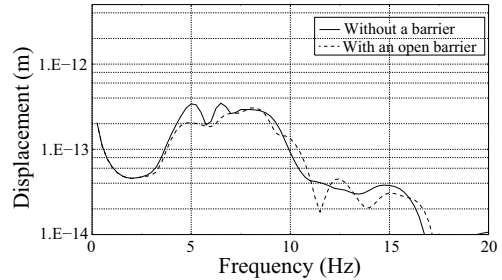
(b) Evaluated 300 m from the excitation point.

Figure 4.14: *Vertical displacement amplitudes versus frequency, with and without considering the FE model of a trench located 60 m from the excitation point.*

Either the vertical or the horizontal components of ground vibrations can generate the highest amplitudes. Which of two is dominant depends in part on their distance from the excitation point. This is exemplified by analysing the vertical and the horizontal displacement amplitudes at the Max IV site. As can be seen in Figure 4.15(a), the vertical and the horizontal responses of the ground surface at a distance of 95 m from the excitation point are somewhat similar in terms of the calculated peak displacement amplitudes obtained from the FE analyses. In Figure 4.15(b), however, at a distance of 300 m from the excitation point, the peak amplitude is nearly twice as high for the horizontal response as it is for the vertical response. For vibrations in buildings, it is often the vertical component that is most critical, because a slab is more stiff in the in-plane direction than in the vertical direction. In high-rise structures, the horizontal component is, however, of interest since it excites the swaying mode of the building.
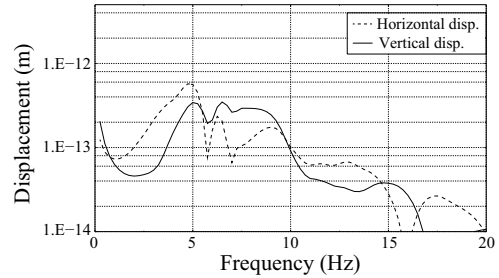
(a) Evaluated 95 m from the excitation point.   *(b) Evaluated 300 m from the excitation point.*

Figure 4.15: *Displacement amplitudes versus frequency for vertical and the horizontal responses.*

4.4 NUMERICAL MODELLING

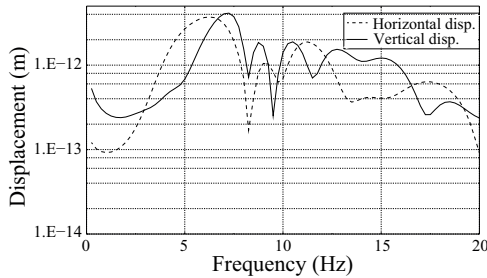There are several reasons why numerical models might be preferred over experimental models in studies, especially concerning large structures and soil-structure interaction. It is often less expensive to conduct numerical investigations and in some cases it is simply not possible the study something experimentally, for example, accidental loads according to building codes. Moreover, in the case of studying the effect of different design solutions, such as vibration-reduction measures, the cost can be very high for construction of mock-ups.

4.4.1 Finite element analysis

FE analyses can be carried out in the time domain or in the frequency domain. The simulation time of steady-state analyses is, in practice, linearly dependent on the number of frequency steps taken. Thus, a frequency range of interest must be determined, along with the resolution in frequency. Because the result at one frequency is not dependent on the result at another frequency, it is possible to divide the frequencies of interest into several ranges and run analyses in parallel on several computers. The simulation time for transient analyses depends on the number of time steps. Therefore, the size of the time steps must be investigated, as well as the total time. Even though the transient analyses can be unconditionally stable, sufficiently small time steps are needed in order to accurately describe the load and to get the sought resolution in the output.

In general, the finer the mesh employed (i.e. the larger the number of dofs), the more accurate the solution becomes. Often the memory capacity or simulation time limits how many dofs can be used. However, it is important to use as many nodes as are needed to describe the geometry sufficiently. In wave propagation problems, a sufficient number of nodes must be used in order to describe the waveforms. Therefore, steady-state analyses involving soft materials (i.e. short wavelengths) and high frequencies results in a dense mesh. It should also be noted that

short wavelengths require, in general, a more detailed representation of the geometry. In the analyses presented in the thesis, at least six to nine nodes to resolve the shortest wavelength were needed for the ground materials. In the FE models applied in this thesis, it was seen that solid, or acoustic for fluids, hexahedral elements obtained by quadratic approximation were preferable to avoid spurious zero energy modes easily developed din large meshes, e.g. soil, where no displacements are prescribed on the boundary. In special cases, certain assumptions can be made about the stress state in order to use structural elements such as beam and shell elements. The latter was used for the pipes analysed in Chapter 6 and in Paper D.

In all appended papers, the FE software package Abaqus [39] was used, and in the appended Paper B, the FE software package HyperWorks [49] was also used.

High-performance computing

Most of the FE calculations presented in this thesis were run on high-performance clusters at Lunarc, the computing centre at Lund University [50]. Since 1986, Lunarc has provided computational resources within all aspects of computational science for Lund University. Moreover, since 2003, Lunarc has provided resources to the whole of Sweden, as part of the Swedish National Infrastructure for Computing (SNIC). The systems Platon and Alarik where used for the simulations. Platon comprised 216 nodes, containing two 64-bit quadcore Intel Xeon E5520 (2.26 GHz) processors, corresponding to a total of 1728 processors. Alarik comprised 208 nodes, containing two 64-bit 8-core AMD6220 (3.0 GHz) processors, corresponding to a total of 3328 processors.

4.4.2 Model calibration

In order to develop numerical models that will produce accurate results, several tasks may be needed. The use and purpose of the numerical model are important to determine initially. This sets the general framework for the calibration process. The quantities to be simulated and measured (e.g. accelerations) must be specified, as well as the type of measure that should be used for calibrating the numerical model to measured data. An example would be to minimise the difference in maximum amplitudes or in RMS values between the measured data and the simulation results. Prior to the development of the numerical model, measurements (geotechnical and geophysical) can be made to determine the stratification and valid intervals for each material parameter. Furthermore, vibration measurements concerning a known load, such as FWD tests, can be used to calibrate the results of the numerical model. In developing a numerical model, one of the first steps is to determine the conceptual behaviour of the model. This involves considering the simulated vibration phenomena, the assumptions regarding material models, the physical domains to be modelled, their interactions and the governing load cases. In establishing the numerical model, decisions must be made regarding discretisation in terms of element types and sizes, the type of analysis (frequency or time domain), and the size of the steps in frequency or time. These decisions pertain to the accuracy of the numerical model.

Numerical parametric studies can be used to obtain the parameters that significantly affect the output, given the uncertainty interval of each parameter obtained from the measurements. Thereafter, the parameters with the most influence on the quantity are used for calibration. Details regarding these matters can be found in [51, 52].

In the analyses involving Max IV, agreement between the results of the numerical simulations and the measurements was achieved by carrying out FE calculations and calibrating these to the measurements. See the appended Paper C for such a model calibration. The FWD tests were used for this comparison since the load involved in the FWD tests was known. These tests were used in conjunction with the FE models, by making use of an iterative process in which each of the material properties (viz. the mass density, the elastic modulus, the Poisson ratio, and the loss factor) was varied within the uncertainty interval obtained from the measurements. Thus, the sensitivity of the simulation results to the material properties involved can be analysed and the best estimate of each of the parameters to be used in numerical simulations can be determined. This was done for the elastic modulus and for the loss factor in particular, since these were found to have the strongest effect on the response at the ground surface given the intervals obtained from the measurements.

5 Vibration-reduction measures

In reducing vibrations affecting either humans or machines, several vibration-reduction measures can be used. In general, these measures can be divided into three types: reduction measures at the source; reduction measures in the medium; and reduction measures at the receiver. Measures at the source include, for example: soil stabilisation [53]; wave-impeding blocks [54] under a track or road; floating slabs on springs and dampers; reducing the speed of the vehicles/trains; a new layer of smooth asphalt; and rail grinding [1]. Reduction measures in the medium and at the receiver are hereafter divided into the following three groups: reducing the incident ground vibrations already in the propagating medium with a wave obstacle, reducing them with measures applied to the building's foundation, and vibration reduction by means of measures within the building itself.

5.1 WAVE OBSTACLES

Most of the vibration energy that originates from excitation on the ground surface propagating in an homogeneous soil is carried by Rayleigh surface waves that propagate close to the ground surface. It is, therefore, possible to reduce the level of the ground vibrations by placing a suitable obstacle in the ground, at the surface, between the source and the receiver. A wave obstacle is designed to reduce externally excited ground vibrations propagating towards a building by reflecting and refracting the waves. Effective wave obstacles include sheet-pile walls and rows of piles [55, 56]. In this section, discussions regarding wave barriers and shaped landscapes are presented.

5.1.1 Barrier

A literature study and a detailed investigation of wave barriers in the form of trenches, solid barriers, and water-infiltrated trenches are presented in the appended Paper A. Installing a barrier in the ground between a vibration source, e.g. a motorway, and the receiver, e.g. a building, engenders discontinuity in the propagating waves. Waves that are incident to a barrier give
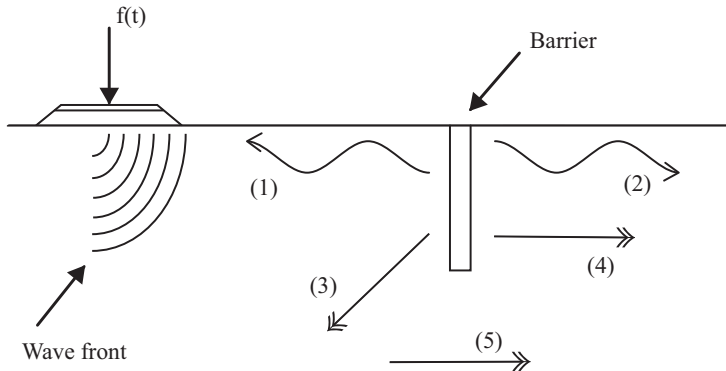
*Figure 5.1: Impinging waves, reflected and transmitted at a barrier.*

rise to different types of waves. These can be divided into five separate groups, see Figure 5.1: (1) Rayleigh waves reflected back by the barrier; (2) Rayleigh waves transmitted through the barrier; (3) body waves from the barrier propagating downwards and back towards the wave source; (4) body waves from the barrier propagating away from the wave source; and (5) waves propagating through the soil and bedrock under the barrier. Ground vibrations after the barrier has been passed are caused by (2) transmitted Rayleigh waves, (4) body waves propagating to the right of the barrier, and (5) waves propagating in the soil and bedrock under the barrier.

The impedance mismatch, which is the controlling parameter for the effectiveness of a barrier, depends on the wave velocity and the mass density. Considering practically feasible material parameters, the mass density of the solid filling the material has little effect. Thus, the wave velocity is the important parameter. The wave velocity, however, can be described by the elastic modulus and the Poisson ratio. Moreover, because the Poisson ratio does not has a marked influence within practical values, the elastic (or shear) modulus is sufficient for determining the effectiveness of a solid barrier material. The infiltration of water and the draining of water in a trench can strongly affect the reduction in the vibration level resulting from the presence of a trench. The effectiveness of a trench decreases when any large amount of infiltrated water is present, since water transmits P-waves.

In the example case of Max IV, which is used in the appended Paper A, it was seen that at long distances of 500–700 m and farther from the vibration source, various phenomena occur that are not seen at shorter distances. At those long distances, the vibration reduction achieved by a trench was markedly decreased. For a certain frequency range, amplification of the ground-surface amplitudes was seen for distances of around 600 m or farther. Moreover, at distances of around 700 m and farther, the vertical displacements of the ground surface follow the vertical displacements of the bedrock.

5.1.2 Shaped landscape

A literature study and a detailed investigation of the effects of using a shaped landscape as a wave obstacle are presented in the appended Paper B. At large construction sites, considerable amounts of soil are usually excavated in order to level the ground surface. This is necessary since, generally speaking, the surface needs to be horizontal prior to the construction. Moreover, the loose topsoil must be removed. A large amount of excavated soil is often transported away from the construction site, a matter which can be costly for the construction project. Alternatively, these soil masses can serve a useful purpose at the construction site. They can be retained and be used to construct a shaped landscape with hills and valleys, or whatever characterises it. A shaped landscape can serve to reduce ground vibrations incident to a facility. Moreover, this can be an aesthetically desirable solution, see Figure 4.1 for an example of a shaped landscape. Constructing a shaped landscape as a wave obstacle located between a vibration source and the receiver engenders discontinuity in the propagating surface waves through the irregular topography of the landscape. Waves that are incident to the shaped landscape behave differently, with changes in the direction of the propagating waves. The waves are subjected to both reflection and diffraction at the irregular ground surface of the shaped landscape. Each of these two phenomena scatters the wave front, thus reducing the level of vibration at the facility.
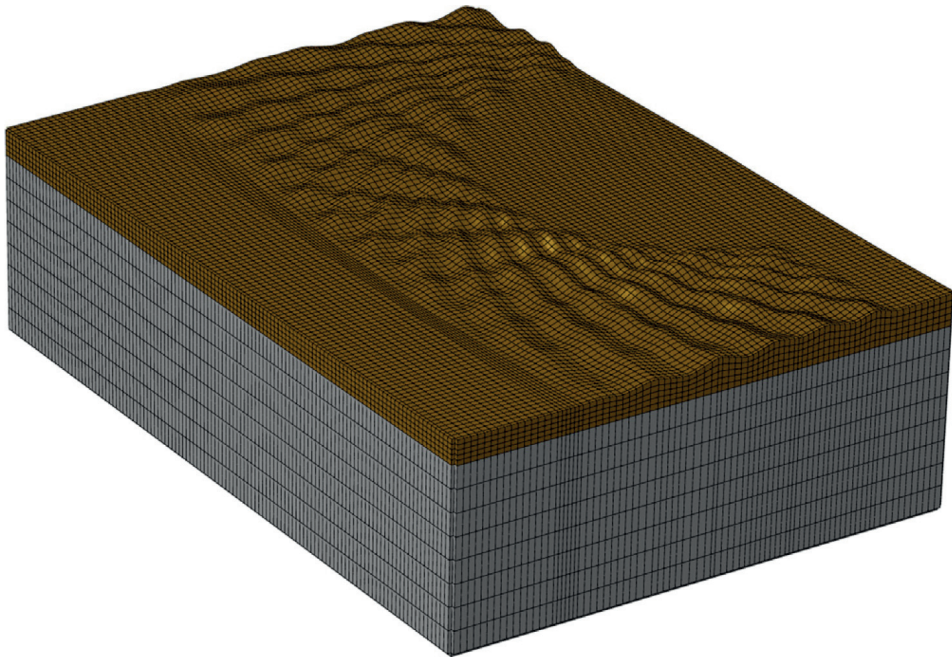
Figure 5.2: *FE mesh for an architectural design of a shaped landscape.*

Concerning the example case of Max IV, which is used in the appended Paper B, the most effective type of pattern used as a shaped landscape was one consisting of alternating hills and valleys. The least effective pattern, which results in an amplification of the vibration level, was one consisting only of valleys. Moreover, different patterns of hills and valley can either result in an appreciable reduction or a marked amplification. A pattern such as the one shown in Figure 5.2 can be used effectively as a vibration-reduction measure.

5.2 FOUNDATION IMPROVEMENT

Rather than reducing incident ground vibrations with wave obstacles, modifications to the building's foundation can be employed. Elastic foundations can be used where the building is placed on springs and dampers [57]. Here, the idea is that the system should have a fundamental frequency well below the frequencies that are to be reduced. Slabs can also be supported on piles or pillars. This section discusses vibration reduction by modifying concrete slabs on soil and by stabilising the soil underneath it. A detailed investigation into these measures (including the results presented below) is provided in the appended Paper C.

5.2.1 Concrete slab

By improving the properties of a concrete slab on soil, vibration reduction can be obtained. In Figure 5.3, a model of a concrete slab on soil involving external and internal loads is shown. There are several ways to improve slabs in terms of vibration reduction: increasing the thickness of the slab; using a type of concrete with a high elastic modulus; and introducing a slit in order to isolate parts. The benefits from increasing the thickness of a concrete slab over increasing the elastic modulus of the concrete relate to the bending stiffness of the slab. Indeed, it is more effective to increase the thickness of the slab. Slitting the slab entails isolating a part of the slab. For short wavelengths, i.e. at high frequencies, this is beneficial. However, the vibration levels on a slab with direct excitation can be amplified. The reduction obtained by increasing
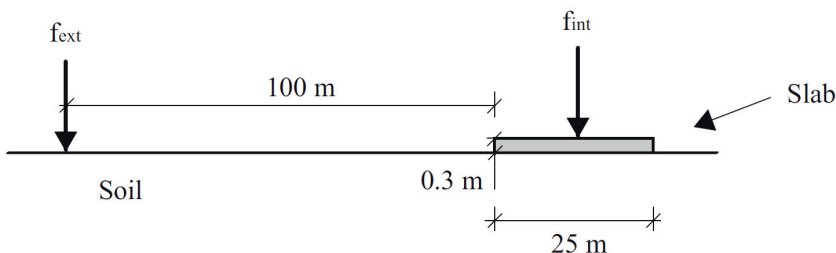
Figure 5.3: Model of a concrete slab on soil. The slab is coloured in grey.

<table>
<tr><td>*(a) Spreading out binder material.*</td><td>*(b) Mixing binder with the original soil.*</td></tr>
</table>

Figure 5.4: *Photographs of the soil-stabilisation process at Max IV [48].*

the thickness or the elastic modulus also depends on the occurring wavelengths in relation to the size of the slab.

5.2.2 Soil stabilisation

The effect from increasing the thickness of a concrete slab on soil motivates the use of soil stabilisation under the slab in order to reduce vibrations in a building. Soil stabilisation involves mixing the soil with a binder in order to increase its stiffness. The procedure is as follows: (i) the soil is dug up down to the desired depth; (ii) a layer of the original soil is spread; (iii) a layer of binder is then spread, see Figure 5.4a; (iv) the original soil is mixed with the binder, see Figure 5.4b; (v) the mixed soil is packed; and (vi) the procedure is repeated from step (ii) until the required thickness of the stabilised soil is achieved. At Max IV, the soil underneath the slab was stabilised to a depth of 4 m. Figure 5.5 shows a model of a concrete slab on stabilised soil with external and internal loads.

For a slab on soil, the reduction obtained by soil stabilisation strongly depends on the Rayleigh
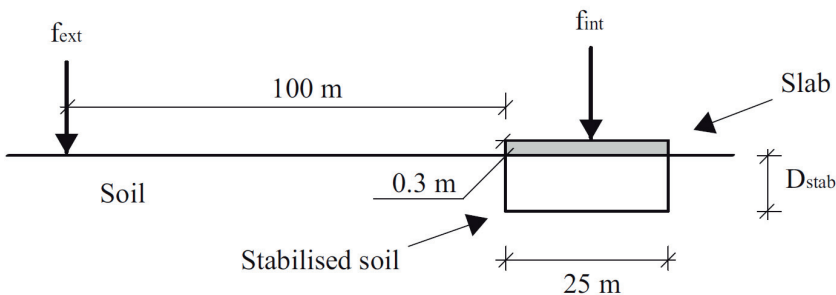

Figure 5.5: *Model of a concrete slab on stabilised soil. The slab is coloured in grey.*

wavelengths that are present. Resonant behaviour can occur for certain wavelengths, thereby amplifying vibration levels. Hence, it is important to use a model that simulates the correct wavelengths, in order to predict the vibration reduction. If vibrations originate from an externally located vibration source, the width of the foundation (i.e. the width of slab and stabilised soil) affects the vibration levels. The most effective way to reduce vibrations is to design a foundation with a width that is 2–4 times the dominant Rayleigh wavelength. The elastic modulus of the stabilised soil significantly affects the obtained reduction for both external and internal loadings. The maximum reduction for external loads increases with the elastic modulus. Increasing the elastic modulus is advantageous for internal loads, independently of frequency. Soil stabilisation is generally more effective the deeper it is. Because soil stabilisation can cause resonant behaviour, however, its design must be evaluated by employing numerical models calibrated to measurements that capture these phenomena. Soil stabilisation is an effective vibration-reduction measure for commonly occurring external and internal sources, such as motorway traffic and indoor pedestrians.

5.3 MEASURES WITHIN BUILDINGS

In order to reduce vibrations by adopting measures within the building several actions can be taken, including: thicker slabs, larger cross-sections, shorter spans, and more rigid connections. To study the vibrations transmitted from internal sources and to suggest vibration-reduction measures, accurate, time-efficient numerical models can be employed. The appended Paper D proposes a numerical procedure for reducing large 3D numerical models of complex vibrating water-pipe systems. The FE model employed includes a water-pipe system, and considers the fluid-structure interaction. To facilitate time-efficient dynamic analyses, reduced order modelling was employed in terms of CMS involving interface reduction. The time-efficiency and accuracy of the proposed model order reduction was demonstrated, using a full FE model as a reference. The following subsection presents an example of a structural measure that can be applied within a building, namely changing the location of the steel supports. The effects on the vibrations transmitted from a vibrating water-pipe system are analysed with the numerical procedure proposed in Paper D.

5.3.1 Pipe supports – example

The effect from the vibrations transmitted from a water-pipe system to adjacent parts of the building was studied. Only dynamic forces were accounted for. Thus, design criteria imposed by static conditions were neglected. Max IV was used as an example case in the investigation. A substructure for the water-pipe system was developed according to the procedure developed in the appended Paper D, involving six retained condensation nodes and 54 retained eigenmodes. The reduced model introduced an average error of less than 2%, compared to the full 3D model.
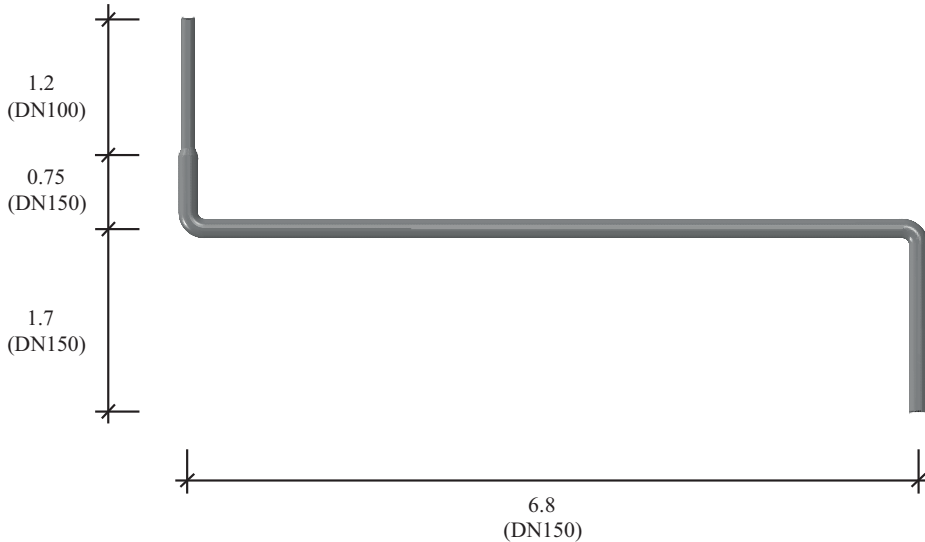
Figure 5.6: Modelled pipe system. The dimensions are in units of meters.

FE model

A water-pipe system constituted of two different pipe cross-sections, DN100 and DN150, that mimics those located in the Max IV facility was used as an example case, see Figure 5.6. A 3D FE model was developed with the use of the FE software package, Abaqus 6.12. The model comprised pipes, the water contained in them, the pipe supports, a concrete tunnel and two layers of soil, see Figure 5.7. The soil consisted of two different clay tills, identified as the Low Baltic clay till (12 m) and the stiffer North-east clay till (4 m). The outer dimensions of the cross-section of the concrete tunnel were 10×4.1 m^2 with a wall thickness of 0.3 m. Each of the pipe supports had a length of 0.2 m and a squared cross-section with a side length of 0.02 m. In parametric FE simulations, it was observed that the bedrock can be excluded from numerical analyses when investigating vibrations stemming from a water-pipe system to the concrete tunnel or the ground surface, without affecting the results to any appreciable extent. Solid 20-node elements with quadratic approximation, using reduced integration, were employed for the supports, the concrete tunnel and the soil. To model the water, 20-node quadratic acoustic pressure elements were used, whereas quadratic 8-node shell elements were employed to model the pipes. In order to simulate the far-field conditions, and to avoid reflecting boundaries, 12-node quadratic one-way infinite elements generating viscous absorbing boundaries were employed.

The materials involved were modelled as isotropic homogeneous materials and linear elasticity was assumed. The ground-material parameters employed were those evaluated as described in Section 4.3.1, see Table 5.1. The water in the pipes was assumed to be inviscid, irrotational, and compressible, and to undergo only small pressure changes. Thus, the water was modelled
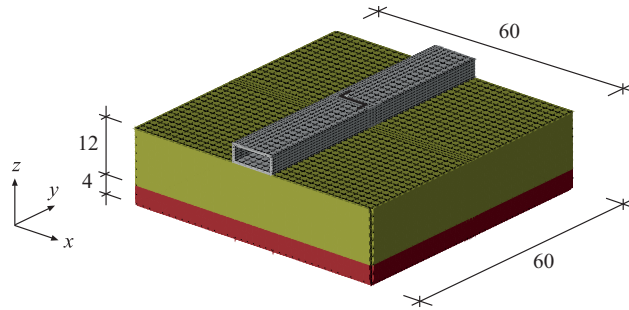
(a) The two soil layers are shown in green and red, and the concrete tunnel is shown in grey.
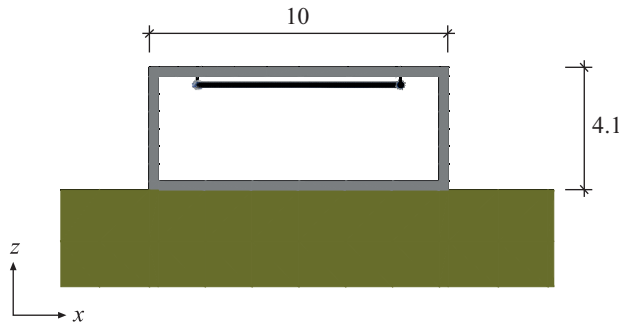
(b) Front view magnifying the pipes, which are shown in black.

Figure 5.7: *The FE model. The dimensions are in units of meters.*

Table 5.1: *Properties of the solid materials employed in the model.*

Property	Steel	Concrete	Low Baltic clay till	North-east clay till
Elastic modulus (MPa)	200,000	40,000	378	1136
Loss factor	0.02	0.04	0.10	0.10
Mass density (kg/m³)	7800	2400	2125	2125
Poisson ratio	0.30	0.25	0.48	0.48

as an acoustic fluid and was investigated by means of FSI analysis. To model the water, 8-node bi-quadratic acoustic pressure elements were employed. The water was assumed to have a temperature of $10\,^{\circ}$C, with its static density, ρ_0, set to 1000 kg/m^3 and the speed of sound, c_0, to 1450 m/s. The bulk modulus, K, was thus 2.10 GPa.

Parametric studies

The effect from changing the location of the supports on the transmitted vibration levels was investigated by steady-state analysis. The frequency range was limited to 5–30 Hz, and a unit of acoustic pressure was applied at the free end of the DN100 pipe section. The displacements
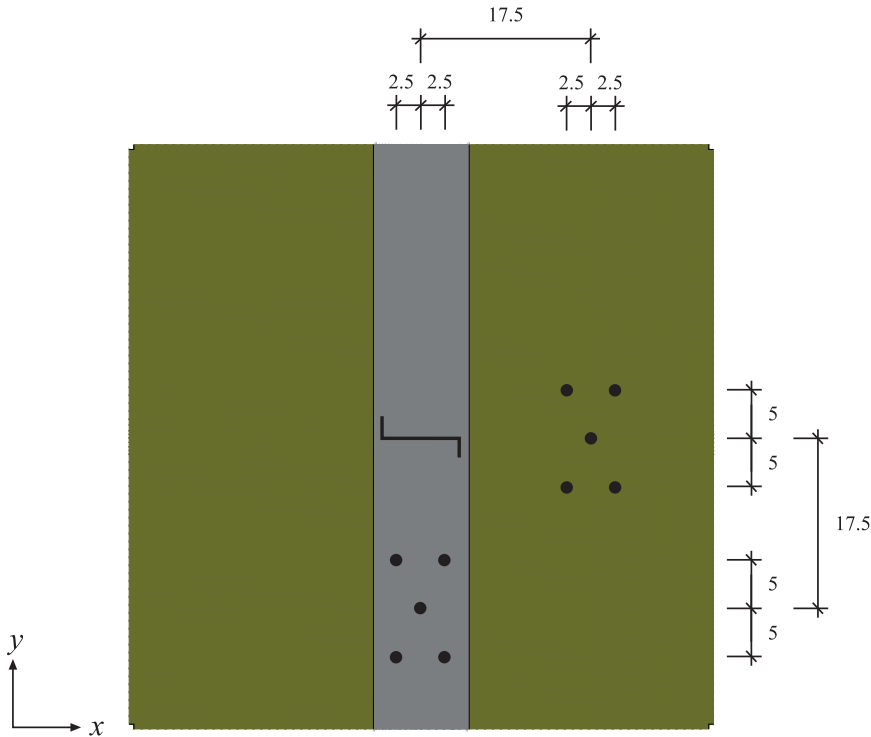
Figure 5.8: *Top view of the FE model. Evaluation points are shown as black dots and the pipe-section as black lines located in the centre of the figure. The dimensions are in units of meters.*

were obtained at two different evaluation point patterns: 'ground surface' and 'tunnel floor', see Figure 5.8. An RMS value (cf. Equation 3.87) for the displacements at the five evaluation points in each pattern was calculated at each frequency step, generating a response spectrum for each evaluation point pattern. Four different types of support setups were investigated, viz. Types A–D in Figure 5.9, where Type A was considered as the reference setup. Because six condensation nodes were retained in the substructure generation, one at each possible location of a support, it was possible to use the same substructure throughout the parametric studies.

Results and discussion

In Figure 5.10, the displacement magnitudes are shown for the two different evaluation point patterns. Table 5.2 and Table 5.3 show by evaluation on the ground surface and the tunnel floor, respectively, the mean value of the RMS spectra and the reduction in the RMS value of the vibration levels for the different setups in relation to the reference setup. By comparing the frequency response for the different types (A–D) in Figure 5.10, it is clear that displacement peaks can be shifted in frequency by changing the location of the supports. In doing so, there is an appreciable difference in the frequency spectrum of the transmitted vibrations,

(a) Type A.

(b) Type B.

(c) Type C.
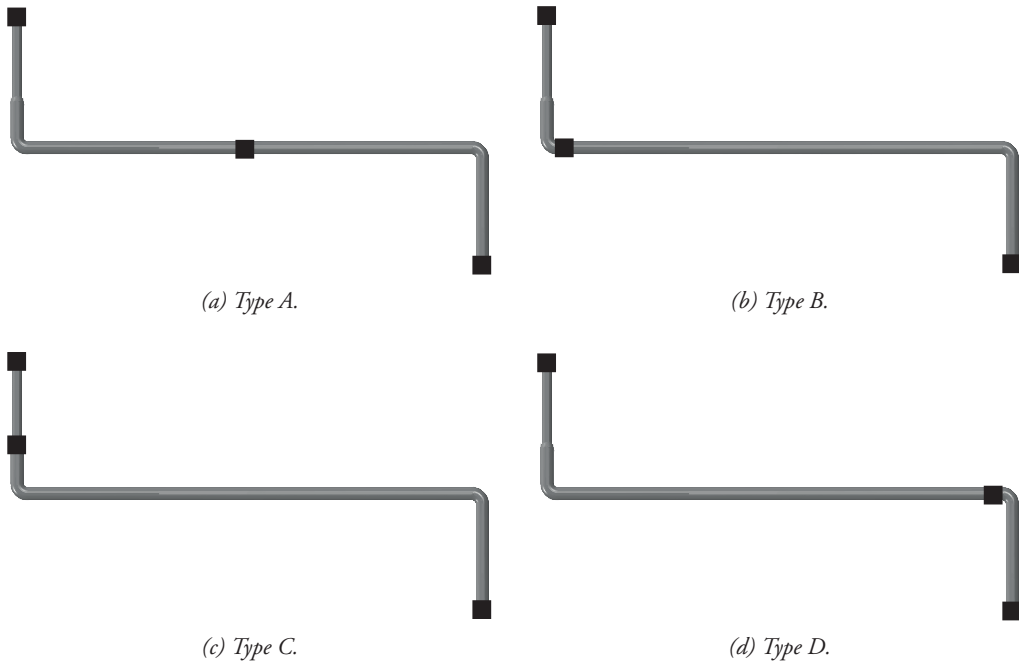
(d) Type D.

Figure 5.9: *Four different support setups (denoted Types A–D). The location of each of the supports is marked by a black square.*

Table 5.2: *Mean RMS values for the different support setups, evaluated on the ground surface, as well as the reduction in the mean RMS values relative to the mean RMS value of the reference setup (Type A).*

Set-up	Mean RMS value (10^{-9}m)	Reduction (%)
Type A	3.71	–
Type B	1.67	55
Type C	1.52	59
Type D	2.58	30

and to the RMS value of the displacements, see Tables 5.2 and 5.3. This shows that it is possible to design a water-pipe system such that the resonance frequencies of the soil can be avoided, thus preventing excessive vibration. Avoiding excitation of resonances is an important design parameter for vibration-sensitive buildings. Table 5.2, where Type A is considered as the reference type, shows that it is possible to achieve a reduction in the vibration level of the ground surface of approximately 60%. This is because the large peak at approximately 11 Hz found for Type A was completely avoided in Type C, and somewhat avoided in Types B and D. By considering the evaluation of displacements at the tunnel floor, a reduction of over 80% was achieved.

(a) Evaluated on the ground surface.   (b) Evaluated on the tunnel floor.
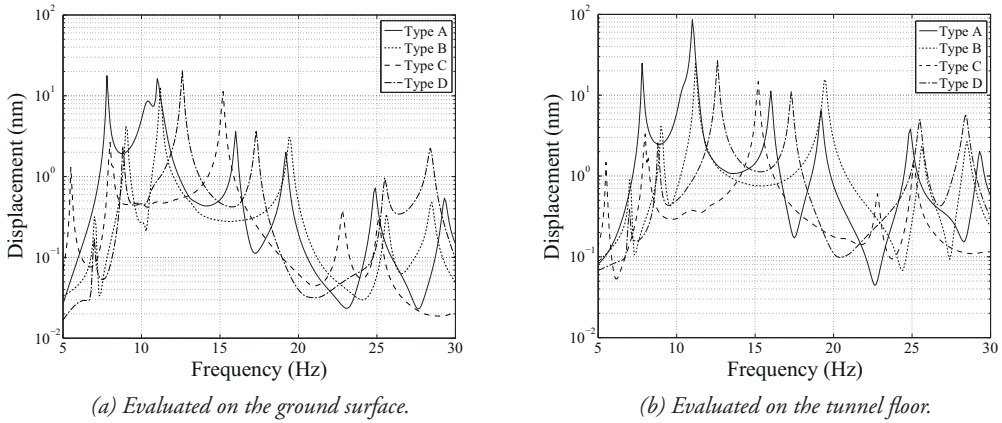
Figure 5.10: *Vertical displacement magnitudes versus frequency for different support setups.*

Table 5.3: *Mean RMS values for the different support setups, evaluated on the tunnel floor, as well as the reduction in the mean RMS values relative to the mean RMS value of the reference setup (Type A).*

Set-up	Mean RMS value (10^{-9} m)	Reduction (%)
Type A	11.3	–
Type B	3.92	65
Type C	1.97	83
Type D	3.91	65

6 Contributions and closing remarks

The main contributions of the research presented in the thesis to the research field are:

- Novelty research regarding analysis of fluid-structure interaction in water-infiltrated trenches. This enables conclusions to be drawn regarding how the effect of trenches in terms of reducing ground vibrations are affected by water infiltration, see the appended Paper A.

- Original investigation of how the effects of vibration reduction change at long distances from the wave barrier, as well as how the vibration propagation in the bedrock affects the vibration propagation in the soil, see the appended Paper A.

- Numerical study of a novel vibration-reduction measure using topographic irregularities of the ground surface, i.e. a shaped landscape, involving investigation of the effectiveness of different patterns of irregularities, see the appended Paper B.

- Innovative study of the effects of using stabilised soil as part of a building's foundation to reduce vibrations produced by external traffic loads and internal pedestrian loads, see the appended Paper C.

- Novelty work on developing a time-efficient numerical model used to study vibrations in liquid-filled pipe systems. The model includes model order reduction, based on component mode synthesis involving interface reduction, see the appended Paper D.

The research presented in this thesis contributes to fulfill the aim of reducing vibration levels in buildings, by using developed and investigated vibration-reduction measures to be used for the construction industry. In this thesis, the need to measure the properties of the ground with adequate accuracy was discussed, in an effort to develop numerical models. By using these numerical models, it is possible to study vibration phenomena and predict the effectiveness of vibration-reduction measures. Thus, the thesis increases the knowledge within the research field and eases the challenges faced by densification of cities.

Closing remarks regarding the prediction of vibrations and their reduction are provided below, along with proposals for future research.

6.1 PREDICTION

In this thesis a method is proposed to obtain the characteristics of a motorway traffic load. However, the method is not only valid when studying vibrations induced by traffic on motorways. It can also be applied to other traffic loads, by using the load spectrum of loads originating from trams and trains, for example. If a frequency spectrum cannot be obtained from measurements at the construction site, it should at least be based on measurements of a similar vibration source at a site with similar geotechnical conditions, since the measured frequency content is affected by the geotechnical conditions on-site.

The effectiveness of the vibration-reduction measures studied in the thesis was found to depend on the geotechnical conditions present at the construction site. For example, a solid barrier with a low elastic modulus was found to be less effective in soft soil than in stiff soil, since the impedance mismatch is greater. Regarding a shaped landscape, small irregularities in the surface in the form of small hills and valleys were found to be less effective at reducing vibrations in stiff soil, owing to the long wavelengths present there. The ability of stabilised soil underneath a concrete slab to reduce vibrations is mitigated when a resonance frequency is excited. It can thus be concluded that it is important to conduct proper measurements at the site in question to adequately evaluate the material parameters needed for the FE analyses. This is necessary in order for the analyses to provide accurate results. In order to obtain an accurate numerical model, it must be calibrated to measurement data. Measurement data are often given in terms of intervals for each of the material parameters. Then, simulations can be used to determine the best estimate within the intervals, to be used for numerical analyses.

The vibration-reduction measures can be evaluated by using the FE method, in order to avoid construction of expensive mock-ups. To be able to simulate large FE models involving several physical domains such as roads, soil, bedrock and building parts in a practical manner, it can be necessary to: reducing the number of dimensions; using viscous absorbing boundaries; or employing model order reduction to enable time-efficient dynamic analyses.

6.2 REDUCTION

The two types of wave obstacles that were investigated, viz. wave barriers and shaped landscapes were shown to achieve an appreciable reduction in the level of vibration. It is clearly difficult to construct a completely open barrier, i.e. a trench, without water infiltrating into it. Because the water level in a trench varies over the course of a year and depends on the groundwater level and the hydraulic conductivity of the soil, it is difficult to draw precise conclusions regarding the presence of water. Given the example case used in the thesis, both barriers and shaped landscapes,were found to achieve a possible reduction of approximately 35%. The vibration-reduction measures can thus be regarded as suitable when constructing buildings close to vibration sources. At long distances around 500 m and longer from a vibra-

tion source, however, an amplification in the vibration levels can be observed when a barrier is employed.

Vibrations from both external and internal sources can be reduced by modifying the properties of concrete slabs and of the soil underneath. The properties of the soil can be improved by mixing it with a binder, with the aim of stiffening the soil. By using stabilised soil underneath a concrete slab at he example case used in the thesis, vibrations originating from motorway traffic can be reduced by almost 60%, and up to 80% for an internal pedestrian load. It should be noted, however, that at some frequencies strong amplification in the vibration levels can occur when the load excites a resonance in the stabilised soil.

By using different locations for the supports of a water-pipe system, the vibrations transmitted into the building can be reduced. This reduction is achieved by avoiding excitation of resonances, resulting in a marked change to the characteristics of the vibrations. This approach results in a reduction of more than 60% for the employed example case.

6.3 PROPOSALS FOR FUTURE WORK

The conclusions draw are general and thus applicable to other example cases than the one used in the thesis. However, specific investigations in each new building project are needed, because the effectiveness of the vibration-reduction measures studied in the thesis was dependent on the ground material properties and the frequency content of the load. Hence, it is pertinent to investigate these measures in conjunction with other geotechnical conditions and loads.

In transient analyses that study how the wave propagation in the ground is affected by wave obstacles, it would be useful to study the flow of the wave energy. This can provide valuable information regarding the direction of the flowing energy. Consequently, this analysis can provide a better understanding of the vibration phenomena occurring and the effect of the vibration-reduction measure.

It is relevant to investigate the extent to which the obtained reduction in the level of vibration by a certain pattern of hills and valleys depends on the occurring Rayleigh wavelengths. It might also be useful to employ a model solely using homogeneous soil, in order to avoid vibration phenomena due to a layered soil profile or bedrock. In the study presented in the thesis, the same material parameters were used for the hills and the undisturbed soil. The hills would really be constructed of excavated soil and thus not having the same stiffness, for example, as the hills. It would be interesting to study how this affects the predicted vibration-reduction ability.

To obtain more time-efficient numerical models, the boundary element method can be employed for the ground at the far-field region in combination with the FE method for both the near-field region of the ground and the building structure. By doing so, the computational

time can be reduced. This is primarily valuable for large 3D FE models, because 2D models are relatively time-effective. The numerical procedure developed in the thesis regarding efficient analyses of liquid-filled pipe systems, which used CMS with a reduction in the number of retained interface dofs, can be further developed in terms of time-efficiency by using a mode-selection method.

A cost- and time-effective strategy when constructing new buildings with the aim of avoiding disturbing external vibrations is to locate them at sites were disturbing ambient vibrations do not occur or where they can be reduced to a sufficient level with a suitable vibration-reduction measure. However, this requires tools for identifying these areas. Such a tool would help engineers select construction sites wisely. The tool might be a computer program with a simplified interface to be used in cases where disturbing vibrations originate solely from external traffic sources. The program could visualise the propagating wavefront and predicting vibration levels, such that the engineer is supplied with information regarding the vibrations. It is vital to have such knowledge in order to suggest the type of structural system for a building or the type of foundation to use, as well as to suggest a suitable vibration-reduction measure. The input for the program could be the type of vibration source (e.g. trains, trams or trucks) along with the material parameters of the site in question and some prerequisites of the building, such as its governing dimensions and the number of floors.

Bibliography

[1] Wilson GP, Saurenman HJ, Nelson JT. Control of ground-borne noise and vibration. Journal of Sound Vibration, 87(2)(1983), 339–350.

[2] Das BM, Ramana GV, Principles of soil dynamics, Cengage Learning, Stamford, 2011.

[3] International Organization for Standardization. Bases for design of structures – Serviceability of buildings and walkways against vibration, ISO 10137:2007.

[4] Brownjohn JMW, Middleton CJ. Procedures for vibration serviceability assessment of high-frequency floors. Engineering Structures 2008;30:1548–1559.

[5] Swedish Geotechnical Society. Markvibrationer (in Swedish), SGF Informationsskrift 1:2012, version 2013-12-18.

[6] Bahrekazemi M. Train-induced ground vibration and its prediction. Doctoral thesis, Royal Institute of Technology, 2004.

[7] Persson P, Persson K, Sandberg G. Numerical study of reduction in ground vibrations by using barriers. Engineering Structures 2016;115:18–27.

[8] Mhanna M, Sadek M, Shahrour I. Numerical modeling of traffic-induced ground vibration. Computational Geotechnics 2012;39:116–23.

[9] Olafsen S. Difference in levels of groundborne noise and vibrations between the T-1300 and MX-3000 metro trains in Oslo. Joint Baltic-Nordic Acoustic Meeting, 18–20 June 2012, Odense, Denmark.

[10] Jones CJC. Use of numerical models to determine the effectiveness of anti-vibration systems for Railways, Proceedings of The Institution of Civil Engineers-transport. 105, Feb., pp. 43–51.

[11] Griffin MJ. Handbook of human vibration, Academic Press Limited, London, UK, 1996.

[12] Pavic A, Reynolds P. Vibration serviceability of long-span concrete building floors. Part 1: Review of background information. The Shock and Vibration Digest 2002;34(3):191–211.

[13] Banverket, Naturvårdsverket. Buller och vibrationer från spårburen linjetrafik – riktlinjer och tillämpning (in Swedish), Dnr. S02-4235/SA60, 2006-02-01.

[14] International Organization for Standardization. Mechanical vibration and shock – Evaluation of human exposure to whole-body vibration – Part 1: General requirements, ISO 2631-1:1997.

[15] Swedish Standard Institute. Vibration and shock - Measurement and guidelines for the evaluation of comfort in buildings (in Swedish), SS 4604861, 1992

[16] Amick CH, Gendreau M, Busch T, Gordon CG, Evolving criteria for research facilities: I – Vibration, SPIE Conference 5933: Buildings for Nanoscale Research and Beyond. San Diego, California (2005).

[17] With C. Train-induced vibrations on embankments and in buildings – Prediction and validation of some models. Doctoral thesis, Royal Institute of Technology, 2008.

[18] Kramer SL. Geotechnical earthquake engineering, Prentice Hall, Upper Saddle River, NJ, 1996.

[19] Richart FE, Hall Jr.JR., Woods RD, Vibrations of soils and foundations, Prentice Hall, Englewood Cliffs, 1970.

[20] Craig Jr RR, Kurdila AJ, 2006. Fundamentals of structural dynamics, John Wiley & Sons, New Jersey.

[21] Chopra A. K., Dynamics of structures, Prentice Hall, Upper Saddle River, 1995.

[22] Zienkiewicz OC, Taylor RL., The finite element method, volume 1 and 2, MacGraw-Hill, London, 1994.

[23] Bathe K-J., Finite element procedures, Prentice Hall, New York, 2006.

[24] Hilber HM, Hughes TJR, Taylor RL. Improved numerical dissipation for time integration algorithms in structural dynamics, Earthquake Engineering and Structural Dynamics, vol. 5, pp. 283–292, 1977.

[25] Brigham EO. The fast Fourier transform, Prentice-Hall Inc., Englewood Cliffs, NJ, 1974.

[26] Roesset JM. Soil amplification of earthquakes, Numerical Methods in Geotechnical Engineering, Chapter 19, ([Eds. Desai CS, Christian JT), McGraw-Hill, 639–682, 1977.

[27] Srikantha Phani A, Woodhouse J. Viscous damping identification in linear vibration. Journal of Sound and Vibration, 2007;303(3–5):475–500.

[28] Lysmer J, Kuhlemeyer RL, Finite dynamic model for infinite media, Journal of Engineering Mechanics (ASCE), 859-877, 1969.

[29] Cohen M, Jennings PC, Silent boundary methods for transient analysis. In: Belytschko T, Hughes TJR, editors. Computational methods for transient analysis, Elsevier, 1983.

[30] Randall J. LeVeque, Finite difference methods for ordinary and partial differential equations, SIAM, 2007.

[31] LeVeque RJ, Finite volume methods for hyperbolic problems, in: Cambridge Texts in Applied Math., Cambridge University Press, Cambridge, 2002.

[32] Atalla N, Sgard F. Finite element and boundary methods in structural acoustics and vibration, CRC press, Taylor & Francis, Boca Ratón, FL, 2015.

[33] Hall WS, Oliveto G, Boundary element methods for soil-structure interaction, Kluwer Academic Publishers, Dordrecht, 2003.

[34] Wolf JP. Dynamic soil-structure interaction. Prentice-Hall, Englewood Cliffs, NJ, 1985.

[35] Sandberg G, Ohayon R. (Eds.) 2008. Computational Aspects of Structural Acoustics and Vibration, CISM Courses and Lectures, vol.505, Springer Wien, New York.

[36] Flodén O, Persson K, Sandberg G. Reduction methods for the dynamic analysis of substructure models of lightweight building structures. Computers and Structures, 138(2014), 49–61.

[37] de Klerk D, Rixen DJ, Voormeeren SN. General framework for dynamic substructuring: history, review, and classification of techniques. AIAA Journal, 46(5) 2008, 1169-1181.

[38] Guyan RJ, 1965. Reduction of stiffness and mass matrices. AIAA Journal, 3, pp. 380.

[39] Dassault Systèmes. Abaqus 6.12 Documentation, USA, 2012.

[40] Allemang RJ, Brown DL, 1982. A correlation coefficient for modal vector analysis, Proceedings of International Modal Analysis Conference, pp. 110–116.

[41] Max IV, Detailed design report of the Max IV facility, 2010.

[42] Fojab, Hallenborgs gata 1A, 211 19 Malmö, Sweden, 2012.

[43] Snøhetta, Akershusstranda 21, N-0150 Oslo, Norway, 2012.

[44] Jonsson P, Jensen B. MAX-IV Vibrationsmätning – datarapport (in Swedish), 2010-12-10.

[45] Middleton CJ, Brownjohn JMW. Response of high frequency floors: A literature review. Engineering Structures 2010;32:337–352.

[46] Tyréns, Geotechnical investigation report, Reference number 225686G, Helsingborg 2010-12-10.

[47] SGU – Geological Survey of Sweden, Max IV - Kartering av kärnborrningarna GS1 och GS2 (in Swedish), Reference number 08-852/2010, Lund 2010-12-02.

[48] Division of Structural Mechanics, Lund University, Lund, Sweden.

[49] Altair Engineering. Hyperworks 11.0.

[50] Lunarc – The center for scientific and technical computing at Lund University.

[51] Paez TL. Introduction to Model Validation. Proceedings of the 27th International Modal Analysis Conference, SEM, Orlando, FL, 2009.

[52] Park KC. Analyses, model tests and design modifications for vibration/noise mitigation. Lecture notes (presented at Lund University on October 28th, 2013). Center for Aerospace Structures, Department of Aerospace Engineering Sciences, University of Colorado at Boulder, CO, USA, 2013.

[53] Andersen L, Nielsen SRK. Reduction of ground vibration by means of barriers or soil improvement along a railway track. Soil Dynamics and Earthquake Engineering 2005;25(7-10):701–16.

[54] Hung HH, Yang YB, Chang DW. Wave barriers for reduction of train-induced vibrations in soils. Journal of Geotechnical Geoenvironmental Engineering (ASCE) 2004;130(12):1283-91.

[55] Kattis SE, Polyzos D, Beskos DE. Modelling of pile wave barriers by effective trenches and their screening effectiveness. Soil Dynamics and Earthquake Engineering 1999;18(1):1-10.

[56] Al-Hussaini TM, Ahmad S. Design of wave barriers for reduction of horizontal ground vibration. Journal of Geotechnical Engineering (ASCE) 1991;117(4):616-36.

[57] Yang YB, Hung HH. A parametric study of wave barriers for reduction of train-induced vibrations. International Journal for Numerical Methods in Engineering, 1997;40(20):3729-47.
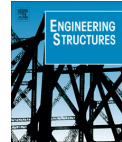
Part II

Appended publications

Paper A

Numerical study of reduction in ground vibrations by using barriers

CrossMark

P. Persson *, K. Persson, G. Sandberg

Department of Construction Sciences, Lund University, P.O. Box 118, SE-22100 Lund, Sweden

ARTICLE INFO

ABSTRACT

Reduction in traffic-induced ground vibrations by the use of barriers is investigated. The traffic load characteristics were measured for motorway traffic. The effects of parameters on various types of barriers were examined by the use of a finite element model that was calibrated to green-field measurements. The model involved a layered soil and bedrock. The depth of a trench and the elastic modulus of a solid back-fill material were found to be the most important parameters to consider. In investigation of the effects of infiltration of water into an open trench, a coupled finite element formulation of the water and the soil was applied. Infiltration of water was found to decrease the achieved reduction. At long distances from the vibration source, of around 500 m and longer, amplification in vibration level can be seen when a trench has been installed. It was also found, at long distances, that the motion of the ground surface follows the motion of the bedrock.

© 2016 Elsevier Ltd. All rights reserved.

1. Introduction

Occasionally, very strict vibrational requirements are specified for vibration-sensitive equipment used in high-tech facilities, such as large ground telescopes, radar towers and synchrotrons. High-tech facilities are often located in the vicinity of vibration sources of significant amplitude, such as trafficked roads and rail- and tramways. Traffic-induced ground vibrations can propagate to facilities nearby and lead to the vibration requirements for sensitive equipment being exceeded. It can be desirable in such cases to reduce the ground vibrations. The traffic-induced vibrations can be reduced by various means, such as shaping the landscape surrounding the facility or by placing a wave barrier in front of the facility [1,2].

Installing a wave barrier in the ground between a vibration source and a facility creates a discontinuity for the propagating waves. Waves that are incident to the trench give rise to different types of waves. These can be divided into five separate groups (see Fig. 1): (1) Rayleigh waves reflected back by the barrier, (2) Rayleigh waves transmitted through the barrier, (3) body waves from the barrier propagating downwards and back, (4) body waves from the barrier propagating forward and (5) waves propagating through the soil and the bedrock, under the barrier. Ground vibrations after the barrier has been passed are caused by (2), (4) and (5).

In the present paper, *barrier* is used as an umbrella term for various types of barriers. More specific, an empty barrier is referred to as a *trench*, a trench back-filled with a solid material is referred to as a *solid barrier*, and a trench infiltrated by water is simply referred to as a *water-infiltrated trench*.

1.1. Earlier studies

Since the pioneering work by Woods in 1968 [5], barriers used for reducing ground vibrations have been studied extensively. Several investigations of the effectiveness of wave barriers in terms of reduction in ground vibrations have been carried out, through field tests and numerical simulations by means of both the boundary element (BE) method and the finite element (FE) method, as well as combination of the two (FE–BE).

Extensive scaled field tests were performed in [5], in order to study the effectiveness of trenches, both close to the vibration source and at a considerable distance from it. On the basis of the experimental findings, certain guidelines concerning the dimensions of a trench to achieve maximal reduction in the ground vibrations are presented. It was also concluded that, because it is difficult to extrapolate full-scale tests from results of small-scale field tests, numerical investigations are of interest. Numerical studies of the effectiveness of barriers in terms of reduction in ground vibrations by means of the BE method have been carried out by, for example, [6–16]. The FE method is also extensively used in studies by, for example, [17–21]. Coupled FE–BE methods for studying the effectiveness of barriers in terms of reduction in ground vibrations have been employed by, for example, [22–26].

---

* Corresponding author. Tel.: +46 46 2228353.
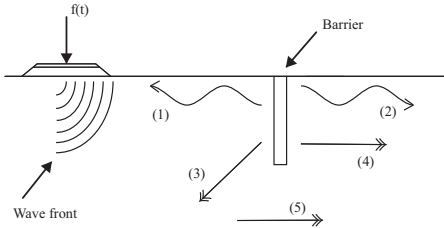 *E-mail address:* peter.persson@construction.lth.se (P. Persson).

Fig. 1. Different waves stemming from waves incident to a barrier.

Some general conclusions from the numerical investigations are that trenches provide a more effective vibration isolation than soil barriers and that the depth of a trench being the one parameter that has the greatest effect on the effectiveness and the width could be negligible while the distance to the vibration source may be important to consider. Further conclusions are that the effectiveness of barriers depend upon the material parameters of the filling material and that barriers, as well as, sheet-pile walls and row of piles can be suitable for reducing ground vibrations. The use of a softer filling material increases the effectiveness of a solid barrier and also permits larger depths to be used than in the case of a trench, the depth of a solid barrier is more effective than increasing its width. Several studies, e.g. [20,24–27], also points out that the impedance mismatch, of the back-filling material and the surrounding ground, is the key factor of determine the efficiency of a barrier. Since the variation of the mass density, Poisson's ratio and the loss factor of the filling material is in practice small, at least compared to the elastic modulus, they were found to not appreciably affect the effectiveness of a solid barrier. Also, a concrete lid placed on top of a trench with double sheet-pile walls, for safety reasons, and the inclination of the trench were found to not affect the effectiveness to any marked extent.

1.2. Present study

The main objective of the study was to investigate the use of barriers for minimising traffic-induced vibrations. This was performed by establishing FE models, validated by green-field measurements, resulting in a model with a layered soil and bedrock able to predict the effectiveness of using a wave barrier. The characteristics of the applied traffic load was determined from vibrational measurements conducted at a motorway. Trenches, solid barriers and water-infiltrated trenches parallel to a motorway were studied. Installation of a wave barrier disturbs the wave front and reflects waves into the bedrock. Wavelengths being less attenuated in the bedrock than in the soil. Therefore, the reduction in ground vibrations at distances far from the barrier may be affected by the waves propagating under the barrier in the bedrock. Thus, the reduction obtained at distances far from the barrier was studied. The effects of infiltration of water into a trench were examined by employing a coupled FE model of the water and the soil, taking the interaction between them into account. Moreover, parametric studies of geometric parameters of a trench and studies of the material parameters of a filling material in a solid barrier were performed.

In the paper, the synchrotron facility, Max IV, serves as an example case. Fig. 2 presents an architectural sketch of the facility. It is built approximately 100 m from the motorway E22. An electron beam is to be controlled by a large number of magnets that are distributed along the ring-shaped building. Since the quality of the measurements obtained is dependent upon the vibration level of the magnets, very strict vibration requirements are specified. The vibration requirements regarding vertical displacements of the magnets are especially strict, its being required that these be less than 20–30 nm in root-mean-square (RMS) per second within a frequency span of 5–100 Hz.

2. Numerical calculations

In the section, the governing theory of structural dynamics and of fluid–structure interaction (FSI) are presented.

2.1. Structural dynamics

The differential equation of motion for the continuum formulation of a three-dimensional solid is written as

$$\tilde{\mathbf{V}}^T \boldsymbol{\sigma}_S + \mathbf{b}_s = \rho_S \frac{\partial^2 \mathbf{u}}{\partial t^2} \tag{1}$$

where $\boldsymbol{\sigma}_S$ is the stress tensor, $\mathbf{b}_s$ is the body force vector, ρ_S is the mass density, $\mathbf{u}$ is the displacement vector, $\tilde{\mathbf{V}}$ is a differential operator and t is the time. With use of Galerkin's method, the FE formulation for a structural domain becomes [28,29]

$$\mathbf{M}_s \ddot{\mathbf{u}} + \mathbf{K}_s \mathbf{u} = \mathbf{f}_s \tag{2}$$

where $\mathbf{M}_s$ is the mass matrix, $\mathbf{K}_s$ the stiffness matrix, $\mathbf{f}_s$ the load vector and $\mathbf{u}$ the nodal displacement vector. Since damping has to be included in the numerical model in order to obtain a realistic response, a rate-independent damping model was assumed since it provides a better match to the real behaviour of soils than other simple available damping models. A limitation of the assumed damping model is that it cannot be used in the time domain. Thus, the damping was described by a loss factor, introduced by the structural damping matrix [30].

2.2. Fluid–structure interaction

In order to investigate a trench infiltrated by water, FSI was considered. Two governing equations can be employed for describing the pressure field of a homogeneous acoustic fluid, which is assumed to be inviscid, irrotational (curl $\mathbf{u}_f = 0$), compressible and to undergo small pressure changes. The equation of motion, the volumetric drag being neglected here, can be written as

$$\rho_0 \frac{\partial^2 \mathbf{u}_f}{\partial t^2} + \mathbf{V}p = 0 \tag{3}$$

where ρ_0 is the static density, $\mathbf{u}_f$ is the fluid displacement vector, t is the time, $\mathbf{V}$ is the gradient operator and p is the acoustic fluid pressure [31,32]. The constitutive equation for a barotropic fluid with constant density can be written as

$$p = -c^2 \rho_0 \mathbf{V} \mathbf{u}_f \tag{4}$$

where c is the speed of sound. With use of Eqs. (3) and (4), the wave equation for the acoustic fluid, the pressure serving as the field variable, can be written as the Helmholtz equation

$$\frac{\partial^2 p}{\partial t^2} - c^2 \mathbf{V}^2 p = 0. \tag{5}$$

By expressing the pressure as a complex harmonic function

$$p = \hat{p} e^{i\omega t} \tag{6}$$

the wave equation in the frequency domain becomes

$$\mathbf{V}^2 \hat{p} + \frac{\omega^2}{c^2} \hat{p} = 0. \tag{7}$$

Thus, with use of Galerkin's method, the FE formulation for the acoustic fluid domain can be written as

Fig. 2. The buildings of the Max IV facility as they are expected to appear, as well as the nearby E22 motorway, as rendering in a drawing [3,4].

$$\mathbf{M}_f \ddot{\mathbf{p}} + \mathbf{K}_f \mathbf{p} = \mathbf{f}_f \tag{8}$$

where **p** is the nodal pressure vector.

2.3. Coupling of domains

Continuity in fluid and structural displacements is assumed in the direction normal to their common boundary S. By introducing a normal vector, **n**, the kinematic boundary condition can be formulated as

$$\mathbf{u}_s \cdot \mathbf{n}|_S = \mathbf{u}_f \cdot \mathbf{n}|_S. \tag{9}$$

Due to the continuity in pressure at S, the static boundary condition for the coupling can be formulated as

$$\sigma_{s,n}|_S = -p \tag{10}$$

where $\sigma_{s,n}$ is the stresses at S in the normal direction.

By introducing a coupling matrix, **H**, the complete fluid–structure system of equations can be written as

$$\underbrace{\begin{bmatrix} \mathbf{M}_s & \mathbf{0} \\ \rho_0 \mathbf{H}_{sf}^T & \mathbf{M}_f \end{bmatrix}}_{\mathbf{M}} \underbrace{\begin{bmatrix} \ddot{\mathbf{u}} \\ \ddot{\mathbf{p}} \end{bmatrix}}_{\ddot{\mathbf{x}}} + \underbrace{\begin{bmatrix} \mathbf{K}_s & -\mathbf{H}_{sf} \\ \mathbf{0} & \mathbf{K}_f \end{bmatrix}}_{\mathbf{K}} \underbrace{\begin{bmatrix} \mathbf{u} \\ \mathbf{p} \end{bmatrix}}_{\mathbf{x}} = \underbrace{\begin{bmatrix} \mathbf{f}_s \\ \mathbf{f}_f \end{bmatrix}}_{\mathbf{q}}. \tag{11}$$

2.4. Characteristics of the road traffic

Experimental testing of traffic-induced vibrations was carried out at the Max IV site. For such vibrations, strains are usually at a level such that the assumption of linear elasticity is applicable. With use of a system of linear equations, the frequency content of the traffic load was considered by scaling the calculated displacements with the obtained frequency spectrum.

It is known from previous work by the authors [33–35] concerning the example case used here, that when taking account of both internal and external vibration sources the material parameters (concerning practical values of them) of the soil have a strong effect on the vibration level that occur in sensitive areas in the facility, whereas structural modifications of the facility itself have only a slight effect. It was also concluded that external vibration source frequencies exceeding 25 Hz are effectively damped out in the soil so that they have only a negligible effect on the vibration level in sensitive areas, which is in line with studies of other site conditions, see for example [36]. As the vibration requirements

for Max IV are especially strict within a frequency span of 5–100 Hz, a frequency span of 5–25 Hz for the traffic load was considered. The frequency range of interest corresponds to Rayleigh wavelengths of the top soil layer of 45–9 m.

The frequency content of the traffic load at the E22 motorway near the facility (cf. Fig. 2) was evaluated on the basis of greenfield in-situ measurements; see Fig. 3 for a schematic presentation of the test set-up. Full velocity–time series were measured by geophones at the top of the slope of the road embankment of the motorway during the passage of trucks, which generated the highest measured velocities. The ten events having the highest velocity amplitudes caused by heavy trucks during the period of one hour were registered. A displacement spectrum was obtained by dividing the velocity spectrum by $i\omega$. Fast Fourier Transformation of the displacement spectrum was performed to determine the frequency content of the response at the embankment. Since high frequencies are damped out quickly in the soil, the measurements on the embankment do not have the same frequency content as the traffic load. However, in the frequency range of interest (below 25 Hz) this difference was assumed to have a negligible effect because of the distances between the load (on the truck wheels) and the embankment being so short.

In order to account for the frequency content of the traffic load, the median value (50% quantile) of the measured data was calculated for each frequency and used for scaling the frequency response function (FRF) obtained from the FE analyses; see Fig. 4.

2.5. Evaluation

An RMS value was used as a measure of the vibration magnitude for evaluation and comparison purposes. The RMS value of the displacements from the steady-state analyses was determined by

$$U_{RMS} = \sqrt{\frac{1}{n} \sum_{i=1}^{m} U(f)_i^2} \tag{12}$$

where U_{RMS} is the RMS value of the displacements, $U(f)_i$ is the magnitude of the displacement at each frequency and n is the number of frequencies in the interval.

To determine the effectiveness of the barrier, an average displacement reduction factor was calculated by the use of five equally spaced evaluation points; see Eq. (14). The points were located at, 100, 150, 200, 250 and 300 m from the load, i.e. at the
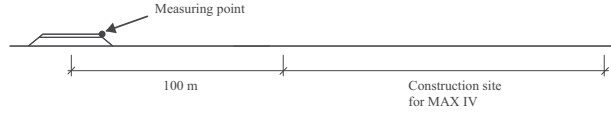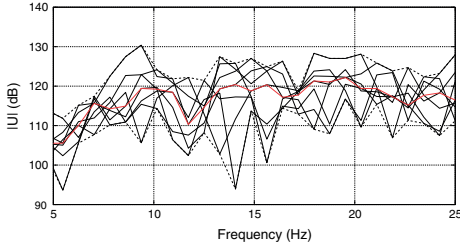
Fig. 3. Schematic measurement setup.

Fig. 4. The magnitude spectrum of displacements, $U(f)$, as obtained on the basis of measurements. The 95% and the 5% quantile curves, respectively, are shown as dashed lines. The median value (50% quantile), being used in the numerical analyses, is shown as a red solid line. A reference displacement of 10^{-12} m being used here.

location of the ring-shaped building; see Fig. 5. The displacement reduction factor, U_{red}, pertains to the vibrational amplitude after a barrier had been installed (post-barrier), U_{post}, to the amplitude prior to its being installed (pre-barrier), U_{pre}, in accordance with Eq. (13). U_{pre} and U_{post} were determined on the basis of the complex displacement magnitudes for the different frequencies and were calculated as the RMS values at the evaluation points, in accordance with Eq. (12). U_{red} and $\bar{U}_{red}$ are defined as

$$U_{red} = \frac{U_{pre} - U_{post}}{U_{pre}} \tag{13}$$

$$\bar{U}_{red} = \frac{1}{m} \sum_{i=1}^{m} U_{red,i} \tag{14}$$

where m is the number of evaluation points.

In order to investigate effects of installation of a barrier on long distances from the vibration source, the action value was used, defined as

$$Action = \int_{\omega} E(\omega) d\omega \tag{15}$$

where the total energy, E, is calculated as

$$E = E_{kinetic} + E_{strain} \tag{16}$$

using the cyclic mean value of the kinetic energy and of the strain energy. The kinetic energy and the strain energy, defined as

$$E_{kinetic} = \int_{V} \frac{1}{2} \rho \mathbf{v} \cdot \mathbf{v} dV \tag{17}$$

$$E_{strain} = \int_{V} \frac{1}{2} \boldsymbol{\sigma} : \boldsymbol{\epsilon} dV \tag{18}$$

were evaluated from the FE analyses.

3. The finite element model

In the numerical example employed, the geotechnical conditions at the Max IV site were employed [37,38]. The soil consisted of 16 m of two different clay tills identified as Low Baltic clay till covering the stiffer Northeast clay till on top of bedrock consisted of sandstone and shale. The geometry of the FE model was that of the road, the barrier, 16 m of soil and 100 m of bedrock; see Fig. 5. The road was modelled as having a layer of asphalt covering a layer of unbounded granular material. A 2D FE model was developed with the use of the FE software package Abaqus [39]. The barrier being assumed to be much longer than the structure to be protected, i.e. wave phenomena that occurs at the edges are assumed to have negligible effect on the obtained ground vibration level and, therefore, not affect the effectiveness. In order to develop an FE model and to ensure that the analyses provided results of adequate accuracy, studies have been conducted to investigate the influence of various parameters such as the aspect ratio and size of the finite elements, the size of the model geometry and reflection of waves at boundaries. The size of the model was determined to be 116×350 m^2 (height $\times$ width). Quadrilateral 8-node plane strain elements obtained by quadratic approximation using reduced integration were employed. To simulate the far-field conditions and avoid boundaries with significant reflections, 5-node quadratic one-way infinite elements were employed. In these elements, viscous absorbing boundaries are employed [40]. The soil materials had for the most part an element size of 2×2 m^2, the bedrock having mainly an element size of 2×9 m^2, thus an element mesh with a minimum of nine element nodes representing the shortest wavelengths was employed; see Fig. 6. The model contained approximately 3800 elements with approximately 11,800 degrees of freedom.

The vibrations with the highest amplitudes occur when the road is heavily trafficked, thus the traffic load can be regarded as a line load. This assumes, however, that all loads acts in phase. In the comparative studies on the effectiveness presented here, it is assumed to have a negligible effect. An FRF was obtained by applying a harmonic load of 1 N for frequencies from 5 to 25 Hz in steps of 0.1 Hz. In order to account for the characteristics of a traffic load, the FRF was scaled with the frequency spectrum of the measured traffic load; see Section 2.4.

Local variations within each layer of the road materials, the soil layers and the bedrock, such as strata and granularity, were assumed to be small as compared with the wavelengths in the frequency range of interest. Thus, the road materials, the soils and the bedrock can be modelled as isotropic homogeneous materials [41]. The material parameters employed were evaluated from both geotechnical and geophysical green-field measurements that were carried out in-situ in collaboration between the authors and participating companies. The mass density was evaluated mainly through soil sampling. The elastic modulus was determined from correlations between the results of numerical simulations and of falling weight deflectometer (FWD) tests and on the basis of relationships between vertical seismic profiling measurements and to surface seismic data. Relating the speed of the pressure wave and of the shear wave to one another enables Poisson's ratio to also be determined. The loss factor was evaluated by comparison
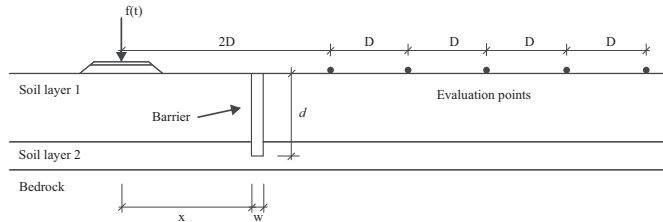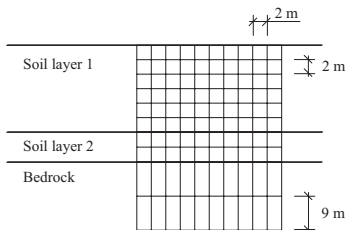
Fig. 5. FE model. Distance, *D* = 50 m.

Fig. 6. Schematic drawing of the FE mesh.

Table 1
Material parameters and stratification [38].

Parameter	Asphalt	UGM	Soil layer 1	Soil layer 2	Bedrock
Depth (m)	0.15	0.5	12	4	100
Elastic modulus (MPa)	5000	315	378	1136	8809
Loss factor	0.10	0.10	0.10	0.10	0.04
Mass density (kg/m^3)	2600	2300	2125	2125	2600
Poisson's ratio	0.25	0.20	0.48	0.48	0.40

between three-dimensional FE simulations and measurements data obtained from FWD tests at site. Thus, the FE model was calibrated with in-situ measurement data; see Table 1 for the employed material parameters and stratification.

The infiltrated water was modelled as an acoustic fluid by means of FSI analyses. In modelling of the water, 8-node biquadratic acoustic pressure elements were employed. The water was assumed to have a temperature of 10 °C, the static density, ρ_0, being set to 1000 kg/m^3 and the speed of sound, *c*, to 1450 m/s resulting in a bulk modulus, *K*, of 2.10 GPa. The pressure at the free surface of the acoustic medium was prescribed to zero.

4. Parametric study of barriers

In order to visualise that wave barriers have an large influence on the propagating wave front, the vertical complex magnitudes of the displacements from simulations with and without a trench are shown for a harmonic load at 15 Hz are shown in Fig. 7. As shown, for the case with a trench, the wave front is directed downwards into the bedrock, propagates forward through the bedrock and excites the soil layers. It is also visible in the figure that the vibration level at the ground surface to the right of the trench are decreased, in comparison to the situation without a trench.

4.1. Trench as wave barrier

A parametric study of trenches was carried out for differing locations, widths and depths. As a base state, the trench was placed at a distance, *x*, of 50 m from the road, having a width, *w*, of 1 m and a depth, *d*, of 12 m (the same as the depth of the top soil layer); see Fig. 5 for the notations. Each parameter was varied from the base state while the other parameters were kept constant.

The reduction in the vibration level is shown in Fig. 8a as a function of the depth of the trench. The depth, *d*, was varied between 0 and 16 m. The reduction becomes larger as the depth is increased. It is evident that in the present case, the trench needs to be deeper

than 4 m in order for the vibration level at the facility to be reduced appreciably. The largest change was found to be for the increase from 6 to 10 m in depth. Between 6 and 10 m the reduction in the vibration level increases from 21% to 55%. For a trench deeper than 10 m, the waves propagating in the bedrock appear to dominate. A reduction of 65% could be obtained by having a depth of 16 m.

The width, *w*, of the trench was varied between 0.25 and 4 m. It was found that the width has only a very slight effect on the reduction in the vibration level. For a shallow trench, the effect of the width was not investigated, although the width may have a stronger effect on the vibration level. A reduction of between just 62% and 65% was obtained for the different widths that were studied.

A barrier reflects incident waves but also contributes to disturbances in the wave front, this causing refraction and diffraction of the propagating waves. The changes in speed and in the direction of the wave front due to reflection, refraction or diffraction results in interference of the waves at certain distances from the barrier. Thus, the most effective location, in terms of reducing vibrations, for the barrier could be sought. A study of the influence of the location of a trench was carried out. The distance between the motorway (the vibration source) and the ring-shaped building (the receiver), was 100 m. In consideration of this, the location of the trench was varied between a distance, *x*, of 10 m (active screening) and a distance of 90 m (passive screening) from the motorway. In Fig. 8b the reduction obtained in the vibration level is shown for various locations of the trench. It was found that the most effective locations of the trench were, in practice, between 20 and 80 m from the road. Note that the effect of the location is somewhat slight.

4.2. Solid wave barrier

In practice, it can be difficult to use trenches due to the infiltration of water and safety aspects that needs to be considered. This motivates the use of barriers with a filling material of some sort. Use of solid barriers also allows a greater depth because of the lack of need for lateral support at the sides. A parametric study of the material properties of the filling material was carried out. Four material parameters were varied, those of the elastic modulus,
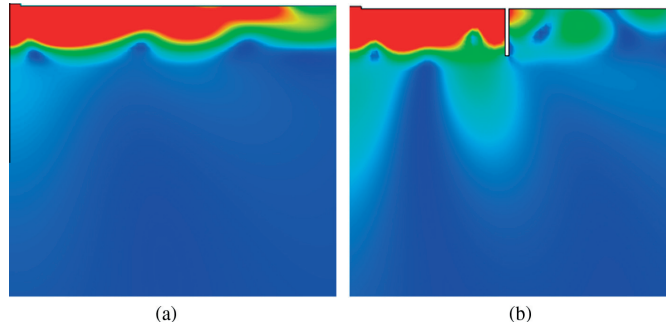
Fig. 7. Simulation results of the complex magnitude of the vertical displacements at 15 Hz, (a) without a trench and (b) for a trench with the geometry $x = 40$ m, $w = 1$ m, $d = 16$ m (same as the soil). Note that the colours in the two plots represents the same values, ranging from zero vibration amplitudes (blue colour) to maximum (0.4 nm, red colour). The full extension of the soil and of the bedrock are not shown here.
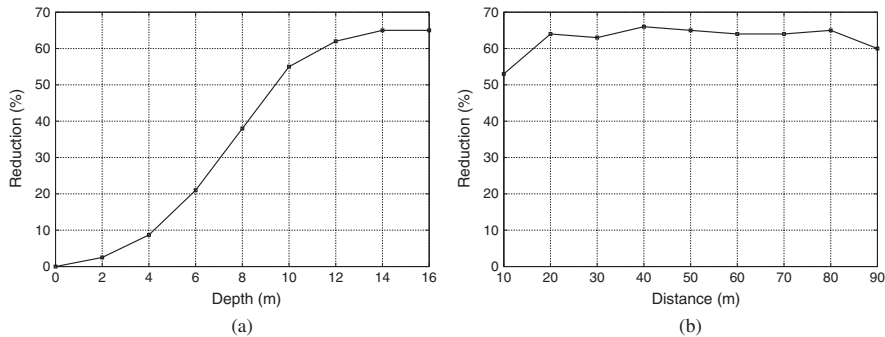
Fig. 8. Average reduction in the vibration level (displacement), (a) versus the depth of the trench and (b) versus the location of the trench.

the loss factor, the mass density and Poisson's ratio. The solid barrier was placed 50 m from the centre of the road, having a width of 1 m and a depth of 12 m (the same depth as the top soil layer). It was assumed, as a base state, that the material properties of the filling material were the same as the top soil layer; see Table 1. Each material parameter was varied from the base state while the others were kept constant.

The elastic modulus was varied between 1 and 50,000 MPa. In Fig. 9a, values of the elastic modulus lower than that of the top soil layer (the base parameter) are shown. As can be seen in the figure, up to a value of approximately 35 MPa, the elastic modulus has a marked influence on the effectiveness of the barrier in reducing the degree of vibration. A reduction of from 39% to 10% was obtained in varying the value of the elastic modulus from 1 to 35 MPa. As the elastic modulus approaches zero, the reduction in the vibration level approaches the same level as that for a trench, although it may not have exactly the same level, due to the mass density of the filling material. For the frequency range considered here (5–25 Hz), with high elastic modulus of the barrier material, e.g. 20 and 50 GPa, the achieved reduction of the barrier was negligible. For those elastic modulus, a reduction of about 3% was seen for the evaluation point located 100 m from the road. However, for the other four evaluation points, amplification of up to 3% was shown. Thus, a very little effect of the barrier was seen during these conditions. A strong frequency-dependence was,

however, seen here. Hence, for higher frequencies the achieved reduction may be different. It should be noted that in other publications, such as [7,8,22,25], a stiff barrier has been shown to be beneficial to install. For the analyses presented in the present paper, varying the elastic modulus to a value larger than that of the top soil layer has only a slight effect on the reduction in the vibration level.

The loss factor was varied between 0.01 and 2, the mass density was varied between 10 and 3000 kg/m³ and Poisson's ratio was varied between 0.01 and 0.48. Since the trench is narrow, varying those parameters of the filling material only has a slight effect of the degree of reduction.

4.3. Water-infiltrated trench

To investigate the effects of water infiltration into a trench, a parametric study was carried out by considering fluid–structure interaction (FSI) in the FE analyses, in which the water level in a trench was varied. The depth of the trench was set to 16 m, was placed 50 m from the motorway and having a width of 1 m. The water level in the trench was varied between 0 and 16 m (0 m corresponding to a trench 16 m deep containing no infiltrated water), while the other parameters were kept constant. Variation of the water level in the trench can be a result of, for example, heavily precipitation or of installation of water pumps that drains the
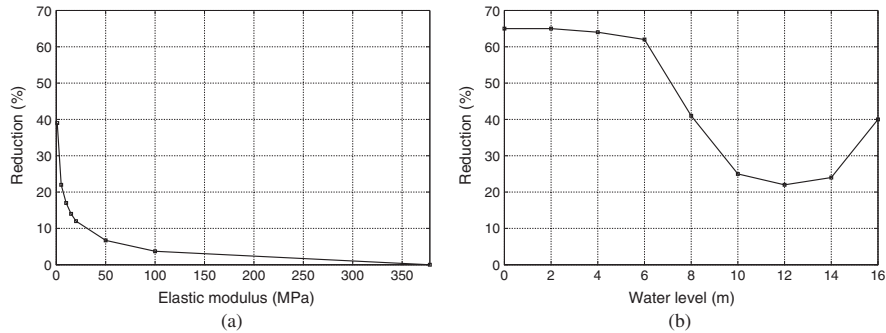
Fig. 9. Average reduction in the vibration level (displacement), (a) versus the elastic modulus of the solid filling material and (b) versus the water level in the trench.

trench by pumping out infiltrated water. The variation of the water level interacts with the groundwater level and can, therefore, affect the material parameters of the soil in proximity to the trench. Due to the clay tills' very low hydraulic conductivity, the changes in the groundwater level were assumed to be a local phenomenon and, therefore, not affecting the relatively long wavelengths in the soil within the frequency range of interest.

As can be seen in Fig. 9b, the water level in the trench can affect very markedly the obtained reduction in the vibration level. A reduction of between 65% and 21% was obtained for the various water levels. The reduction, caused by the trench when it is empty, decreases only very slightly up to a water level of 6 m, and decreases rapidly then up to a water level of 10 m, these higher water levels enabling more of the P-waves to travel through the trench (S-waves cannot propagate in water). Within the water levels of 10–14 m the phenomena involved seeming to interact and to have about the same effect. At higher water levels, between 14 and 16 m, the reduction increases.

4.4. Effects of long distances from the source

As mentioned in the beginning of Section 4, the presence of a wave barrier in the ground directs incident waves into the bedrock, then propagating forward through the bedrock and excites the soil far from the barrier. The distances considered in the previous parametric studies, lead to a reduction in the vibration level at the location of the facility. It has been noted, however, that the reduction is decreasing with larger distances from the vibration source. In this subsection, the causes for the reduction achieved by installing a wave barrier decreases, or even leading to occurrence of amplification, at long distances from the vibration source, are presented.

The length of the FE model used in the previous subsections is extended here to 1500 m in order to evaluate vibration level at very long distances from the source. For the simulation results presented in this subsection, the barrier involved constitutes of a trench with base parameters according to Section 4.1.

The average reduction in vibration level versus the location of the evaluation is shown in Fig. 10 for two different frequency ranges. The reduction achieved is somewhat constant at distances of around 500 m and further from the vibration source. Applying the frequency range of interest (5–25 Hz), a reduction is shown at all distances considered, i.e. 100–1200 m in steps of 100 m. If, however, frequencies between 10 and 25 Hz is considered, amplification occurs at distances of 600 and 800–1200 m from the vibration source.
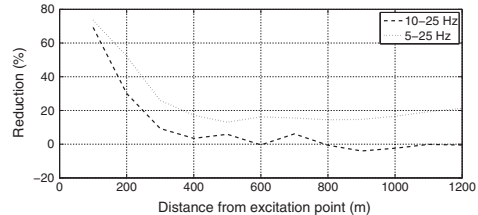

Fig. 10. Average reduction in the vibration level (displacement) by a trench with base parameters versus the location of the evaluation.

In Fig. 11, each subfigure (a–f) consists of two plots (upper and lower), valid for evaluation at 200–1200 m from the vibration source. In the upper plots the obtained reduction by installing a trench is shown and in the lower plots the displacement response on the ground, with and without a trench, is shown. By comparing the responses on the ground surface (lower plots) at the various distances, it is found that the response is somewhat similar at distances of about 700–800 m and further away from the vibration source.

The displacements evaluated on both the ground surface and at the interface between the lower soil layer and the bedrock are shown in Fig. 12 for two different distances from the vibration source. Considering a distance of 200 m from the source and comparing the response on the ground surface with the response on the bedrock, there is a marked difference in the frequency response. At a distance of 1000 m, however, the behaviour of the response on the ground surface and at the interface, respectively, are somewhat similar, i.e. the frequency peaks occurring at the same frequencies. Since waves in the soil are dampened out faster than in the bedrock, the vertical motion of the soil layers follows the vertical motion of the bedrock at long distances from the vibration source. In Fig. 12b it is shown that the vertical displacements are larger, for some frequencies, at the soil–bedrock interface than on the ground surface. Applying a lower loss factor of the bedrock leads to an even larger difference in the response at those frequencies (especially 13–17 Hz), where the displacements are larger on the soil–bedrock interface than on the ground surface. Note that this is only valid for lowering the loss factor of the bedrock. By, increasing the loss factor of the soil, not only the attenuation of the waves in the soil increases but also results in that the amount of energy propagating down into the bedrock decreases.
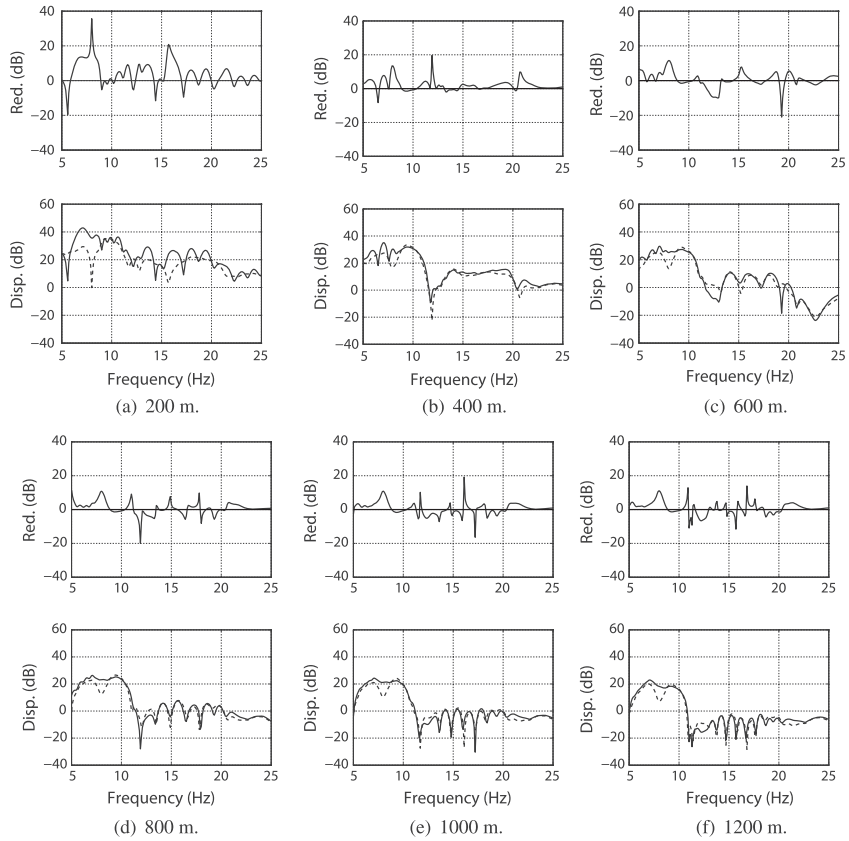
Fig. 11. Lower plots; complex magnitude of the vertical displacements, evaluated on the ground surface at various distances from the vibration source (solid line: without trench, dashed line: with trench). Upper plots; the reduction for the case of with and without a trench, respectively. Amplification is shown as negative reduction, a reference displacement of 10^{-12} m being used here.
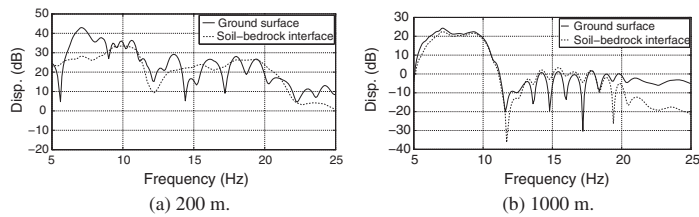
Fig. 12. Complex magnitude of vertical displacements, evaluated on the ground surface as well as at the interface between the lower soil layer and the bedrock, at 200 and 1000 m, respectively, from the vibration source. A reference displacement of 10^{-12} m being used here.

In Fig. 13, the location of the element sections (I, II and III) used for evaluating the energy is shown. The volume used for calculating the energy according to Eqs. (17) and (18), is here defined as a unit length in the direction of the road multiplied with the finite element area. Section I is located 50 m from the vibration source,

i.e. at the same location as the trench. Section II is located 100 m from the source and Section III is located 1000 m away. Table 2 presents values of the *Action* (frequency-integrated energy), for the three different element sections; see Eq. (15). In Table 2 it is seen that at the location of the trench (Section I), the action is
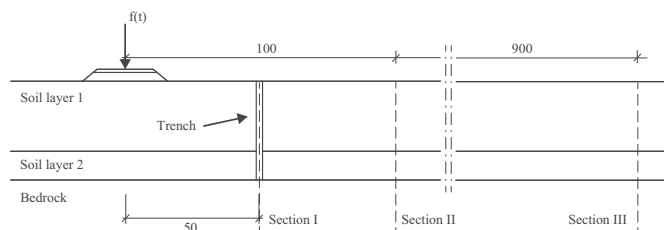
Fig. 13. Location of the element sections where the total energy being evaluated. The element sections are one finite element long in the orthogonal direction to the road. The dimensions are in the units of metres.

Table 2
Frequency-integrated energy, here denoted as Action. The actions are in the unit of pJ rad/s.

Distance (m)	Section	Ref. model (no trench)	Trench model
50 (at trench)	Soil$_I$	900	–
	Bedrock$_I$	65.8	92.7
	Complete$_I$	966	92.7
100	Soil$_{II}$	125	12.1
	Bedrock$_{II}$	40.5	40.8
	Complete$_{II}$	166	52.9
1000	Soil$_{III}$	0.23	0.15
	Bedrock$_{III}$	0.90	0.56
	Complete$_{III}$	1.13	0.71

41% higher in the bedrock for the FE model with a trench as compared to the bedrock in the model without a trench. It is also seen that at 100 m (Section II) from the location of the excitation, the energy in the bedrock for the trench model represents 77% of the energy present in the complete section, as compared to the model without a trench where the energy in the bedrock only represents 24% of the energy present in the complete section. The action in the bedrock at 100 m from the vibration source was, however, essentially the same for the two different models. The installation of a trench resulting therefore in higher energy content in the bedrock as compared to prior an installation.

Note that the direction of the flowing energy was not analysed in the study, i.e. energy in the bedrock directed away from the ground surface is still accounted for in determining the action value. The direction of the energy flow may be calculated applying transient loads and determining the gradient of the total energy.

5. Concluding remarks

Reduction in traffic-induced ground vibrations through the use of wave barriers was investigated in a numerical parametric study employing a FE model, validated by green-filed in-situ measurements. The effects of the geometric parameters of a trench, the material parameters of a solid filling material, and of the infiltrated water into a trench considering FSI were examined, as well as the effect on obtained reduction at long distances away from the barrier.

The results obtained from the investigation of wave barriers, considering the measured frequency content of a traffic load are in line with the general conclusions drawn from the earlier studies in the area (cf. Section 1.1); the depth of a trench being the one parameters that has the greatest influence on the effectiveness, the width could be negligible while the distance to the vibration source may be considered. The findings regarding the material parameters of the filling material are also matching the general conclusions; the effectiveness of barriers depends upon the material parameters of the filling material. The use of a softer filling material increases the effectiveness of a barrier, the depth of a barrier is more effective than increasing its width. Since the barriers investigated here are narrow, the mass density, Poisson's ratio and the loss factor of the filling material, within practically values of them, were found to not appreciably affect the effectiveness of a barrier.

On the basis of the results obtained, the following conclusions are highlighted.

- The infiltration of water into, as well as draining of water in, a trench can strongly affect the reduction in the vibration level that the presence of a trench results in. The effectiveness of a trench decreases when any large amount of infiltrated water is present since water transmits P-waves. A water level of 12 m in a trench 16 m deep was found, for example, to decrease the reduction in the vibration level from 65% to 21%.
- The impedance mismatch, which is the controlling parameter for the effectiveness of a trench, depends on the wave velocity and the mass density. Considering practically possible useful material parameters, the mass density of the solid filling material has little effect, thus the wave velocity being the important parameter. The wave velocity, however, could be described by the elastic modulus and Poisson's ratio, and since Poisson's ratio do not has a marked influence on the effectiveness (within practical values), the elastic (or shear) modulus can be sufficient to consider in determining the effectiveness of a solid barrier material.
- At distances of 500–700 m and further from the vibration source, various phenomena occurs that are not seen at shorter distances. At those distances, the reduction achieved in the vibration level by installing a trench in the ground is decreased to a plateau of approximately 15% for the frequency range of interest. By considering a different frequency range, amplification of the ground surface amplitudes can be seen for distances of around 600 m or longer. It was also concluded that at distances of around 700 m and longer, the vertical displacements of the ground surface follows the vertical displacements of the bedrock.

Acknowledgments

References

[1] Persson P, Persson K, Sandberg G. Reduction in ground vibrations by using shaped landscapes. Soil Dyn Earthq Eng 2014;25:31–43.
[2] Richart FE, Hall Jr JR, Woods RD. Vibrations of soils and foundations. Englewood Cliffs: Prentice Hall; 1970.

[3] FOJAB arkitekter Malmö. Hallenborgs gata 1A, 211 19 Malmö, Sweden; 2012.
[4] Snøhetta. Akershusstranda 21. N-0150 Oslo, Norway; 2012.
[5] Woods RD. Screening of surface waves in soil. J Soil Mech Found Eng (ASCE) 1968;94(4):951–79.
[6] Emad K, Manolis GD. Shallow trenches and propagation of surface waves. J Eng Mech Div (ASCE) 1985;111:279–82.
[7] Beskos DE, Dasgupta G, Vardoulakis IG. Vibration isolation using open or filled trenches Part 1: 2-D homogeneous soil. Comput Mech 1986;1(1):43–63.
[8] Dasgupta G, Beskos DE, Vardoulakis IG. Vibration isolation using open or filled trenches Part 2: 3-D homogeneous soil. Comput Mech 1990;1:129–42.
[9] Leung KL, Beskos DE, Vardoulakis IG. Vibration isolation using open or filled trenches Part 3: 2-D non-homogeneous soil. Comput Mech 1990;1:137–48.
[10] Leung KL, Vardoulakis IG, Beskos DE, Tassoulas JL. Vibration isolation by trenches in continuously nonhomogeneous soil by the BEM. Soil Dyn Earthq Eng 1991;10(1):172–9.
[11] Al-Hussaini TM, Ahmad S. Design of wave barriers for reduction of horizontal ground vibration. J Geotech Eng (ASCE) 1991;117(4):616–36.
[12] Ahmad S, Al-Hussaini TM, Fishman KL. An investigation on active isolation of machine foundation by open trenches. J Geotech Eng (ASCE) 1996;122(6):454–64.
[13] Klein R, Antes H, Le Houédec D. Efficient 3D modelling of vibration isolation by open trenches. Comput Struct 1997;64(1–4):809–17.
[14] Al-Hussaini TM, Ahmad S. Active isolation of machine foundations by in-filled trench barriers. J Geotech Eng (ASCE) 1996;122(4):288–94.
[15] Kattis SE, Polyzos D, Beskos DE. Modelling of pile wave barriers by effective trenches and their screening effectiveness. Soil Dyn Earthq Eng 1999;18(1):1–10.
[16] Tsai PH, Feng ZY, Jen TL. Three-dimensional analysis of the screening effectiveness of hollow pipe barriers for foundation-induced vertical vibration. Comput Geotech 2008;35:489–99.
[17] Yang YB, Hung HH. A parametric study of wave barriers for reduction of train-induced vibrations. Int J Numer Meth Eng 1997;40(20):3729–47.
[18] Shrivastava RK, Kameswara Rao NSV. Response of soil media due to impulse loads and isolation using trenches. Soil Dyn Earthq Eng 2002;22(8):695–702.
[19] Hung HH, Yang YB, Chang DW. Wave barriers for reduction of train-induced vibrations in soils. J Geotech Geoenviron Eng (ASCE) 2004;130(12):1283–91.
[20] Wang JG, Sun W, Anand S. Numerical investigation on active isolation of ground shock by soft porous layers. J Sound Vib 2009;321:492–509.
[21] Alzawi A, El Naggar MH. Full scale experimental study on vibration scattering using open and in-filled (GeoFoam) wave barriers. Soil Dyn Earthq Eng 2011;31:306–17.
[22] Andersen L, Liingaard M. Vibration screening with sheet pile walls. In: Takemiya H, editor. Proceedings of the 2nd international symposium on environmental vibrations. Okayama, Japan; 2005. p. 429–37.
[23] Andersen L, Frigaard P, Augustesen AH. Mitigation of ground vibration by double sheet-pile walls. In: Proceedings of the 8th international congress on advances in civil engineering, vol. 2. Famagusta, Cyprus; 2008. p. 247–54.
[24] Adam M, von Estorff O. Reduction of train-induced building vibrations by using open and filled trenches. Comput Struct 2005;83(1):11–24.
[25] Andersen L, Nielsen SRK. Reduction of ground vibration by means of barriers or soil improvement along a railway track. Soil Dyn Earthq Eng 2005;25(7–10):701–16.
[26] Andersen L, Augustesen AH. Mitigation of traffic-induced ground vibration by inclined wave barriers – a three-dimensional numerical analysis. In: Proceedings of the 16th international congress on sound and vibration. Kraków, Poland; 2009.
[27] Massarsch KR. Vibration isolation using gas-filled cushions. Soil dynamics symposium in Honour Prof. Richard D. Woods. Geo-Frontiers 2005, Austin, Texas; 2005.
[28] Bathe KJ. Finite element procedures. New York: Prentice Hall; 2006.
[29] Zienkiewicz OC, Taylor RL. The finite element method, vol. 1 and 2. London: MacGraw-Hill; 1994.
[30] Craig Jr RR, Kurdila AJ. Fundamentals of structural dynamics. New Jersey: John Wiley & Sons; 2006.
[31] Morand H, Ohayon R. Fluid-structure interaction. Chichester: Wiley; 1995.
[32] Sandberg G, Ohayon R, editors. Computational aspects of structural acoustics and vibration. CISM courses and lectures, vol. 505. New York: Springer Wien; 2008.
[33] Persson P. Analysis of vibrations in high-tech facility. Report TVSM-5164. Lund (Sweden): Division of Structural Mechanics, Lund University; 2010.
[34] Persson P, Persson K. Analysis of dynamic soil-structure interaction at high-tech facility. In: Eriksson A, Tibert G, editors. Proceedings of NSCM-23: the 23rd nordic seminar on computational mechanics. Stockholm, Sweden; 2010.
[35] Persson P, Persson K, Sandberg G. Reduction of traffic-induced vibrations at high-tech facility using trenches. In: Freund J, Kouhia R, editors. Proceedings of NSCM-24: the 24rd nordic seminar on computational mechanics. Helsinki, Finland; 2011.
[36] Mhanna M, Sadek M, Shahrour I. Numerical modeling of traffic-induced ground vibration. Comput Geotech 2012;39:116–23.
[37] SGU – Geological Survey of Sweden. MAX IV – Kartering av kärnborrningarna GS1 och GS2. Reference number 08-852/2010. Lund 2010-12-02.
[38] TYRÉNS. Geotechnical investigation report. Reference number 225686G. Helsingborg 2010-12-10.
[39] Dassault Systémes SIMULIA. Abaqus 6.11.
[40] Lysmer J, Kuhlemeyer RL. Finite dynamic model for infinite media. J Eng Mech Div (ASCE) 1969:859–77.
[41] Das BM, Ramana GV. Principles of soil dynamics. Stamford: Cengage Learning; 2011.

Paper B
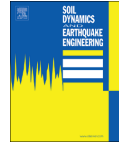
Reduction in ground vibrations by using shaped landscapes

Peter Persson *, Kent Persson, Göran Sandberg

Department of Construction Sciences, Lund University, Sweden

ARTICLE INFO

ABSTRACT

Reduction in traffic-induced ground vibrations by the use of shaped landscapes is investigated here by shaping the landscape surrounding a high-tech facility, using the landscape thus produced as a wave obstacle. The effects of the geometric parameters of a shaped landscape were examined in parametric studies. An architectural landscape design was also investigated in terms of its effectiveness in reducing traffic-induced ground vibrations. Finite element models, analysed in the frequency domain, were employed. The models involve a layer of soil and the underlying bedrock. It was found that anywhere from an appreciable reduction to an appreciable amplification of the vibrations produced can occur, depending upon the geometric parameters of the shaped landscape involved. The most effective shape was found for a topography that acted as a waveguide that reduced the level of vibration by approximately 35%.

© 2014 Elsevier Ltd. All rights reserved.

1. Introduction

Occasionally, very strict vibrational requirements are specified for sensitive equipment used in high-tech facilities, such as radar towers and synchrotron facilities. Regardless of whether the sensitive equipment in itself is a significant source of vibration, or not, it is important to isolate it from external vibrations. High-tech facilities are often located in the vicinity of sources of vibrations of significant amplitude, radar towers often being found near rocket-launching facilities, for example, and synchrotrons near heavily trafficked roads, the latter for logistic reasons. The traffic-induced ground vibrations can propagate to facilities nearby and lead to the vibration requirements for sensitive equipment there being exceeded. It can be desirable under such conditions to reduce the ground vibrations by the use of wave obstacles. The traffic-induced vibrations can be reduced by various means, such as by shaping the landscape between the road and the facility.

It is known from the previous studies [1–3] concerning the synchrotron facility MAX IV in Lund, Sweden, that the material parameters of the soil there have a strong effect on the vibration levels that occur in sensitive parts of the facility, whereas structural modifications of the facility itself have only a negligible

effect. Most of the vibration energy produced by vibrations induced on the ground surface is transmitted by Rayleigh surface waves that propagate close to the ground surface. Since Rayleigh waves attenuate with horizontal distance as well as with depth, the ground vibrations can be reduced by constructing a suitable wave obstacle in the ground between the wave source and the facility that is to be protected. Body waves propagate as a hemispherical wave front, whereas Rayleigh waves propagate radially as a cylindrical wave front [4]. The attenuation of the body waves is thus proportional to $1/r$, the attenuation of the Rayleigh waves, in contrast, being proportional to $\sqrt{1/r}$. Thus, at a relatively large distance from a vibration source the Rayleigh waves become the dominant wave form.

Constructing a shaped landscape as a wave obstacle between a vibration source and a facility creates a discontinuity for the propagating waves. Waves that are incident to the shaped landscape show different types of behaviours that are associated with changes in direction of the propagating waves. They are subjected to reflection as well as diffraction at the boundaries of the landscape. These two phenomena scatter the wave front and reduce the level of vibration at the facility.

At large construction sites, large amounts of soil are excavated in order to level the ground surface. This is necessary since, generally speaking, the surface needs to be horizontal before the construction of a building begins, the loose topsoil needing to be removed. The large amounts of excavated soil produced often need to be transported away from the construction site, which can be

---

* Corresponding author.
E-mail address: peter.persson@construction.lth.se (P. Persson).

Fig. 1. The buildings of the MAX IV facility as they are expected to appear, as well as the nearby E22 motorway, as rendering in a drawing [5,6].

costly for the construction project. If instead, these soil masses can serve a useful purpose at the construction site, they can be retained and be used to construct a shaped landscape with hills and valleys, for example, see Fig. 1. The architect bureaus associated with the MAX IV project, *Fojab* and *Snøhetta* [5,6], developed an architect-designed geometry of a shaped landscape (cf. Fig. 1) surrounding the MAX IV facility, one based on ideas partly introduced by the Department of Construction Sciences at Lund University. This shaped landscape can serve to reduce traffic-induced ground vibrations incident to the facility and is regarded as representing an aesthetically desirable solution.

In the paper, the reduction in vibrations that shaped landscapes are expected to bring about were investigated, the MAX IV synchrotron facility serving as an example case here. Fig. 1 presents an architectural sketch of the facility as planned. MAX IV is to be built approximately 100 m from the motorway E22. In the MAX IV facility, a beam of electrons is to be controlled by a large number of magnets that are distributed along the ring-shaped structure and along beam lines that lead beams of electrons to measurement stations. Since the quality of the measurements obtained is dependent upon the levels of vibration of the magnets, very strict requirements regarding the vibration levels have been specified. The vibration requirements for MAX IV regarding vertical displacements of the magnets are especially strict, its being required that these be less than 20–30 nm in RMS per second within a frequency span of 5–100 Hz.

1.1. Literature review

Several investigations of the effects of irregular topography on ground vibrations have been carried out.

Lee and Wu [7,8] presented a numerical solution for the two-dimensional (2D) scattering and diffraction of plane P, SV and SH waves by canyons of arbitrary shape in an elastic half space. The displacements were computed numerically using the method of weighted residuals (moment method). It was concluded that the ground vibrations were frequency dependent and were also dependent upon the orientation of the incident waves. It was found that the shape of the canyon had an effect on the displacement amplitudes at the surface of the canyon and in the nearby half-space [8]. Zhou and Chen [9] investigated the effect of topography on Rayleigh waves excited by an explosive source near the surface, their employing the local indirect wave-number method. The energy and the frequency content of waves before and after passing through the topography involved were compared in order to evaluate the effect of the steepness of the topography. Reduction in the energy of the waves and loss of their high frequency content were found to occur. The authors

concluded that these effects were more obvious where the topography was steeper.

Mossessian and Dravinski [10] investigated the diffraction of plane harmonic waves by three-dimensional (3D) surface irregularities by the use of an indirect boundary integral method. The irregular shapes were arbitrary and were embedded in the half-space. It was found to be important to use 3D numerical models when investigating the scattering of elastic waves by surface topographies of arbitrary shape. Sánchez-Sesma and Campillo [11] investigated the topographical effects for P, SV and Rayleigh waves in an elastic half-space, through the use of the indirect boundary element (BE) method, their finding that the topography can have an appreciable effect on both the amplification and the reduction in the level of vibration at or nearby the topographic features in question. Reinoso et al. [12] investigated through the use of a direct BE method the 3D scattering of seismic waves from irregular topographies, due to the presence of incident P-, S- and Rayleigh waves in the time domain. The irregular shapes were those of both mountains and valleys. It was found that an irregularity affects by way of its geometry the level of amplification achieved. It was concluded that mountains with vertical walls generate higher amplification levels than walls of mountains with a smooth slope. Nguyen and Gatmiri [13] used a 2D direct BE method for examining the scattering of seismic waves by topographic features of different types. They found that a topographic feature modifies the seismic waves at and near to the topographic feature in question. Zhenning and Jianwen [14] investigated the scattering of incident SV waves by a canyon in a layered half-space through use of an indirect BE method. They found that the presence of a layered half-space affects both the displacement amplitudes on the ground surface and the frequency content of the displacements. They observed that the displacements obtained depended upon the type of excitation.

Bouckovalas and Papadimitriou [15] employed the finite difference (FD) method to study the effects of the topography and of vertically propagating SV waves on seismic ground vibration in step-like ground slopes. It was found that the topography involved can lead to either an amplification or a reduction in the level of vibration at the crest of the slope or nearby. Amplification generally occurs near the crest of the slope and reduction at the toe of the slope. Ducellier and Aochi [16] developed an FD-FE method for modelling seismic wave propagation in a 2D elastic medium having an irregular surface topography. To study amplification effects there, numerical simulations of seismic wave propagation in a series of hills were carried out and were compared with a single-hill case. The authors found that the presence of several hills, as opposed to a single hill, can increase the amplification effects produced by the topography of the ground surface. They concluded that in evaluating topographic site effects the

surrounding topography needs to be taken into account alongside the local topography.

Chongbin Zhao and Valliappan [17] used a coupled finite and infinite element method to develop a numerical model for studying wave scattering effects in the frequency domain. They concluded that the effect of canyon topographic and geologic conditions on ground vibrations due to P and SV earthquake waves can affect dramatically both the peak value and the frequency content of the free-field vibration occurring along the canyon surface during an earthquake. Athanasopoulos et al. [18] investigated surface topography effects through carrying out 2D seismic response analyses based on the use of the finite element (FE) method. They found that a step-like topography amplified the intensity of vibration considerably without affecting the frequency content of the vibration. They concluded that surface topography plays an important role in affecting the intensity of the ground vibration induced by seismic waves. Assimaki et al. [19] performed 2D FE analyses in the time domain for analysing topographic effects, as well as additive contributions of the soil stratigraphy, the heterogeneity of the material and the soil–structure interactions in the ground vibrations induced by an earthquake. They found the topography to have a strong effect on the seismic waves produced by ground vibrations. Gatmiri et al. [20] investigated, by the use of the FE method in the near-field and the BE method in the far-field, seismic effects due to irregularities of the topography at the ground surface, their carrying out parametric studies of slopes, ridges and canyons. They concluded that ground vibration is generally amplified at the crest of ridges, at the upper corner of slopes and at the edges of canyons, but that ground vibration is reduced at the base of the different features. Gatmiri and Arson [21] investigated, by means of the FE method in the near-field and the BE method in the far-field, seismic effects due to the topography and the geotechnical characteristics of valleys. They found that horizontal displacements tended to be amplified at the edge and reduced at the centre of empty valleys, but that the horizontal displacements tended to be reduced near the edge and amplified at the centre in the case of sedimentary valleys. Duzgun and Budak [22] investigated the effects of canyon-shaped topographies on ground vibration by the use of a finite and infinite element method. They found that both the topography and the geotechnical properties have an appreciable effect on the ground vibration occurring along a canyon.

Beskou and Theodorakopoulos [23] investigated various ways of modelling a road pavement, foundation soil, loads and material behaviour. Analytical and numerical methods, as well as combinations of them were considered under both plane strain and 3D conditions. It was concluded that the FE method appears to be the best numerical method with respect to efficiency, versatility and availability without compromising on accuracy.

Some general conclusions from the papers referred to above can be drawn. In case of seismic waves, topographic features could affect the wave propagation by either amplifying or reducing the level of vibration. The effects on the vibration levels depend on the topography, also the presence of several topographic features may affect the wave propagation near the ground surface.

None of the investigations referred above considered the characteristics of the traffic loads to be expected. Also, none of them explored the usefulness of shaping the surrounding landscape so as to construct a wave obstacle with the intention of reducing incident ground vibrations.

1.2. The present study

The main objective of the present study was to investigate the use of shaped landscapes (man-made ground surface irregularities) as wave obstacles for minimising traffic-induced vibrations in vibration-sensitive parts of a high-tech facility such as the MAX IV one. Investigating this here was done by creating FE models for predicting the effectiveness of using a shaped landscape as a wave obstacle. The FE models employed was applied both to the soil layer and to the bedrock. The vibrations involved were investigated in the frequency domain by means of steady-state analyses, the traffic load on the motorway being taken into account in the analyses. The intention here was to extend the knowledge of the use of shaped landscapes as wave obstacles. Some preliminary calculations were made in cooperation with the former master thesis student Jørstad [24].

The general knowledge of the reduction in the vibration level achieved by the use of a shaped landscape needs to be extended so as to encompass traffic-induced vibrations from motorways, generally, to make it possible to meet the increasing needs in the future of placing buildings closer to vibration sources.

2. Governing theory

2.1. Structural dynamics

The equation of motion of a body, assuming small deformations, can be described by the differential equation

$$\tilde{\nabla}^T \boldsymbol{\sigma} + \mathbf{b} = \rho \frac{\partial^2 \mathbf{u}}{\partial t^2} \tag{1}$$

where $\tilde{\nabla}$ is a differential operator matrix, $\boldsymbol{\sigma}$ is the stress vector, $\mathbf{b}$ the body force vector, ρ the mass density, $\mathbf{u}$ the displacement vector and t is time [25,26]. The governing finite element formulation of a dynamic problem, as derived from Eq. (1), can be written as

$$\mathbf{M\ddot{u}} + \mathbf{C\dot{u}} + \mathbf{Ku} = \mathbf{f} \tag{2}$$

where $\mathbf{M}$ is the mass matrix, $\mathbf{C}$ the damping matrix, $\mathbf{K}$ the stiffness matrix, $\mathbf{f}$ the load vector and $\mathbf{u}$ the nodal displacement vector. In harmonic loading, steady-state vibration occurs. The load and the corresponding displacements can be expressed, therefore, as complex harmonic functions

$$\mathbf{f} = \hat{\mathbf{f}} e^{i\omega t}; \quad \mathbf{u} = \hat{\mathbf{u}} e^{i\omega t} \tag{3}$$

where $\hat{\mathbf{f}}$ and $\hat{\mathbf{u}}$ denote the complex load amplitude and the displacement amplitude, respectively, i is the complex number involved and ω is the angular frequency. Inserting Eq. (3) into Eq. (2) results in the following equation of motion in the frequency domain:

$$\mathbf{D}(\omega)\hat{\mathbf{u}} = \hat{\mathbf{f}} \tag{4}$$

where $\mathbf{D}$ is the frequency-dependent dynamic stiffness matrix, which can be expressed as

$$\mathbf{D}(\omega) = -\omega^2 \mathbf{M} + i\omega \mathbf{C} + \mathbf{K}. \tag{5}$$

Since damping generally plays an important role in the dynamic response in soils and therefore has to be included to obtain realistic output from the calculations, a damping in the system was assumed. Rate-independent damping model has been found to provide good approximation to the realistic behaviour of soils. The loss factor which represents the attenuation of the propagating waves is defined as

$$\eta = \frac{1}{2\pi} \frac{E_D}{E_{So}} \tag{6}$$

where in a steady-state, the energy dissipated in the form of viscous damping in a given cycle of harmonic vibration being denoted as E_D and the strain energy as E_{So} [27]. E_D can be written as

$$E_D = \pi c \omega u_0^2 \tag{7}$$

where c is the damping constant, u_o is the amplitude of the motion and E_{S_o} can be written as

$$E_{S_0} = k u_0^2 / 2 \tag{8}$$

where k is the stiffness. Inserting Eqs. (7) and (8) into Eq. (6) gives

$$\eta = \frac{\omega c}{k}. \tag{9}$$

In generalising this to multiple degrees of freedom (dofs), Eq. (9) can be written as

$$\mathbf{K}\eta = \omega \mathbf{C}. \tag{10}$$

Inserting Eq. (10) into Eq. (5) results in

$$\mathbf{D}(\omega) = -\omega^2 \mathbf{M} + (1 + i\eta)\mathbf{K}. \tag{11}$$

The imaginary part of the stiffness matrix is referred to as the structural damping matrix [28].

2.2. Evaluation

The RMS value can be used as a measure of the vibration magnitude. The RMS value of the displacements obtained from the steady-state analyses was determined by

$$u_{RMS} = \frac{1}{n}\sqrt{(u_1^2 + u_2^2 + \cdots + u_n^2)} \tag{12}$$

where u_{RMS} is the RMS value of the displacements, u_i is the magnitude of the displacement at each frequency and n is the number of frequencies in the interval.

3. Traffic load and evaluation

Several factors need to be considered in investigating traffic loads such as the speed and weight of passing vehicles, as well as irregularities of the road and inhomogeneous soil conditions [4]. Traffic-induced ground vibrations are transmitted as both body and surface waves.

The vibration requirements for MAX IV are especially strict within a frequency span of 5–100 Hz, and various studies of the MAX IV site [1–3] have concluded that vibration source frequencies exceeding 25 Hz have only a negligible effect on the amplitudes of vibrations in the facility. From the initial simulations in the present study, it was found that the limit of 25 Hz can be lowered to 20 Hz, due to the ground material parameters being slightly different here compared to the values in the studies [1–3]. The soil of the present studied location has lower elastic modulus and higher damping than the one in the mentioned studies, the lowering of the limit was therefore possible. Thus, a frequency span of 5–20 Hz for the traffic load was considered. The frequency content of the traffic load at the motorway near MAX IV was evaluated on the basis of green-field in-situ measurements; see Fig. 2 for a schematic presentation of the measurement setup. Velocity versus time was measured at the top of the slope of the road embankment of the motorway during the passage of trucks, which generated the highest velocities at the measuring point. The ten events having the highest velocity amplitudes, caused by heavy trucks at a speed of approximately 80–90 km/h, during a 1-h period were registered. The displacements involved, $U(t)$,
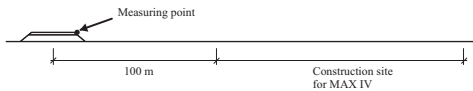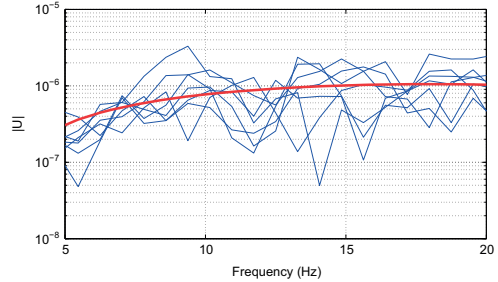

Fig. 2. Schematic measurement setup.

Fig. 3. The magnitude spectrum of $U(t)$, as obtained on the basis of measurements.

were evaluated and a Fast Fourier Transform (FFT) of the displacement–time curves was performed to determine the frequency content of the response at the embankment. Since high frequencies are damped out quickly in the soil, the measurements on the embankment do not have the same frequency content as the traffic load. However, in the frequency range of interest (below 20 Hz) this difference in location was assumed to have only a negligible effect on the frequency content of the load because of the distances between the load (the truck wheels) and the embankment being so short. A second-degree polynomial was fitted well to the experimental data; see Fig. 3, the second-degree polynomial, normalised by its largest magnitude, being considered to be representative of the frequency content of the traffic load.

Distributed evaluation points were used to calculate an average displacement reduction factor, see Eq. (14). It was used as a measure of the effectiveness of the shaped landscape as a wave obstacle. The displacement reduction factor, U_{red}, pertains to the relationship of the vertical vibrational amplitude after a shaped landscape has been introduced (post-shaped landscape), U_{post}, to the amplitude prior to its being introduced (pre-shaped landscape), U_{pre}, in accordance with Eq. (13). U_{pre} and U_{post} were determined on the basis of the complex displacement magnitudes for the different frequencies, these being calculated as the RMS values at the evaluation points, in accordance with Eq. (12)

$$U_{red} = \frac{U_{pre} - U_{post}}{U_{pre}}. \tag{13}$$

$$\overline{U}_{red} = \frac{1}{n}\sum_{i=1}^{n} U_{red,i} \tag{14}$$

where n is the number of evaluation points.

For traffic-induced ground vibrations, strains are usually at a level such that the assumption of linear elasticity is applicable, in the case of soil and of bedrock, $\mathbf{M}$, $\mathbf{C}$ and $\mathbf{K}$ thus being constant matrices. With the use of a system of linear equations, the frequency content of the traffic load can be employed for scaling the calculated displacements in order to account for the traffic load.

4. Material parameters considered

In the example case studied here, that of the synchrotron facility MAX IV, the soil between the motorway and the facility consisted of 14 m of a clay till and the bedrock consisted of shale, sandstone and limestone. The soil in the hills was assumed to have the same material properties as the soil prior to its being excavated. Note that it may be difficult to compact the soil in such a way that the original material parameters applies, such as the density and the elastic modulus, after reshaping the landscape.

Local variations in the soil layer and the bedrock, such as stratum and granularity, were assumed to be small as compared with the wavelengths in the frequency range of interest. Thus, the soil and the bedrock were modelled as being isotropic homogenous materials. The material parameters employed here were evaluated by FE simulations of geotechnical and geophysical measurement data that were obtained at the MAX IV site in collaboration with the companies *PEAB*, *TYRÉNS* and *NGI*, see Table 1 [29]. The loss factors include material damping and attenuation effects due to the varying topography of the soil and of the bedrock.

5. A two-dimensional parametric study

A 2D parametric study of shaped landscapes was carried out for differing geometric parameters of the shapes involved. The height (depth) of the hills (valleys), their width and the total number of shapes in the landscape considered were varied. The shapes and the configurations of them are described in detail in Subsection 5.2.

5.1. The finite element model

The geometry was that of 14 m of soil and 200 m of bedrock, see Fig. 4. The FE model involved the use of a harmonic point load, $f(t)$, applied to the middle of the modelled ground surface, its representing the traffic from the nearby motorway, see Fig. 4. The harmonic load was applied for frequencies of 5–20 Hz in steps of 0.5 Hz. To determine the effectiveness of a shaped landscape evaluation points were used to evaluate the displacements present where MAX IV is being built. The main evaluation point was located 10 m from the shaped zone (100 m from the excitation point), see Fig. 4. An additional evaluation point was introduced to ensure that the response obtained at the main evaluation point was not a local phenomenon. A 2D FE model was developed with the use of the FE software package *HyperWorks 11.0* [30]. The size of the model was 214×560 m^2 (height(z) × width (x)). The distances from the region of interest to the boundaries were large, in

order to avoid disturbing reflections at the boundaries. Quadrilateral 4-node plane strain elements with linear approximation were employed. To ensure that the analyses provided results of adequate accuracy, an element mesh with a minimum of seven element nodes that represented the shortest wavelengths were employed. The element size was set to 2×2 m^2 so as to be able to describe accurately the geometry of the hills and valleys in the shaped landscape, the same size being used throughout in the FE model. The model contained approximately 30,000 elements with approximately 60,000 dofs.

5.2. Configuration of shapes

The shapes were located in a zone 80 m wide, starting 10 m after the excitation point had been passed and ending 10 m before the evaluation point was reached, see Fig. 4. The constant curvature of the various shapes, the maximum slope angle being one of $30°$, served as a constraint. This constraint was employed with the idea that the shapes were to be retained over an extended period of time. The number of shapes was varied across the 80 m wide zone, there being one to six shapes introduced. The shaped landscapes studied consisted of a configuration of different shapes. In Fig. 5, the basic geometry that applied to each of the shapes in the configuration is shown, the dimensions of each of the shapes being shown in Table 2. Note that the height, h, could just as well be used to describe the opposite, i.e. the depth of the valleys involved (Table 3).

In order to indicate whether a given shape is to be regarded as creating a hill or a valley, a notation of [X X X X] was introduced, where the number of Xs denotes the number of shapes in a given configuration, and where X was either H or V, H denoting a hill and V a valley. A geometric scale factor was used to scale the height of the shapes in a given configuration. This factor was varied between 0.25 and 1 in steps of 0.25. An extra notation, [Y], was introduced so as to be able to denote the geometric scale factor in the form [Y][X X X X], where [0.75][H V H V], for example, implies the geometric scale factor to be 0.75 applied to a configuration of four shapes that began with a hill, and was followed by a valley, then a hill and finally a valley.

For additional examples of the notation of the configurations of the different shapes, see the configuration in Figs. 6 and 7.

Table 1
Material parameters.

Property	Soil	Bedrock
Density (kg/m^3)	2125	2600
Elastic modulus (MPa)	476	8809
Loss factor	0.14	0.04
Poisson's ratio	0.48	0.40
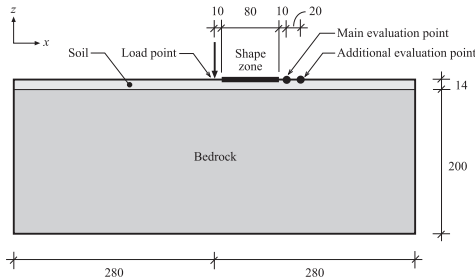
Fig. 4. FE model. Dimensions, materials, location of the excitation point, evaluation points and the zone where the shapes were employed are shown. The dimensions are in units of meters.

Fig. 5. Geometry of one shape. The width (l), the height (h) and the maximum slope are indicated.

Table 2
Width and maximum height of each shape in a configuration.

Configuration	Width, l (m)	Height, h (m)
1 shape	80.0	10.7
2 shapes	40.0	5.36
3 shapes	26.7	3.57
4 shapes	20.0	2.89
5 shapes	16.0	2.14
6 shapes	13.3	1.79

Table 3
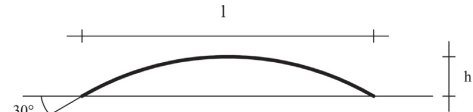The configurations that were analysed, involving geometric scale factors (pertaining to the height) of 1, 0.75, 0.5 and 0.25.

Configuration	1 shape	2 shapes	3 shapes	4 shapes	5 shapes	6 shapes
Only hills	[H]	[H H]	[H H H]	[H H H H]	[H H H H H]	[H H H H H H]
Alternating hills and valleys		[H V]	[H V H]	[H V H V]	[H V H V H]	[H V H V H V]
Alternating hills and valleys		[V H]	[V H V]	[V H V H]	[V H V H V]	[V H V H V H]
Only valleys	[V]	[V V]	[V V V]	[V V V V]	[V V V V V]	[V V V V V V]
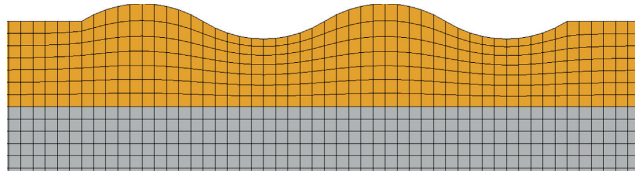
Fig. 6. The configuration of four shapes having the geometric scale factor of 1, [1][H V H V]. The full extension of the soil and of the bedrock is not shown.
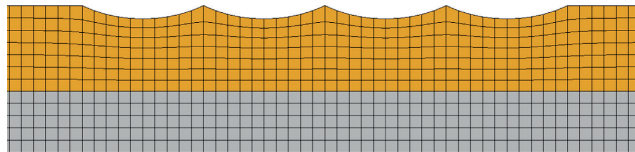
Fig. 7. The configuration of four shapes having the geometric scale factor of 0.75, [0.75][V V V V]. The full extension of the soil and of the bedrock is not shown.

5.3. Results

Fig. 8 presents simulation results concerning the vertical displacements produced in connection with a configuration consisting of two shapes, [1][V H], at a frequency of 9.5 Hz. As is shown, the level of vibration is lower, at the main evaluation point, after the vibrations have passed through the shaped landscape than it is at the same distance on the other side of the excitation point. It can also be seen that the shaped landscape directs waves into the bedrock.

In Fig. 9, the frequency response spectrum for the configurations [1][H V] and [1][V H], is shown as examples, as well as the frequency response spectrum for a flat landscape. In the figure it is shown that there is a resonance peak in the ground at around 9, 12 and 18 Hz, considering the frequencies of interest (5–20 Hz).

The degree of reduction (and amplification) in the level of vibration for different number of shapes and different geometric scale factors for only hills and only valleys is shown in Fig. 10. As can be seen, for three or more shapes, up to six at least (when there are only hills or only valleys), the behaviour shown is quite similar in each case. Valleys with a geometric scale factor of 1 (the same as hills with a geometric scale factor of −1) have the largest amplification (which is the same as the largest negative reduction) in the level of vibration. Also, the level of amplification in the vibration level achieved is decreased when the value of the geometric scale factor approaches zero. The degree of reduction in the level of vibration for positive values of the geometric scale factor (hills) is, in general, increased when the value of the scale factor increases.

In Fig. 11, a tendency for the degree of reduction in the level of vibration to decrease as the number of shapes increases can be noted. The plot also shows the complexity of drawing general conclusions, a matter which is especially clear in the case of three shapes (for which the difference in the level of reduction that can be seen are immense).

Fig. 12 illustrates how a configuration of hills alone generally results in an appreciably larger reduction in the level of vibration than a configuration of valleys alone produce. Also, a configuration of only one shape deviates from the other numbers of shapes considered here, this illustrating the complexity of drawing general conclusions, especially in the case of three or fewer shapes.

In Table 4, the 10 most effective configurations of 2D shapes, in terms of their reduction of vibrations, are shown. The two most effective configurations consist of two shapes, a valley followed by a hill. Four of the five most effective configurations of shapes consist of two shapes, the one a hill and the other a valley, employed in an alternating manner. None of the top five configurations consisted of more than two shapes. Eight of the nine most effective configurations consisted of alternating hills and valleys (the configuration of one shape was the one that deviated). The most effective configuration, [1][V H], reduced the vibration level by 22.1%.

The 10 least effective configurations of 2D shapes in terms of reducing vibrations are shown in Table 5. All of these configurations consist of valleys only, each of them resulting in an amplification of the level of vibration. The least effective configuration for each of the different numbers of shapes involved was a configuration of valleys only (Table 6).

All the configurations involving an even number of shapes (2, 4 or 6 shapes) and alternating hills and valleys that started out with a valley were just as effective or more effective than those that started out with a hill. For configurations of five or six shapes, the most effective configurations were those involving hills only, something that was not found to be the case for configurations of fewer shapes. For configurations of two or more shapes, the presence of only valleys led to an amplification of the vibration level, regardless of the geometric scale factor that was applied. Generally speaking, configurations having more valleys than hills showed an amplification in the level of vibration (though not in
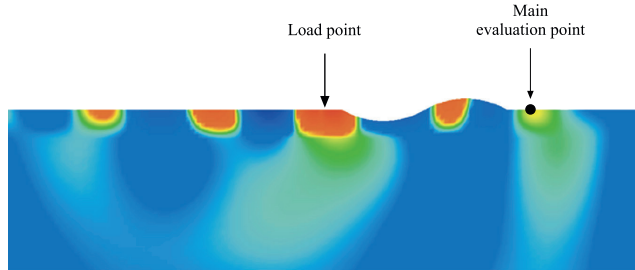
Fig. 8. Simulation results for the magnitude of the vertical displacements found at 9.5 Hz for the configuration [1][V H]. The blue colour corresponds to the minimum value (zero) and the red colour to the maximum value.
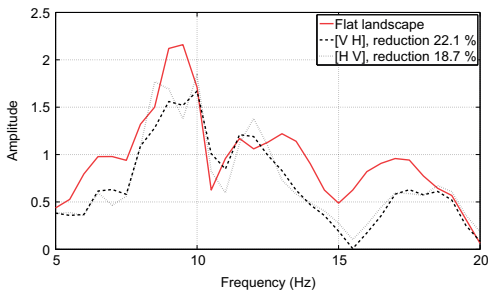
Fig. 9. A frequency response spectrum for two different configurations and for a flat landscape, the configurations involved having a geometric scale factor of 1.
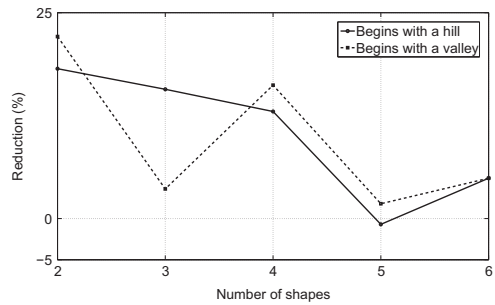
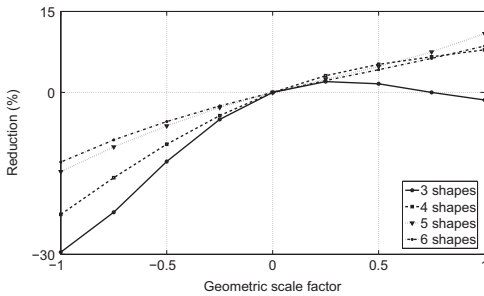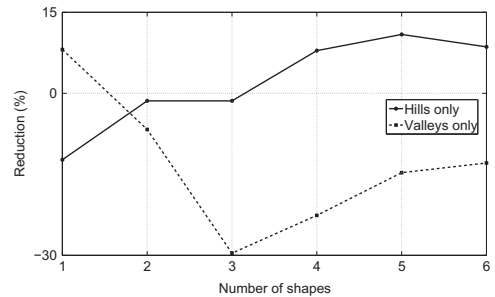**Fig. 11.** The degree of reduction (amplification is shown as a negative reduction) in the level of vibration in the case of alternating hills and valleys, beginning with a hill and with a valley. A geometric scale factor of 1 is employed here.

Fig. 10. The degree of reduction (amplification is shown as a negative reduction) in the level of vibration in the case of only hills and only valleys (valleys are denoted by use of a negative geometric scale factor).

Fig. 12. The degree of reduction (amplification is shown as a negative reduction) in the level of vibration for only hills and only valleys. A geometric scale factor of 1 is employed here.

the case of a configuration involving only one shape). This emphasises how important it is to be careful, in designing a shaped landscape, to make the correct decision regarding whether to employ a hill or a valley. In configurations containing only a valley, a reduction in the vibration level was achieved with use of a geometric scale factor of 0.75 or more.

The level of vibration was also evaluated at an additional evaluation point that was located 10 m from the main evaluation point, i.e. 20 m from the shaped zone and 110 m from the excitation point, for each of the configurations involving use of a

geometric scale factor of 1. The responses at the additional evaluation point were found to show basically the same tendencies as those at the main evaluation point.

6. A three-dimensional parametric study

A 3D parametric study of shaped landscapes for differing geometric parameters of the shapes involved was carried out. The height (depth) of the hills (valleys), their width and the numbers of

Table 4
The 10 most effective 2D configurations in terms of reducing the level of vibration (displacement).

Configuration	Reduction (%)
[1][V H]	22.1
[0.75][V H]	20.7
[0.75][V]	19.1
[1][H V]	18.7
[0.75][H V]	17.9
[1][V H V H]	16.2
[1][H V H]	15.7
[1][H V H V]	13.0
[0.75][H V H]	12.8
[1][H H H H]	10.9

Table 5
The 10 least effective configurations of 2D shapes in terms of amplifying the level of vibration (displacement). Amplification is shown as a negative reduction.

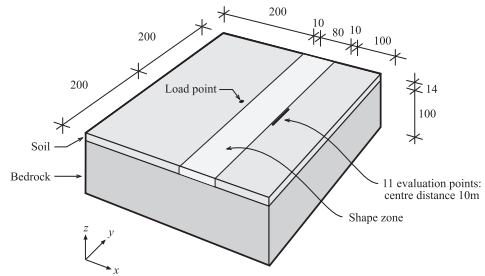| Configuration	Reduction (%)
[1][V V V]	−29.6
[1][V V V V]	−22.6
[0.75][V V V]	−22.2
[0.75][V V]	−21.3
[0.5][V V]	−19.1
[0.25][V]	−18.6
[0.75][V V V V]	−15.8
[1][V V V V V]	−14.7
[1][V V V V V V]	−12.9
[0.5][V V V]	−12.8

Table 6
The analysed configurations of straight shapes and of rotated shapes, as well as the analysed chequered configurations of shapes.

Configuration	2 shapes	3 shapes	4 shapes
Only hills	[H H]	[H H H]	[H H H H]
Alternated hills/valleys	[H V]	[H V H]	[H V H V]
Alternated hills/valleys	[V H]	[V H V]	[V H V H]
Only valleys	[V V]	[V V V]	[V V V V]

Fig. 13. The FE model, showing the dimensions and the materials involved, the location of the excitation point and the locations of the evaluation points, and the zone in which the different shapes were employed. The dimensions are given in units of meters.

Fig. 14. Examples of different configurations: (a) a configuration of four straight shapes, [H H H H], (b) a configuration of four rotated shapes, [H V H V] and (c) a chequered configuration of four shapes, [H V H V].
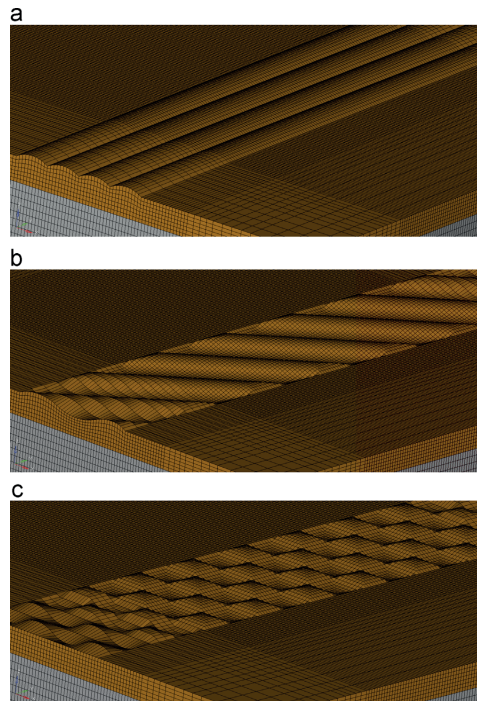
shapes in the landscape were varied. Use of 3D FE models also allowed the traffic load to be applied as a point load rather than as a line load as it is in the case of 2D plain strain models. The shapes employed and the types of configuration of them involved are described in detail in Subsection 6.2 configuration of shapes.

6.1. The finite element model

A 3D FE model was developed with use of the FE software package *HyperWorks 11.0* [30]. The size of the model was $400 \times 400 \times 114 \text{ m}^3$ ($x \times y \times z$)). In the z-direction, the geometry was that of 14 m of soil and 100 m of bedrock, see Fig. 13. It was seen to it that the distances from the region of interest to the boundaries were large throughout, in order to avoid occurrence of disturbing reflections at the boundaries. Quadrilateral 8-node hexahedron solid elements with linear approximation were employed. To ensure that the analyses provided results of adequate accuracy, an element mesh with a minimum of seven element nodes representing the shortest wavelengths were employed. The element size was set to $2 \times 2 \text{ m}^2$ in the shape zone, in order to be able to describe accurately the geometry of the hills and valleys in the shaped landscape. The model was meshed symmetrically in the horizontal (x–y) plane, the x–z-plane and the y–z-plane being the planes of symmetry. An element size of 2×2

m^2 was employed in the x–y plane, in a 120 m long zone stretching from the excitation point on through zones of increasing element size (four elements having an element length of 4 m, followed by four elements having an element length of 6 m, and finally four elements with an element length of 10 m). In the vertical (z) direction, use was made of elements 2 m in length in the soil, in the bedrock the first eight elements in the vertical direction each

being 4 m in length, these being followed by six elements each 6 m in length, and then by four elements each 8 m in length. The FE mesh can be seen in Fig. 14. Since the bedrock is much stiffer than the soil, which contributes to the longer wavelengths in the bedrock, the element sizes in the bedrock were larger than the element sizes in the soil. The model contained approximately 518,000 elements, and it is having approximately 1,700,000 dofs.

The FE model involved the use of a harmonic point load, $f(t)$, applied to the centre of the modelled ground surface, representing the traffic from the nearby motorway, see Fig. 13. The harmonic load was applied for frequencies of 5–20 Hz, in steps of 1/3-octave bands (5, 6.3, 8, 10, 12.5, 16 and 20 Hz).

For determining the effectiveness of a shaped landscape in 3D terms, use was made of several evaluation points in evaluating the displacements at the MAX IV site. The main evaluation point was located 10 m from the shaped zone (and 100 m from the excitation point), see Fig. 13. Because of the scattering of the propagating waves when considered in 3D terms, the displacements were evaluated along a straight line, see Fig. 13. A total of 11 evaluation points, with a distance of 10 m between successive ones, were placed along this line, the main evaluation point in the middle corresponding to the shortest distance to the excitation point. In comparing the results obtained from the 3D analyses with the values obtained for the 2D analyses, the use was made of the main evaluation point in the 2D analyses and the corresponding main evaluation point in the 3D analyses.

6.2. Configuration of shapes

In the same manner as for the configuration of 2D shapes, the shapes here were employed in a zone 80 m wide, starting 10 m after the excitation point had been passed and ending 10 m before the evaluation point was reached, see Fig. 13. A constant curvature of the shapes, as well as a maximum slope angle of 30°, served as geometric constraints here, just as for the 2D shapes. The number of shapes was varied, between the use of two and four different shapes over the 80 m wide zone, each of the shaped landscapes studied consisting of a configuration of different shapes. The geometry of each shape in the configuration is shown in Fig. 5, and the dimensions of each of the shapes in Table 2. Note that the height, h, here just as in the case of the 2D shapes, could just as well be directed in the opposite direction, i.e. for denoting the depth of a valley. The 3D shapes here followed the same name conventions as in the study of 2D shapes. In this 3D study, only a geometric scale factor of 1 was considered.

Three different types of configurations were investigated: straight shapes, rotated shapes and a chequered configuration of shapes, see Fig. 14. A configuration of straight shapes corresponded, geometrically, to a configuration of 2D shapes, since the 2D shapes were extended in the out-of-plane direction. In the configurations of rotated shapes, the shapes were rotated 45° in the horizontal (x–y) plane in relation to the straight shapes. The chequered configuration of shapes was the one that in geometric terms resembled the architect-designed landscape the most, see Fig. 1.

6.3. Results

In all of the configurations, an appreciable reduction in the level of vibration could be found. The results obtained are presented in three separate subsections, each dealing with a different type of configuration.

6.3.1. Configurations of straight shapes

For the simulation results, it was found that a part of the wave entered the first hill that was reached, its then being reflected

along inside the hill. This was a particular reason for investigating rotated shapes, in an attempt to guide the waves. This can be seen in Fig. 15a.

The frequency response spectrum for configurations of alternating hills and valleys involving two, three and four shapes,

Fig. 15. Different subfigures concerning the result of configurations of straight shapes. (a) Simulation results for the magnitude of the vertical displacements connected with a configuration of three shapes, [H V H], the blue colour corresponds to the minimum value (zero) and the red colour to the maximum value. (b) A frequency response spectrum for each of three different configurations, as well as the frequency response spectrum for a flat landscape. (c) The degree of reduction in the level of vibration for cases of alternating hills and valleys, beginning in the one with a hill and in the other one with a valley.

Table 7
Reduction and amplification in the level of vibration for different configurations of straight shapes. Amplification is shown as a negative reduction.

2 shapes	Reduction (%)	3 shapes	Reduction (%)	4 shapes	Reduction (%)
[H H]	2.4	[H H H]	− 5.2	[H H H H]	− 2.8
[H V]	19.6	[H V H]	10.5	[H V H V]	17.3
[V H]	20.9	[V H V]	23.8	[V H V H]	22.8
[V V]	− 19.4	[V V V]	− 70.0	[V V V V]	− 58.4

respectively, is shown in Fig. 15b, in which use is made of the main evaluation point. The degree to which a reduction in the level of vibration was achieved is shown in the legend of the plot. As can be seen, the degree of reduction in cases of the three types was somewhat similar, although there was a clear difference between the response for the four shapes configuration and the other two configurations, especially at 10 Hz. Also, of the three types of configurations shown, it is the one with four shapes that resembles the flat landscape most closely in terms of the response spectrum.

In Fig. 15c, as one can see, there is a larger reduction in the vibration level for configurations that begin with a valley than for those that begin with a hill, the difference here is valid for the shapes involved within the range of two to four shapes, at least.

In Table 7, the degree of reduction or amplification in the level of vibration occurring for each of the different configurations of straight shapes examined is shown. As can be seen, a stronger effect on the degree of reduction achieved in the vibration level occurring was found for configurations that began with a valley than in those that began with a hill. Configurations of valleys alone showed an appreciable amplification in the level of vibration that occurred, whereas configurations of hills alone showed only a slight effect on the vibration level. The most effective configuration of shapes was one consisting of three shapes, with alternating hills and valleys, beginning with a valley. The reduction in the level of vibration there was found to be one of 23.8%. Configurations of alternating hills and valleys starting out with a valley were found to be the most effective configurations, regardless of the number of shapes included in the configurations, all such configurations resulting in an appreciable reduction in the level of vibration. Configurations of valleys only were found to be the least effective, all of them resulting in an appreciable amplification in the vibration level.

6.3.2. Configurations of rotated shapes

In the configurations of rotated shapes the incident waves had a different incident angle than in the configurations of straight shapes. The horizontally rotated shapes here were different from the straight shapes in being non-symmetrical in the x–z-plane. This resulted in the responses at the different evaluation points varying, depending upon at which side of the main evaluation point they were located, see Fig. 16a. For some configurations, reduction in the level of vibration on the one side and amplification on the opposite side were found. These differences were expected, however, since the phenomenon of the waves being guided by hills was observed already for the straight shapes. Fig. 16b shows the frequency response spectrum for a configuration of alternating hills and valleys, three shapes being shown for two different evaluation points. One of the evaluation points was located at the same level on the y-axis as the load point, and the other evaluation point was located 40 m from it in the positive direction of the y-axis. The degree of reduction or amplification in the vibration level that was achieved is shown in the legend of the plot. One can note that at the main evaluation point ($y=0$) an appreciable reduction in the level of vibration was attained, whereas at the other evaluation point ($y=40$ m) there was an appreciable degree of amplification. The rotated shapes behaved as waveguides, meaning that the degree both of reduction and of amplification achieved in the vibration level was very sensitive to the evaluation point selected.

Fig. 16c shows there to be a significant greater reduction in the level of vibration for configurations that begins with a valley, as shown for various numbers of shapes involved. As can be seen, in the case of two-shape configurations in particular, there is a much larger degree of reduction for a configuration that starts off with a
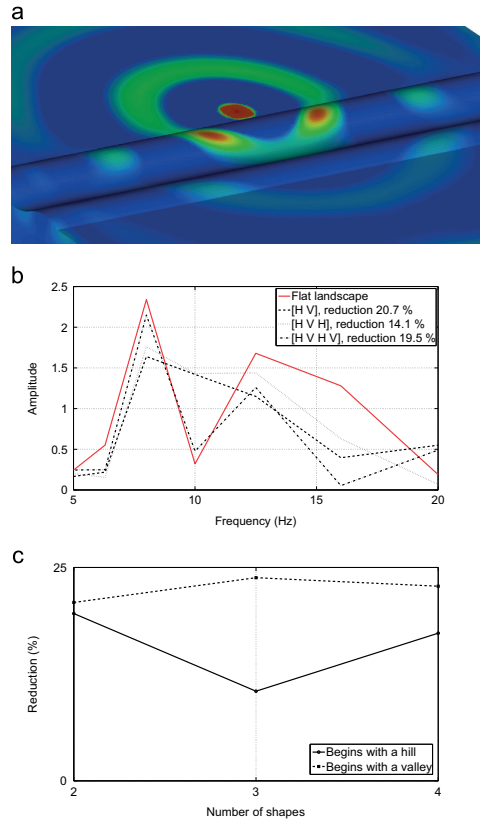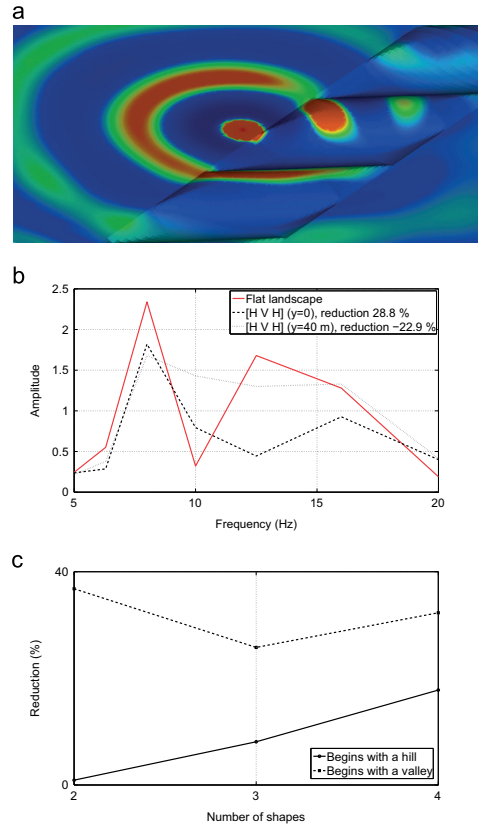

Fig. 16. Different subfigures concerning the result of configurations of rotated shapes. (a) Simulation results for the magnitude of the vertical displacements in a configuration consisting of two shapes, [H V], the blue colour corresponds to the minimum value (zero) and the red colour to the maximum value. (b) A frequency response spectrum for two different configurations of shapes, as well as the frequency response spectrum for a flat landscape. Amplification being shown as negative reduction. (c) The degree of reduction in the level of vibration in cases of an alternation of hills and valleys, one set of cases beginning with a hill and the other beginning with a valley.

Table 8
Reduction and amplification in the level of vibration for the configurations of rotated shapes. Amplification is shown as a negative reduction.

2 shapes	Reduction (%)	3 shapes	Reduction (%)	4 shapes	Reduction (%)
[H H]	− 1.4	[H H H]	− 3.3	[H H H H]	− 8.9
[H V]	0.9	[H V H]	8.1	[H V H V]	17.8
[V H]	36.8	[V H V]	25.8	[V H V H]	32.3
[V V]	− 10.8	[V V V]	− 49.2	[V V V V]	− 56.3

valley than for one that starts off with a hill. One that started off with a valley was found to generate a very appreciable reduction in the level of vibration, whereas one that started off with a hill was found to have only a very slight effect on the degree of reduction that was achieved in the vibration level.

The reduction and the amplification of the level of vibration for configurations of rotated shapes are shown in Table 8. As can be seen, configurations of hills only had only a slight effect on the degree of amplification achieved in the vibration level. The most effective configuration of shapes was found to be one of the two shapes in which there were alternating hills and valleys, beginning with a valley. The reduction in the level of vibration there was found to be 36.8%. Configurations of alternating hills and valleys starting out with a valley were found to be the most effective configurations, regardless of the number of shapes that were included in the configuration, each of the numbers involved resulting in an appreciable reduction in the vibration level. Configurations of valleys only were found to be the least effective configurations, all of them resulting in an appreciable amplification in the level of vibration.
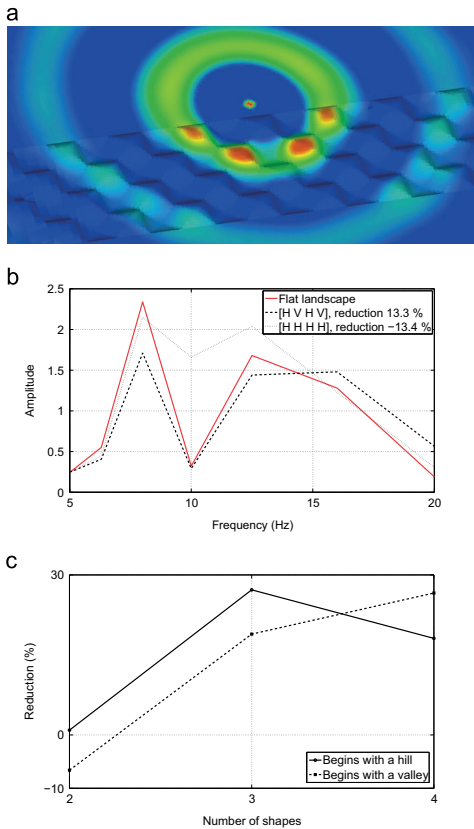
6.3.3. Chequered configurations of shapes

On the basis of the simulation results, it could be seen that configurations of four shapes with alternating hills and valleys created more obvious diagonals made up of hills, into which the waves were guided, than was the case for constellations of fewer shapes, analogous to the results obtained for rotated shapes, see Fig. 17a.

The frequency response spectrum for each of two chequered configurations of four shapes, the one of them with alternating hills and valleys and the other with hills alone, is shown in Fig. 17b. Use is made of the main evaluation point here. The degree of reduction in the level of vibration achieved is shown in the legend of the plot. As can be seen, there are appreciable differences between the two configurations, both in the degree of reduction achieved in the vibration level and in the response obtained. Also, the response that the configuration of hills alone produces resembles most the response to a flat landscape.

Table 9
Reduction and amplification, respectively, in the level of vibration in different chequered configurations of shapes. Amplification is shown as a negative reduction.

2 shapes	Reduction (%)	3 shapes	Reduction (%)	4 shapes	Reduction (%)
[H H]	10.9	[H H H]	−8.8	[H H H H]	−10.2
[H V]	0.9	[H V H]	27.2	[H V H V]	18.1
[V H]	−6.6	[V H V]	18.9	[V H V H]	26.6
[V V]	−44.9	[V V V]	−54.7	[V V V V]	−42.0

Fig. 17. Different subfigures concerning the result of chequered configurations of shapes. (a) Simulation results for the magnitude of the vertical displacements in a configuration consisting of four shapes, [H V H V], the blue colour corresponds to the minimum value (zero) and the red colour to the maximum value. (b) A frequency response spectrum for two different configurations of shapes, as well as the frequency response spectrum for a flat landscape. Amplification being shown as negative reduction. (c) The degree of reduction (amplification being shown here as negative reduction) in the level of vibration for cases of alternating hills and valleys, those beginning with a hill and those beginning with a valley.
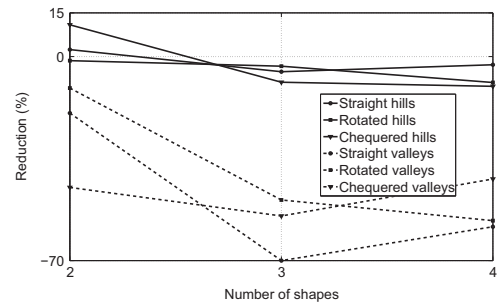

Fig. 18. The degree of reduction (amplification being shown as negative reduction) in the level of vibration for different configurations of hills only and of valleys only, all three types of configurations being involved.
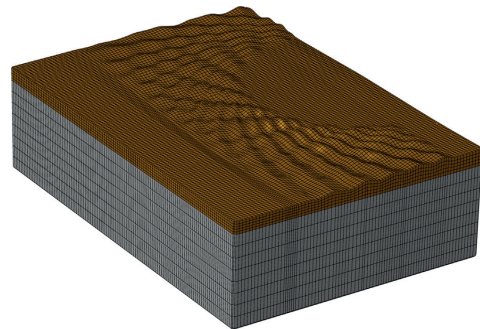

Fig. 19. The FE mesh of the architectural landscape design.

In the case of a chequered configuration with alternating hills and valleys, a hill (or a valley) has neighbouring valleys (or hills). This means that it is only a part of the wavefront that hits a hill (or a valley) first, since on each side the wave front hits a valley (or a hill). This can explain why the difference in the degree of reduction in the level of vibration is no greater than it is in the case of the wavefront hits a hills first compared to a valley first. The results for configurations that begin with a valley being shown in Fig. 17c and also in Figs. 15c and 16c.

The degree of reduction and of amplification in the level of vibration for chequered configurations of shapes are shown in Table 9. As can be seen there, configurations of valleys only result in an appreciable amplification in the vibration level, for this reason they are being found to be the configurations that are the least effective. Configurations of hills only were found to have a lesser effect on the degree of amplification achieved in the level of vibration, than configurations of valleys only had, a reduction in the vibration level also being seen for two-shape configurations. Three- and four-shape configurations were found to be the most effective configurations in the case of alternating hills and valleys, whereas for two-shape configurations, those of hills alone were found to be the most effective ones. The most effective configuration was a three-shape one involving alternating hills and valleys, beginning with a valley. The reduction in the level of vibration there was found to be 27.2%.

In comparing the three different types of configurations, both of hills alone and of valleys alone, marked differences in the degree of reduction achieved between configurations of hills alone and valleys alone were found, as can be seen in Fig. 18.

7. Three-dimensional architectural design

The landscape architect bureaus within the MAX IV project created an architectural design (geometry) of a shaped landscape around the MAX IV facility, see Fig. 1. In the present investigation, the landscape design was extended to include the area between the motorway and the research facility, see Figs. 19 and 20. The architect-designed geometry was given to the authors in order for it to be analysed by the use of finite element software and evaluated from a vibration reduction point-of-view.
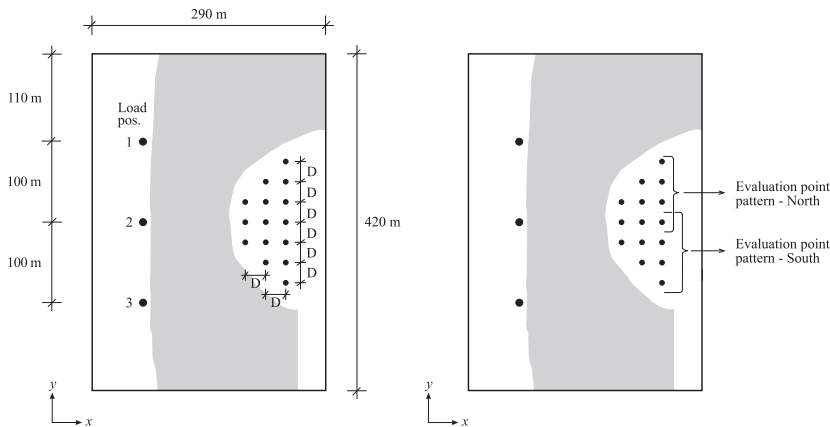
7.1. Finite element model

The shapes contained in the architectural landscape design have a rounded and natural form, which applied as well to the shapes considered in the parametric analyses. The maximum slope angle for the shapes was one of about 30°, similar to the shapes employed in the parametric studies. The hills had a height of up to about 5.5 m and the valleys a depth of approximately 2.5 m. Both measures concern the vertical distance to the initially flat ground surface. The maximum vertical distance between an adjacent hill and valley was approximately 6 m. The shortest width (distance in along the x-axis) of the shaped landscape was approximately 90 m, its being located at the same level along the y-axis as load position 2.

A 3D FE model was developed with the use of the FE software package *Abaqus 6.11* [31]. The model was $420 \times 290 \times 114$ m³ (length $(x) \times$ width $(y) \times$ height (z)) in size. In the z-direction, the geometry was that of 14 m of soil and 100 m of bedrock, see Fig. 19. Quadrilateral 20-node hexahedron solid elements obtained by quadric approximation using reduced integration being employed. To simulate far-field conditions and avoid reflecting boundaries, 12-node quadratic elements were used that use viscous absorbing boundaries [32]. In order to ensure that the analyses provided results of adequate accuracy, an element mesh with a minimum of seven element nodes representing the shortest wavelengths was employed. The element size in the soil was generally $4.5 \times 4.5 \times 4.5$ m³, so as to able to accurately describe the geometry of the hills and valleys in the shaped landscape. The bedrock was significantly stiffer than the soil, which contributed to long wavelengths being produced there, the element length in the z-direction being increased to 12.5 m in the bedrock. The model

Table 10
Reduction in the level of vibration for different patterns of evaluation points and load positions.

Evaluation point pattern	Load position 1 (%)	Load position 2 (%)	Load position 3 (%)
North	17.4	15.2	12.7
South	19.6	14.9	14.2
All	18.2	16.4	13.0

Fig. 20. (a) Load positions and the evaluation point pattern *All* are shown. Distance, $D=25$ m. (b) Evaluation point patterns *North* and *South* are shown. The grey shading shows the location of the shaped landscape.

contained approximately 60,000 elements with a total of approximately 700,000 dofs. See Fig. 19 for details regarding the FE mesh.

The FE model involved the use of a harmonic point load, representing the traffic from the nearby motorway. The traffic load was applied in three different load positions, so as to be able to investigate different regions of the shaped landscape in terms of its non-symmetric design, see Fig. 20a. The different load positions are each located approximately 10 m (in the direction of the x-axis) from where the shape landscape begins, just as in the parametric studies. Load position 2 corresponds to the position of the load in the 3D parametric study. The harmonic load was applied at frequencies ranging from 5 to 20 Hz in steps of 0.1 Hz.

To determine the effectiveness of the architectural landscape design, in terms of reducing the level of vibration, several evaluation points were used for evaluating the displacements that occurred. Three different patterns of evaluation points were employed. The pattern *All* included all the 15 evaluation points shown in Fig. 20a. The patterns *North* and *South* included 9 evaluation points each, see Fig. 20b. The first column of evaluation points is located approximately 20 m (in the direction of the x-axis) from the shaped landscape.

7.2. Results

The reduction in the vibration level obtained for different evaluation point patterns and load positions is shown in Table 10. One can note that the largest reductions in the level of vibration were for load position 1 and the lowest reductions were for load position 3, regardless of which evaluation point pattern was considered. The difference between load positions 1 and 3 in the degree of reduction achieved was one of approximately 5% for each of the evaluation point patterns. Thus, the shaped landscapes were more effective in the region between load position 1 and the construction site than between load position 3 and the construction site.

8. General conclusions

The degree of reduction in traffic-induced ground vibrations expected to be achieved by shaping the surrounding landscape of the high-tech facility MAX IV was investigated. The effects of the geometric parameters of such a shaped landscape were examined by means of parametric studies. An architectural design of a shaped landscape was investigated in terms of its effectiveness in terms of reducing ground vibrations.

On the basis of the results of these investigations, the following general conclusions can be drawn:

- The most effective shaped landscape, within each configuration, was the one consisting of alternating hills and valleys.
- The least effective shaped landscape (which resulted in amplification of the vibration level) within each configuration was the one consisting of valleys only.

The conclusions drawn can be used at an early stage of a construction project to improve the effectiveness of an architectural landscape design with the intention to reduce incident ground vibrations.

References

[1] Persson P. Analysis of vibrations in high-tech facility. Report TVSM-5164, Division of Structural Mechanics, Lund University, Lund, Sweden; 2010.

[2] Persson P, Persson K. Analysis of dynamic soil–structure interactions at high-tech facility. In: Eriksson A, Tibert G, editors. Proceedings of the 23rd Nordic seminar on computational mechanics (NSCM-23). Stockholm, Sweden; 2010.

[3] Persson P, Persson K, Sandberg G. Reduction of traffic-induced vibrations at high-tech facility using trenches. In: Freund J, Kouhia R, editors. Proceedings of the 24th Nordic seminar on computational mechanics (NSCM-24). Helsinki, Finland; 2011.

[4] Das BM, Ramana GV. Principles of soil dynamics. Stamford: Cengage Learning; 2011.

[5] FOJAB arkitekter Malmö, Hallenborgs gata 1A, 211 19 Malmö, Sweden; 2012.

[6] Snøhetta, Akershusstranda 21, N-0150 Oslo, Norway; 2012.

[7] Lee VW, Wu X. Application of the weighted residual method to diffraction by 2-D canyons of arbitrary shape. I. Incident SH waves. Soil Dyn Earthq Eng 1994;13:355–64.

[8] Lee VW, Wu X. Application of the weighted residual method to diffraction by 2-D canyons of arbitrary shape. II. Incident P, SV and Rayleigh waves. Soil Dyn Earthq Eng 1994;13:365–75.

[9] Zhou H, Chen X-F. A study on the effect of depressed topography on Rayleigh surface wave. Chin J Geophys 2007;50(4):1018–26.

[10] Mossessian TK, Dravinski M. Scattering of elastic waves by three-dimensional surface topographies. Wave Motion 1989;11:579–92.

[11] Sánchez-Sesma FJ, Campillo M. Topographic effects for incident P, SV and Rayleigh waves. Tectonophysics 1993;218:113–25.

[12] Reinoso E, Wrobel LC, Power H. Three-dimensional scattering of seismic waves from topographical structures. Soil Dyn Earthq Eng 1997;16:41–61.

[13] Nguyen K-V, Gatmiri B. Evaluation of seismic ground motion induced by topographic irregularity. Soil Dyn Earthq Eng 2007;27:183–8.

[14] Zhenning B, Jianwen L. 2.5D scattering of incident plane SV waves by a canyon in layered half-space. Earthquake Eng Eng Vib 2010;9:587–95.

[15] Bouckovalas GD, Papadimitriou AG. Numerical evaluation of slope topography effects on seismic ground motion. Soil Dyn Earthq Eng 2005;25:547–58.

[16] Ducellier A, Aochi H. Interactions between topographic irregularities and seismic ground motion investigated using a hybrid FD–FE method. Bull Earthq Eng 2012;10:773–92.

[17] Zhao C, Valliappan S. Seismic wave scattering effects under different canyon topographic and geological conditions. Soil Dyn Earthq Eng 1993;12:129–43.

[18] Athanasopoulos AG, Pelekis PC, Leonidou EA. Effects of surface topography on seismic ground response in the Egion 15 June 1995 earthquake. Soil Dyn Earthq Eng 1999;18:135–49.

[19] Assimaki D, Kausel E, Gazetas G. Wave propagation and soil–structure interaction on a cliff crest during the 1999 Athens Earthquake. Soil Dyn Earthq Eng 2005;25:513–27.

[20] Gatmiri B, Arson C, Nguyen K-V. Seismic site effects by an optimized 2D BE/FE method I. Theory, numerical optimization and application to topographical irregularities. Soil Dyn Earthq Eng 2008;28:632–45.

[21] Gatmiri B, Arson C. Seismic site effects by an optimized 2D BE/FE method II. Quantification of site effects in two-dimensional sedimentary valleys. Soil Dyn Earthq Eng 2008;28:632–45.

[22] Duzgun OA, Budak A. A study on soil–structure interaction analysis in canyon-shaped topographies. Sadhana 2010;35(3):255–77.

[23] Beskou ND, Theodorakopoulos DD. Dynamic effects of moving loads on road pavements: a review. Soil Dyn Earthq Eng 2011;31:547–67.

[24] Jørstad P. Vibration reduction by shaping the terrain topography. Report TVSM-5183, Division of Structural Mechanics, Lund University, Lund, Sweden; 2012.

[25] Bathe KJ. Finite element procedures. New York: Prentice Hall; 2006.

[26] Zienkiewicz OC, Taylor RL. The finite element method, vols. 1 and 2. London: MacGraw-Hill; 1994.

[27] Chopra AK. Dynamics of structures. Upper Saddle River: Prentice Hall; 1995.

[28] Craig Jr RR. Structural dynamics. New York: John Wiley & Sons; 1981.

[29] TYRÉNS, Geotechnical investigation report. Reference number 225686G, Helsingborg 2010-12-10.

[30] Altair Engineering. HyperWorks 11.0.

[31] Dassault Systémes SIMULIA. Abaqus 6.11.

[32] Lysmer J, Kuhlemeyer RL. Finite dynamic model for infinite media. J Eng Mech Div ASCE 1969;859–77.

Paper C

Numerical study on reducing building vibrations by foundation improvement

P. Persson, K. Persson, G. Sandberg

Department of Construction Sciences, Lund University
P.O. Box 118, SE-22100 Lund, Sweden
Tel. +46 46 2228353
peter.persson@construction.lth.se

Abstract

Vibration disturbances in buildings may stem from ambient sources, such as motorway traffic, or from internal sources such as people walking inside the building itself. Vibrations may exceed requirements for sensitive equipment or cause annoyance to humans and therefore the vibrations may need to be reduced. Vibrations from both external and internal sources can be reduced by modifying the properties of concrete slabs and of the soil underneath. Soil can be improved by being mixed with a binder in order to increase its stiffness. In this study, parametric finite element analyses were conducted on the achieved vibration reduction from improving the properties of a concrete slab on soil or of the soil underneath. The size, elastic modulus, and depth of the stabilised soil were found to markedly affect the level of reduction obtained. The soil stabilisation at a vibration-sensitive facility was used as an example case. The developed finite element model was calibrated to green-field measurements carried out on-site. Frequency spectra of both road traffic loads and internal pedestrian loads were considered in the model. The validated finite element model predicted reductions of almost 60% for the road traffic and 80% for the pedestrian load.

Keywords: soil improvement, vibration reduction measure, soil stabilisation, wave propagation, soil dynamics, finite element method, vibration measurements

1. Introduction

A vibration-reduction problem can be divided into three parts: the *source* generating vibrations, the *medium* in which vibrations are propagated, and the *receiver* that is to be protected. Each of these three parts need to be considered in today's urban planning developments. The desification that occurs increases the risk of vibration disturbances. An example of a source is faster trains, and an example of a receiver is more advanced and therefore more sensitive medical equipment. The medium is affected by the densification of cities, i.e. having buildings closer to existing vibration sources such as motorways or railways. Owing to economic and environmental reasons, there is a trend in the building industry to build with lighter elements and thus use less material, such as wooden structural parts and hollow-core concrete slabs. Thus, the building industry is facing increasing challenges regarding vibrations. In such cases, effective measures to reduce vibrations are desirable.

Since Woods' pioneering field-tests of trenches in 1968 [1], there have been extensive studies on several measures aimed at reducing incident ground vibrations stemming from external sources. Since then, several research groups have investigated the vibration reduction effects of various types of wave obstacles, such as trenches (open, back-filled, and water-infiltrated) [2, 3] and shaped landscapes [4]. The idea of placing a wave obstacle is to introduce a disturbance in the incident wavefront by reflection and refraction of the waves.

Other techniques aim at reducing vibrations at the externally located source. Yang and Hung [5] developed a finite element (FE) model to investigate the reduction in train-induced vibrations by various measures, such as an elastic foundation below the train track. They concluded that a soft foundation performs better than a stiff one. However, they did not account for static loads. They also showed that the elastic foundation performs poorly at low frequencies (i.e. long wavelengths); hence, a large foundation in relation to the vibration wavelength may be beneficial. Andersen and Nielsen [2] used a coupled FE–boundary element (FE-BE) model to study the effects of improving the soil underneath a train track on ground vibrations. They improved the soil by increasing the elastic modulus by a factor of ten from 200 to 2000 MPa. They found that soil improvement was especially efficient at reducing ground vibrations at and close to the track compared to trenches. For some frequencies and loading situations, a larger vibration reduction was achieved by soil improvement then by a trench. In general, however, trenches resulted in larger reductions than soil improvement for the increase in elastic modulus that they considered. Hung et al. [6] used a coupled FE-BE model to investigate the vibration reduction effect on train-induced ground vibrations of different measures, such as trenches and wave-impeding blocks (WIBs). They found that a WIB may be an efficient vibration reduction measure. However, the width of the WIB is much smaller than the occurring wavelengths at low frequencies. Then, the waves will not be trapped, which can result in a poor vibration reduction performance. In general, the WIBs did not perform as well as open trenches but better than in-filled ones.

Methods for reducing vibrations at the building to be protected usually involve thickening the whole slab, slitting the slab into isolated islands, or supporting the slab with piles. Sanayei et al. [7] studied using a thickened lower floor in a multi-story building as a vibration reduction measure for train-induced ground vibrations. They tested a full-scale building to verify an analytical prediction model created with a methodology which they previously developed [8, 9]. They investigated the vibration reduction efficiency of the thickened floor for various thicknesses and concluded that it can be used as a reduction measure for external vibration sources. Xiong et al. [10] studied the effect of various cases on reducing train-induced building vibration levels. They concluded that, for example, a stiffened foundation–slab system may an effective vibration reduction measure. They found that an island of a thicker slab-on-grade reduced the vertical vibrations compared to the surrounding conventional slab-on-grade but increased the horizontal vibrations at some frequencies. Note that the reduction in vertical vibrations was strongly dependent on the occurring wavelengths; thus, the conclusions may differ under other site conditions. Amick et al. performed vibrational measurements [11] in order to evaluate how the stiffness of a slab-on-grade or of a building affected the vibrations at a construction site. They concluded that isolating part of the slab where vibration-sensitive equipment is to be placed is only effective for vertical vibrations with frequencies higher than a certain limit (20 Hz in this specific case). Thus, for low frequencies (i.e. long wavelengths), there is no positive

<table>
<tr><td>(a) Spreading out binder material.</td><td>(b) Mixing binder with original soil.</td></tr>
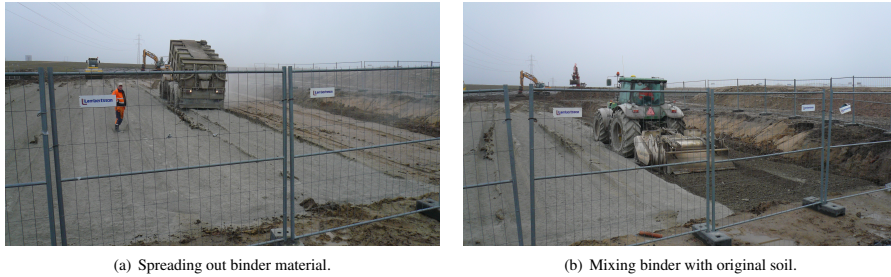</table>

Figure 1: Photographs of the soil stabilisation process at MAX IV Laboratory.

effect from using isolated islands, and horizontal vibrations may even be amplified. They noted that the obtained vibration reduction depends on the ratio of the present wavelength and dimensions of the slab-on-grade. Amick et al. [12] conducted an experimental study on three types of concrete slabs to determine their vibration reduction ability: (i) a 300 mm solid slab, (ii) 300 mm slab with a separated island of 900 mm, and (iii) the same as the latter but the island was placed on concrete piles instead of soil. The vibrations were evaluated with both external and internal excitation sources. For the externally excited vertical vibrations, the slab with piles performed the best, and the continuous slab performed the worst. For the internally excited vertical vibrations, the slab type resulting in the largest vibration reduction depended on the frequency of interest. In general, they concluded that the performances of the different slab types depend on the frequency range of interest and on the excitation type. Note that the island they considered was three times thicker than the continuous slab. Thus, their study was not complete in terms of investigating the benefits of a slit/gap in a slab.

The authors [13, 14] previously found that improvement of the soil parameters have a greater effect on the vibration levels in a building than structural modifications have when internal loads are applied. The soil parameters were also found to have a major effect when external loads are applied [15].

1.1. Soil stabilisation as a vibration reduction measure

One approach to improve the soil parameters is to stabilise the soil by mixing it with a binder in order to increase its stiffness. The procedure of mixing various types of binders with soil was developed both in Sweden and Japan in the 1970s. It is frequently used to improve soft soils for road and railway construction and for building foundations to decrease settlement. There are several types of binders that can be used for this purpose, either singly or in conjunction with one another, such as cement, lime, blast furnace slag, and fly ash. The first two are used most frequently. The fundamental aim is to increase the elastic modulus of the soil by adding an adequate amount of binder, the procedure is as follows: (i) the soil down to the desired depth is dug up, (ii) spreading out a layer of original soil, (iii) spreading out a layer of binder (cf. Fig. 1a), (iv) mixing the original soil with the binder (cf. Fig. 1b), (v) the mixed soil is packed, and (vi) the procedure is repeated from step ii until the required thickness of the stabilised soil is achieved. Fig. 1 shows two photographs of the stabilisation process.

By improving the soil underneath the building to be protected, both externally and internally induced vibrations

may be reduced. However, soil stabilisation underneath a slab-on-grade as a vibration reduction measure is not well-examined in the literature. The vibration reduction effect of stiffening the soil underneath a slab-on-grade is twofold. First, the bending stiffness of the foundation is increased from solely incorporating the slab-on-grade to also include the stabilised soil. This is advantageous for vibrations stemming from both external and internal sources. If different material properties of the stabilised soil and ambient soil are used, differences in the wave speed and mass density occur between the stabilised soil and ambient soil. Since the mechanical impedance is defined as the wave speed multiplied by the mass density ($Z = c\rho$), an impedance mismatch occurs between the two materials. Thus, when an incident wave front hits the boundary of the stabilised soil, energy is reflected since the impedance mismatch governs the amount of energy reflected [26]. The impedance mismatch also results in refraction of the incident wave front. Thus, improving the soil by stabilisation may reduce vibrations from both internal and external vibration sources in an efficient manner.

1.2. Present study

The present study has its origin in the conceptual design of the MAX IV Laboratory research facility. See Section 6 for more information about the facility (hereafter referred to as 'Max IV'). In the design of the facility, numerical conceptual studies were carried out to investigate the effects of modifications to the soil and structure on vibration levels within the facility to satisfy the strict vibrational requirements applied there.

In the paper, parametric FE analyses were conducted to investigate the vibration reduction from improvements to a slab and the soil underneath and to develop general guidelines to be used for the design stage of vibration-sensitive buildings. A calibrated FE model was used to predict the obtained vibration reduction by soil stabilisation at a real-life example case.

The study was divided into two major parts. As discussed in Section 3, the first part involved creating an FE model including a concrete slab located on a homogeneous soil. Various parameters of the slab were varied, and the related vibration phenomena were examined. As discussed in Section 4, the influence of soil stabilisation was included in the parametric studies; different parameters of the soil and stabilisation were varied. The influence of bedrock underneath the soil on the vibration reduction was investigated. Section 5 summarises the findings from the parametric studies as guidelines. In the second major part, soil stabilisation at the vibration-sensitive research facility was used as an example case. This is discussed in Section 6. Frequency spectra of occurring road traffic loads and internal pedestrian loads were considered in the model.

2. Numerical modelling

Local variations in the concrete, soil, and bedrock such as strata and granularity are small compared with the wavelengths involved in the frequency range of interest. Thus, isotropic homogeneous materials were used in the numerical model. The present study focused on vibrations stemming from road traffic, people walking on a slab, and similar sources. For such vibrations, strains are usually at a level that the assumption of linear elasticity is applicable.

The FE formulation for the equation of motion can be written as [16, 17]

$$\mathbf{M\ddot{u}} + \mathbf{C\dot{u}} + \mathbf{Ku} = \mathbf{f}, \tag{1}$$

where $\mathbf{M}$ is the mass matrix, $\mathbf{C}$ is the damping matrix, $\mathbf{K}$ is the stiffness matrix, $\mathbf{f}$ is the load vector, and $\mathbf{u}$ is the nodal displacement vector. A rate-independent (hysteretic) damping model was assumed because it provides a good match to real soil behaviour. Therefore, the damping can be described by a loss factor introduced by the structural damping matrix [18]. A limitation of the assumed damping model is that it cannot be used in the time domain (non-causal). Hence, for the calibration of the numerical model in the example case with the measurement data in the time domain (see Section 6), the rate-dependent Rayleigh damping was used instead. Rayleigh damping provided an adequate damping model for the narrow frequency range of interest in the example case (5–25 Hz). The relationship between the loss factor η and Rayleigh damping ratio ξ can be expressed in steady-state analyses as

$$\eta = \frac{1}{2\pi}\frac{E_D}{E_{So}} = 2\xi\frac{\omega}{\omega_n}, \tag{2}$$

where the energy dissipated per unit volume in the form of viscous damping of a given cycle of harmonic vibrations is denoted as E_D and the strain energy is denoted as E_{So} [19]. When the exciting angular frequency ω is equal to the natural angular frequency ω_n, the loss factor (see Eq. 2) can be expressed as

$$\eta = 2\xi. \tag{3}$$

Waves in a continuum comprise pressure (P) and shear (S) waves. Their wave speeds in a linearly elastic homogeneous isotropic medium are given by

$$c_P = \sqrt{\frac{\lambda_L + 2\mu}{\rho}}; \qquad c_S = \sqrt{\frac{\mu}{\rho}}, \tag{4}$$

where λ_L and μ are the first and second Lamé constants, respectively [20]. The Lamé constants are related to the engineering constants as follows:

$$\lambda_L = \frac{\nu E}{(1+\nu)(1-\nu)}; \qquad \mu = \frac{E}{2(1+\nu)}, \tag{5}$$

where ν is Poisson's ratio and E is the elastic modulus. The second Lamé constant μ is identified as the shear modulus. P- and S-waves are derived under the assumption of an infinite medium. In a finite medium, boundary waves occur near the boundaries, such as Rayleigh waves. The wave speed of Rayleigh waves c_R can be determined on the basis of

$$V^6 - 8V^4 - (16\alpha^2 - 24)V^2 - 16(1 - \alpha^2) = 0, \tag{6}$$

where $V = c_R/c_S$ and $\alpha = c_S/c_P$ [20].

The FE software package Abaqus 6.12 [21] was used to develop the FE models. Plane strain conditions were employed in the parametric studies; these are applicable to line loads and elongated structures. In the analyses of the example case, however, a full 3D FE model was used because the applied loads and geometry did not allow

for a reduction in the dimensions. The FE models were reduced in size by using viscous absorbing boundaries (VABs) developed by Lysmer and Kuhlemeyer [22]; boundary conditions in terms of dashpots were used to absorb incident waves. In the following derivation of the VAB [21], only plane longitudinal waves are considered. By using Lamé's constants, the stress–strain relation can be written as

$$\sigma_{xx} = 2\mu\epsilon_{xx} + \lambda(\epsilon_{xx} + \epsilon_{yy} + \epsilon_{zz}). \tag{7}$$

The incoming plane longitudinal waves and reflected wave can be written as

$$u_x = f_1(x - c_p t); \qquad u_x = f_2(x + c_p t). \tag{8}$$

Distributed damping constants can be introduced on the absorbing boundary such that the stress there becomes

$$\sigma_{xx} = -d_p \dot{u}_x. \tag{9}$$

The damping constants for P-waves can be obtained as follows:

$$d_p = \rho c_p; \qquad d_s = \rho c_s. \tag{10}$$

The damping constants for S-waves can be obtained in a similar manner. The VAB are completely effective for orthogonally impinging plane body waves assuming a linear elastic material model. For waves that do not propagate in the normal direction of the boundary and for surface waves such as Rayleigh waves, the boundary damping still works sufficiently well from an engineering point of view [23].

In order to develop an FE model and to ensure that the analyses provided results of adequate accuracy, studies have been conducted to investigate the influence of various parameters such as the aspect ratio of the finite elements, the size of the model geometry and reflection of waves at boundaries. An element mesh with a minimum of six element nodes representing the shortest wavelengths in each developed model was employed.

Root mean square (RMS) values were used to indicate the resulting vibration magnitudes. The RMS values were calculated according to the complex magnitude of the vertical displacements obtained from the steady-state analyses. The following RMS value (see Eq. 11) was used in order to obtain a frequency-dependent function for plotting a graph of the selected evaluation points selected:

$$u_{RMS}^I(f) = \frac{1}{n}\sqrt{\sum_{i=1}^{n} u_i^2}, \tag{11}$$

where u_i is the magnitude of the displacement at node i and n is the number of evaluation nodes. A second RMS value was used in order to determine a single value indicating the vibration level and is defined here as

$$u_{RMS}^{II} = \frac{1}{m}\sqrt{\sum_{j=1}^{m} u_{RMS}^I(f_j)^2}, \tag{12}$$

where $u_{RMS}^I(f_j)$ is the magnitude of the displacement at frequency step j in the steady-state analyses and m is
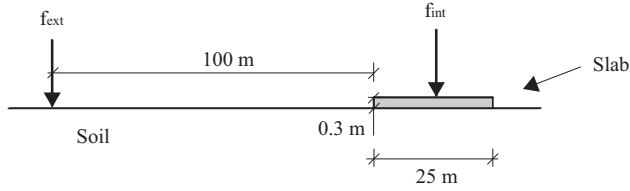
Figure 2: Model of slab on soil used for parametric studies. The concrete slab is coloured in grey.

Table 1: Material properties used for the reference model [24].

Property	Concrete	Soil
Density (kg/m^3)	2400	2100
Elastic modulus (MPa)	35,000	480
Loss factor	0.04	0.14
Poisson's ratio	0.25	0.48

the number of frequency steps considered.

3. Slab on homogeneous soil

Parametric FE analyses were conducted in order to investigate the vibration reduction from improving the properties of a slab on soil. A 2D FE model included a concrete slab on a homogeneous soil was developed. As reference geometry, the concrete slab had a width of 25 m and thickness of 0.3 m. Frequency sweeps were carried out with a unit line load applied at frequencies of 1–100 Hz. Two different loads were investigated: one externally located on the ground surface, f_{ext}, and one located on the midpoint of the slab itself, f_{int}. The geometry of the model using the external load position was 200×300 m^2 (height×width). In the model using the internal load position, the width was reduced to 150 m due to symmetry conditions. The model is shown in Fig. 2. Quadrilateral 8-node plane strain elements obtained by quadratic approximation were employed. The model contained between approximately 150,000–300,000 degrees of freedom (dofs), depending on if the external or the internal load position was used. The soil properties used in the study (see Table 1) are typical for a stiff clay till in southern Sweden. The vibration response, and thus the obtained vibration reduction, was presented as a function of the Rayleigh wavelength in the soil. For the soil properties applied here, frequencies between 1 and 100 Hz corresponded to Rayleigh wavelengths of 257–2.57 m.

3.1. Slit in slab

A common measure to isolate vibrations stemming from machines or to sensitive areas is to make use of a slit in the slab. To evaluate the vibration reduction effect achieved, a slab separated into two equally sized parts (12.5 m each) was considered, as shown in Fig. 3a. The load was applied in the middle of one of the parts, i.e. 6.25 m from the outer edge. The obtained displacements on the slab parts (see Eq. 11) were compared to that of a continuous slab with a 25 m width and the load at the same position, as shown in Fig. 3b. Fig. 4 shows the reduction in displacement versus the Rayleigh wavelength on both sides of the slit. It is seen in the figure that the vibration
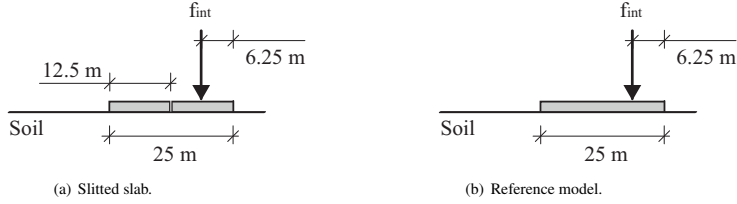
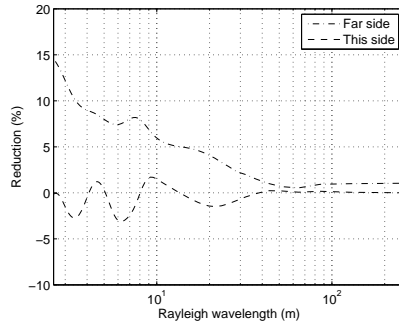Figure 3: Models used to study the effects of a slit in a slab. The concrete slabs are coloured in grey.

Figure 4: Reduction in displacement as a function of the Rayleigh wavelength with internal loading. The displacements were evaluated on the far and near sides of the slit in relation to the loading, and the results were compared with those for a continuous slab.

levels could be reduced if the target being protected was located on the far side of the slit compared to the position of the excitation. However, this only had a slight effect; the effect became stronger as the wavelengths became less than 50 m. Long Rayleigh waves go deep into the soil. At the depth of $0.8\lambda_R$, for example, the amplitude is still 50% of the surface amplitude [25]. Because the slab was only 0.3 m thick while the occurring wavelengths were several meters in depth, the long waves were more strongly affected by the soil properties because most of the particle motion occurred in the soil. This explains why the slit is more effective for short wavelengths.

When loading occurred on the same side as the target, the vibration levels were amplified for Rayleigh wavelengths shorter than about 40 m. Thus, using a slit in a slab with a vibration source producing wavelengths in such a range may amplify the vibration level in that part of the slab.

3.2. Bending stiffness of the slab

To study the influence on the obtained reduction by increasing the stiffness the expression of a Kirchoff plate bending assuming isotropic material with constant thickness was used. The bending stiffness was defined as

$$D = \frac{Et^3}{12(1 - \nu^2)}, \tag{13}$$

where E is the elastic modulus, t is the thickness, and ν is Poisson's ratio.

The effect of varying the bending stiffness of the slab was investigated for the externally located load. Fig. 5
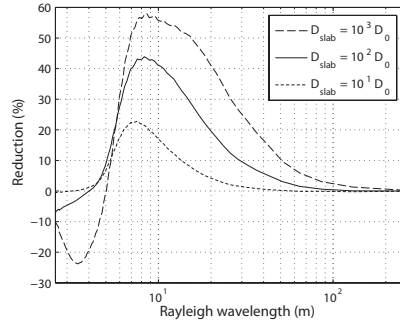
Figure 5: Reduction in displacement as a function of the Rayleigh wavelength for external loading. The displacements on the slab were evaluated for various bending stiffness of the slab. D_0 denotes the bending stiffness of the original slab. The displacements were averaged for a sweeping window of 10 Hz over the frequency range, and the mean value of the frequencies was calculated within the window for each frequency.

shows the reduction in the vibration level as a function of the the Rayleigh wavelength for various bending stiffness levels of the slab. The bending stiffness of the slab was increased by increasing the elastic modulus E. According to Eq. 13, changing the thickness and Poisson's ratio of the slab changes the bending stiffness of the slab. However, the results concerning the change in thickness are somewhat questionable. For example, increasing the stiffness 10^3 times corresponds to increasing the thickness by 10 times, e.g. from 0.3 to 3 m. Then wave propagation within the slab affects the vibration level obtained. For a moderate increase in the thickness, however, the same degree of reduction was observed when the bending stiffness was increased with the elastic modulus in relation to the thickness, given that the density was reduced to preserve the mass of the slab. It is not realistic to vary Poisson's ratio in order to increase the bending stiffness to any appreciable extent because this would require a negative Poisson's ratio (i.e. auxetic material).

Fig. 5 shows that a larger reduction occurred with a higher bending stiffness. However, amplification was observed for Rayleigh wavelengths shorter than 5 m when the bending stiffness was increased by a factor of 1000, i.e. resonance occurred. The stiffened slab resulted in a marked reduction at wavelengths from about 6 to 15 m, however the interval depended of the bending stiffness of the slab. Because the width of the slab used here was 25 m, the width of the slab should be about 2–4 times the dominating wavelength in order to reduce the displacement as effectively as possible and to minimise the risk of amplification. The positive effect of increasing the bending stiffness of the slab motivated the study on stabilising the soil underneath the slab in order to achieve a higher bending stiffness of the foundation, which includes both the slab and stabilised soil.

3.3. Slab stiffness in relation to the soil stiffness

Fig. 6 shows the reduction obtained by increasing the elastic moduli of the soil and concrete compared to their reference values, which are given in Table 1. The internally located load was considered. The figure shows that increasing the elastic modulus of the soil is far more effective at reducing vibrations than increasing the elastic modulus of the concrete slab. This is most obvious at low frequencies (long wavelengths) because the larger part
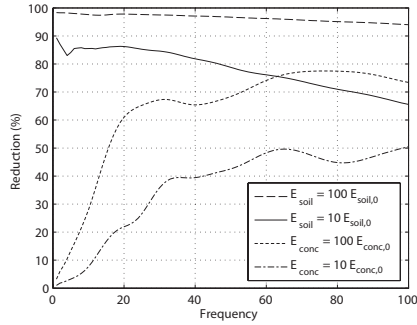
Figure 6: Reduction in displacement as a function of frequency for internal loading. Displacements on the slab were evaluated. The elastic modulus of soil E_{soil} and concrete E_{conc} were varied.

of the Rayleigh wave particle motion occurred in the soil compared to shorter waves. Note that the soil volume in the model was much larger than the slab volume; hence, changing the stiffness of the soil had an appreciable influence on the global stiffness of the model. The positive effect of increasing the soil stiffness motivated the investigation on stabilising the soil underneath a slab in terms of a vibration reduction measure.

4. Slab on stabilised soil volume

Parametric studies were conducted on both external and internal loading of a slab on stabilised soil. Fig. 7 shows the model used. Here, the same FE model was used as in Section 3 with the exception of different material properties of the volume under the slab, denoted as 'Stabilised soil' in the figure. The wavelengths in bedrock being longer than in soil. Thus, the number of dofs was reduced to between approximately 100,000–250,000, depending on if the external or the internal load position was used, for the models involving bedrock.

As discussed in Section 4.1, one material parameter at a time was varied from its reference value for the stabilised volume. Here, the material parameters of the original soil were used as reference values. Table 1 presents
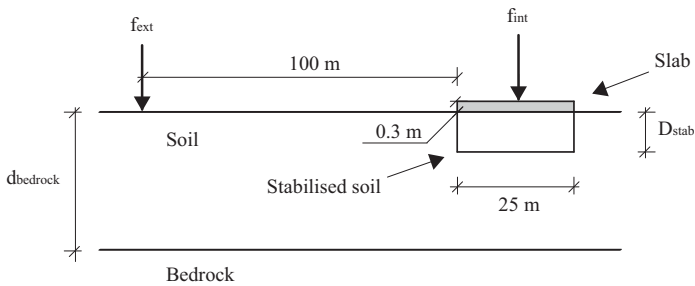

Figure 7: Model used for parametric studies of slab on stabilised soil volume. The concrete slab is coloured in grey.
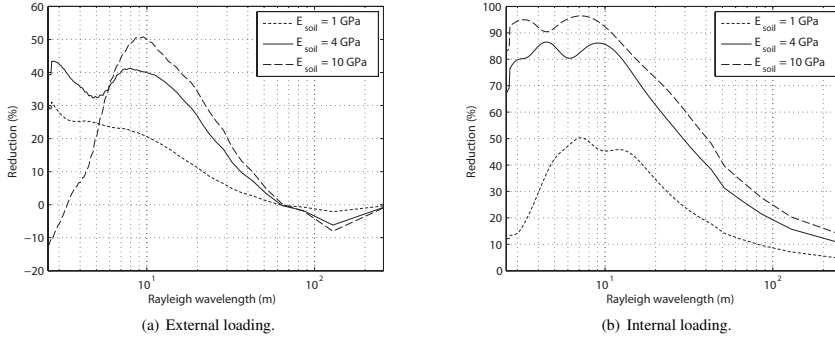
(a) External loading.

(b) Internal loading.

Figure 8: Reduction in displacement as a function of the Rayleigh wavelength for different elastic modulus of the soil at the stabilisation volume. The reference value of the elastic modulus was 480 MPa.

the reference values of the material parameters. As discussed in Section 4.2, the elastic modulus and depth of the stabilised soil were each varied because they had the largest effect on the vibration reduction and are easier to modify during the stabilisation process. Here, the material parameters of the stabilised soil were used as reference values Table 2 presents the reference material parameters of the stabilised soil. As discussed in Section 4.3, the influence of bedrock at certain distances from the ground surface on the vibration reduction was investigated. The reduction of displacements shown in Figs. 8–13 was evaluated in terms of RMS values (see Eq. 11) for all nodes on top of the slab relative to a slab on soil with reference material parameters. For those figures, the displacements were averaged by sweeping a window of 10 Hz over the frequency range and calculating the mean value of the frequencies within the window for each frequency. Note that the sweeping window is truncated at the frequency limits. The plots show amplification of the vibration levels as a negative reduction. The displacements are shown as a function of the Rayleigh wavelength of the original soil with the reference material parameters.

4.1. Parameters of soil

The soil material properties of the soil volume underneath the slab were varied in a parametric study (Fig. 7). The elastic modulus, Poisson's ratio, the loss factor, and the mass density were varied one at the time while the others were kept constant. The parameters were varied in intervals assumed to cover the practical useful values for a stabilised soil. Hence, they were varied between the reference values of the soil and concrete, as presented in Table 1. The elastic modulus was the exception; the upper limit was set to 10 GPa.

4.1.1. Elastic modulus

The elastic modulus was varied between 480 and 10,000 MPa. As shown in Fig. 8a, the elastic modulus had a marked effect on the vibration levels of the slab when an external load was applied. The results showed a maximum reduction of approximately 55% and amplification of up to approximately 10% depending on the excitation frequency and elastic modulus. For some Rayleigh wavelengths, a higher elastic modulus resulted in greater reduction but also higher amplification. The amplification was due to resonances of the stabilised soil.
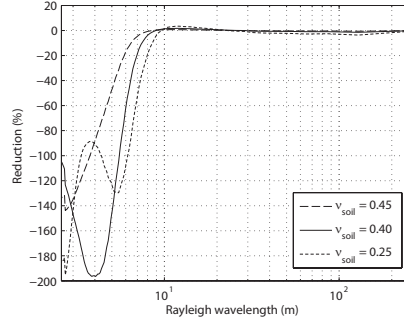
11

Figure 9: Reduction in displacement as a function of the Rayleigh wavelength for different Poisson's ratios of the soil in the stabilisation volume. External loading was applied, and the reference value of Poisson's ratio was 0.48.

Fig. 8b shows that the influence of varying the elastic modulus on the vibration levels of the slab was also significant for internally located loads. In contrast to external loading, increasing the elastic modulus was beneficial for all investigated wavelengths.

4.1.2. Poisson's ratio

Poisson's ratio was varied from 0.48 to 0.25. As shown in Fig. 9, the effect on the vibration levels of the slab relative to the reference model was significant for the shorter Rayleigh wavelengths with an externally located load. The vibration levels of the slab were amplified for wavelengths shorter than approximately 8 m independent of the value of the Poisson's ratio. However, the resonance peak was slightly shifted. When Poisson's ratio was lowered, the shear stiffness (see Eq. 5) increased, and the bending stiffness (see Eq. 13) decreased. However, the stiffness in the vertical direction markedly decreased, which is given by

$$D_{zz} = \frac{E(1 - \nu)}{(1 + \nu)(1 - 2\nu)}.$$

(14)

For internal loading, varying Poisson's ratio resulted in both reduction and amplification. However, there was only a slight effect.

4.1.3. Loss factor

The loss factor was varied between 0.14 and 0.04. For external loading, the loss factor had a marked effect on the vibration levels of the slab for Rayleigh wavelengths between 5–15 m, as shown in Fig. 10a. The highest amplification from lowering the loss factor was 25% and occurred at a wavelength of 8 m.

For internal loading, varying the loss factor affected the response of the slab for Rayleigh wavelengths shorter than the slab itself, as shown in Fig. 10b. For external loading, the effect of changing Poisson's ratio was largest between wavelengths of about 5 and 15 m with a peak amplification of approximately 18%.
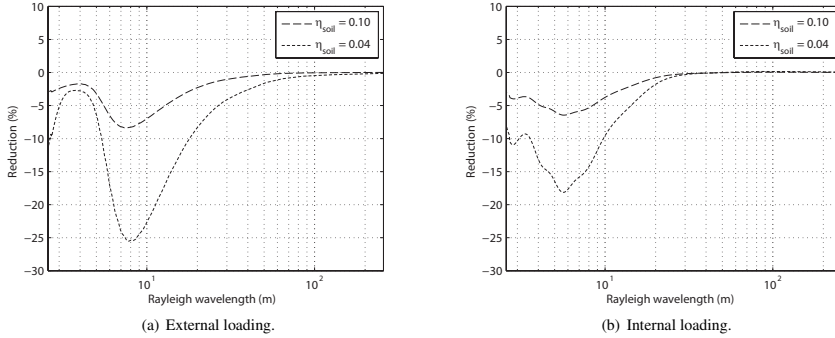
12

Figure 10: Reduction in displacement as a function of the Rayleigh wavelength for different loss factors of the soil at the stabilisation volume. The reference value of the loss factor was 0.14.

Table 2: Reference values for the stabilised soil. The values within brackets show the intervals used in the parametric studies of the soil stabilisation.

Property	Stabilised soil
Depth (m)	4 (2–10)
Density (kg/m^3)	2400
Elastic modulus (GPa)	4 (1–10)
Loss factor	0.04
Poisson's ratio	0.25

4.1.4. Mass density

The mass density was varied from 2100 to 2400 kg/m^3. With external loading, the effect on vibration levels was negligible. With internal loading, a somewhat larger effect was obtained. For a mass density of 2400 kg/m^3, the reduction reached a maximum of 8% for Rayleigh wavelengths shorter than 5 m. Overall, the mass density of the soil had a slight effect on the vibration levels of the slab. If the mass density would be varied for a larger soil volume, it may have a larger effect.

4.2. Parameters of the stabilised soil

The elastic modulus and the depth of the stabilised soil were varied one at the time while the other parameters were kept constant. Table 2 presents the reference material parameters used for the stabilised soil. According to a geotechnical report [24], the elastic modulus is the material property of the soil that can be changed the most by stabilisation. The obtained displacements are presented as the reduction (or amplification) relative to having the original soil underneath the slab.

4.2.1. Elastic modulus

The elastic modulus of the stabilised soil was varied from 1 to 10 GPa. Fig. 11a shows that the obtained reduction by stabilising the underlying soil is highly dependent on the incident Rayleigh wavelengths for the external load. Both large reductions and large amplifications can be obtained. The behaviour was similar to increasing the bending stiffness of the slab, as discussed in Section 3.2. The largest reduction was obtained for wavelengths of
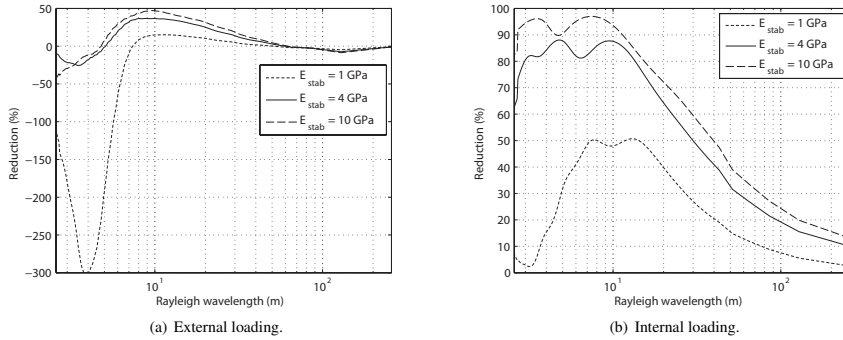
13

Figure 11: Reduction in displacement as a function of Rayleigh wavelength when the elastic modulus of the stabilised soil was varied. The reference case was a slab on homogeneous soil.

5–25 m. Fig. 11a shows that increasing the elastic modulus of the stabilised soil increased the maximum reduction and decreased the maximum amplification. Thus, increasing the elastic modulus of the stabilised soil is beneficial. Moreover, the displacements on the slab were amplified at wavelengths shorter than approximately 6 m depending on the elastic modulus of the stabilised soil. At those wavelengths, a resonance occurred because of the large influence of the low Poisson's ratio of the stabilised soil relative to the original soil. In order to compensate for the loss of stiffness in the normal direction resulting from the lowered Poisson's ratio and therefore to avoid large amplification of the vibration levels, the elastic modulus should be at least 4 GPa.

Fig. 11b shows that, similar to the results for external loading, increasing the elastic modulus of the stabilised soil is also beneficial for internal loads. However, for internal loading, reduction was seen for all investigated Rayleigh wavelengths. The largest reductions occurred for wavelengths shorter than the slab. For the shortest and longest wavelengths considered in the study, a stabilised soil with an elastic modulus of 1 GPa resulted in negligible reduction levels.

4.2.2. Stabilisation depth

The depth of the stabilised soil was varied from 2 to 10 m. Figs. 11 and 12 show somewhat similar tendencies when either the elastic modulus or depth of the stabilised soil was increased. As shown in Fig. 12a, the vibration levels of the slab were considerably amplified for frequencies generating Rayleigh wavelengths shorter than approximately 5 m, depending on the depth of the stabilised soil. The vibrations of the whole stabilised volume were amplified, which indicates resonant behaviour. Thus, resonances from the stabilisation affected the response of the slab.

Fig. 12b shows that the depth of the stabilised soil had a marked effect on the vibration levels of the slab with internal loading. In contrast to the elastic modulus (Fig. 11b), increasing the depth of the stabilised soil was not beneficial for all investigated Rayleigh wavelengths.
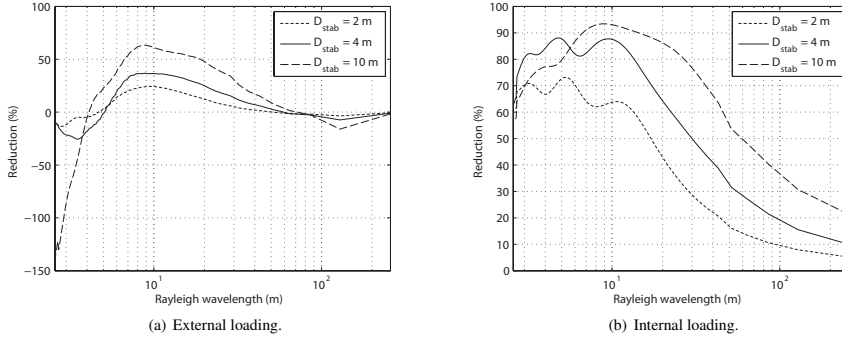
14

Figure 12: Reduction in displacement as a function of the Rayleigh wavelength for different depths of the stabilised soil. The reference case was a slab on homogeneous soil ($D_{stab} = 0$).

4.3. Influence of bedrock

In previous studies by the authors found that including bedrock in the FE models can have a large influence of the level of reduction obtained when a vibration reduction measure was applied [3]. It was concluded that the wavefront propagates through the bedrock and affects the soil layer at long distances from the vibration source. The effect of bedrock included in the model on the reduction achieved through soil stabilisation was investigated for both external and internal loadings. Fig. 7 shows the model used. The depth of the soil layer (i.e. distance from the ground surface to the bedrock $d_{bedrock}$) was varied between 4 m (i.e. stabilised soil all the way down to the bedrock) and infinity (i.e. no bedrock). Thus, the depth of the stabilised soil was kept constant in the analysis at $D_{stab} = 4$ m.

Fig. 13a shows that, for external loading, the maximum reduction increased as the distance to the bedrock decreased. In other words, the maximum reduction obtained by soil stabilisation increases when there is a short distance between the ground surface and the bedrock. However, when the soil was stabilised down to the bedrock, a marked amplification was obtained at a Rayleigh wavelength of about 3 m, which is equivalent to a frequency of 83 Hz. This corresponds somewhat to the eigenmode of the stabilised volume having its horizontal surface pulsating in the vertical direction. The large reduction at a wavelength of 10 m occurred at the same frequency where the model without stabilisation had its peak response. Because the stabilised soil was located directly on the bedrock, this effect was significantly decreased.

For internal loading, the achieved reduction generally increased as the depth to bedrock decreased, as shown in Fig 13b. Similar to external loading, when the soil was stabilised down to the bedrock ($d_{bedrock} = 4$ m), resonances of the stabilised soil became important. The large reduction obtained at a Rayleigh wavelength of the soil of 8 m corresponded to the frequency where the model without stabilisation had a peak response. A peak was not observed in the model including the stabilisation. The reduction decreased for frequencies corresponding to wavelengths shorter than approximately 5 m because the resonant behaviour of the soil in the model without
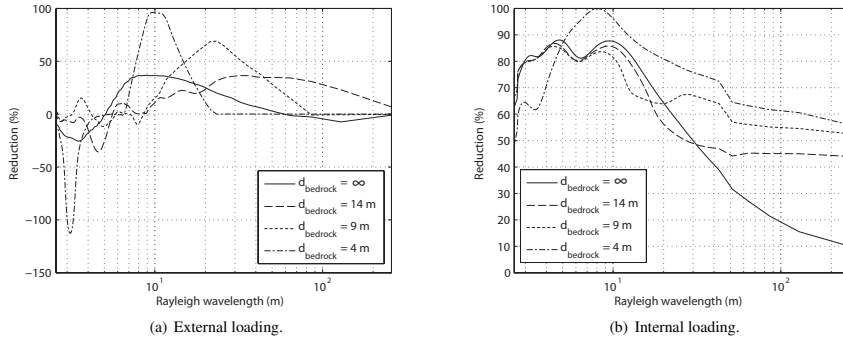
Figure 13: Reduction in displacement as a function of the Rayleigh wavelength for various distances to the bedrock from the ground surface. An infinite distance denotes a model without any bedrock present. The depth of the stabilised soil was kept constant at 4 m.

stabilisation was less significant at those frequencies.

5. Guidelines

The most important findings from the parametric studies are summarised below in the form of general guidelines which can be used at the design stage of vibration-sensitive buildings.

- *The slab and stabilisation width should be 2–4 times the dominant Rayleigh wavelength*

  If vibrations stemming from an externally located vibration source should be addressed, the widths of the slab and stabilised soil are important. The foundation (slab and stabilised soil) is most effective at reducing vibrations from Rayleigh wavelengths of about 5–15 m. It can therefore be concluded that This corresponds to a slab width of approximately 2–4 times the dominant Rayleigh wavelength. This should also be considered if a slitted slab is to be used because the width of the slab changes. Making use of a slit may be beneficial for isolating internal vibration sources but only for shorter Rayleigh wavelengths (up to a couple of meters for the model used in the study). However, vibrations on the same side of the slit as the source may be amplified.

- *The elastic modulus of the stabilised soil should be high*

  Varying the elastic modulus of the stabilised soil was observed to have a significant effect on the obtained reduction for both external and internal loadings. The maximum reduction for external loading increases with the elastic modulus. Increasing the elastic modulus is always advantageous for internal loading. However, resonant behaviour was observed for certain wavelengths and may therefore amplify the vibration levels.

16

Figure 14: Architectural sketch of Max IV [27, 28].

- *The selected depth of the stabilised soil should be large*

  Soil stabilisation is generally more effective the deeper it is. For external loads, however, some resonance behaviour was observed at certain stabilisation depths for certain wavelengths, especially when the stabilised soil reached the bedrock. Thus, investigations must be performed to prevent amplification.

- *Numerical simulations needed*

  As stated in the aforementioned guidelines, soil stabilisation can cause resonant behaviour leading to amplified vibration levels on the slab. Therefore, the design of the stabilisation needs to be evaluated by employing models capturing these phenomena. Numerical simulations provide an adequate tool for such purposes. The resonant behaviour is strongly dependent on the properties of the ground materials and the properties of the stabilisation. It is therefore necessary to calibrate the numerical model to measurements carried out on-site or at sites with similar conditions.

6. Example case

As an example of the reduction in vibration levels which can be achieved by soil stabilisation, the research facility Max IV was considered involving its governing loads. The large ring-shaped building, as shown in Fig. 14, has a circumference of about 650 m and is approximately 12 m in height. It has a 0.3 m thick concrete slab which is 25 m wide. Fig. 15 shows the cross-section of the concrete structure. The distance A varies between 6 and 8 m because of the serrated geometry of the outer wall, as shown in Fig. 16. Below the concrete slab, the soil was stabilised to a depth of 4 m. Table 2 presents the values of the material parameters used for the stabilised soil. Because the Max IV site is large at around 300,000 m^2, the stratification of the soil varies throughout the site. The soil comprises 14–16 m of two different clay tills: Low Baltic clay till covers the stiffer Northeast clay till, which rests on top of bedrock consisting of sandstone and shale. In the building, electron beams producing synchrotron light are controlled by magnets. Since the quality of the measurements depends upon the vibration levels of the magnets, there are strict requirements regarding displacements. The vibration requirements regarding
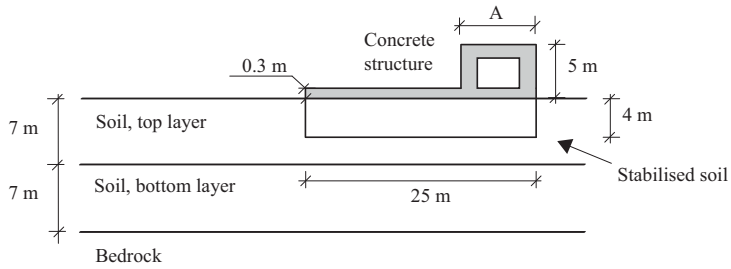
17

Figure 15: Cross-section of the model. The distance *A* varies between 6 and 8 m. The concrete structure is coloured in grey.

vertical displacements are especially strict; these must be less than 30 nm in 1 s RMS in the frequency range of 5–100 Hz.

In the design process of Max IV, a group of experts in dynamics was composed. The authors belonged to that group, together with people from companies in the building industry. The main goal of the work of the group was to ensure that the vibration requirements could be fulfilled. Conceptual studies were performed to specify and verify design solutions aiming at minimising the vibration level in the sensitive areas. As examples of the adopted design solutions developed by the authors may be the use of a shaped ambient landscape [4] (see Fig. 14) and the work presented in the present paper. Both used as vibration reduction measures. To exemplify the outcome of the parametric studies performed in the present paper, the applied solution at Max IV serves as an example case.
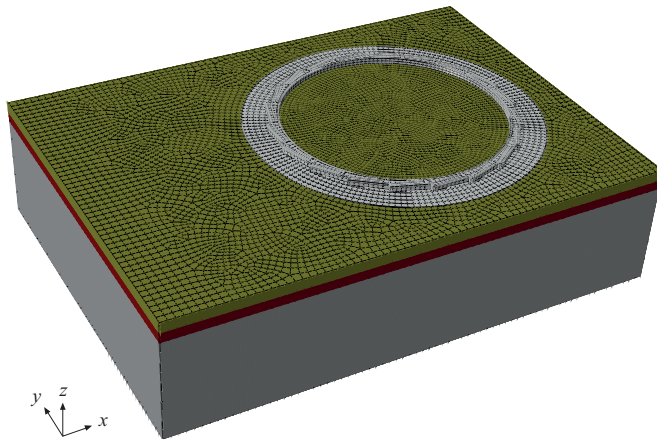

Figure 16: FE mesh of the calibrated model. The concrete structure of the building is in grey, the top soil layer is in green, the bottom soil layer is in red, and the bedrock is in dark grey.

18

Table 3: Material parameters used in calibrating the FE model and layering used in model. The calibration parameters being: E_1, E_2, ξ_1, and ξ_2.

| Property	Soil, top layer	Soil, bottom layer	Bedrock
Depth (m)	7	7	75
Density (kg/m^3)	2100	2100	2500
Elastic modulus (MPa)	E_1	E_2	10,000
Damping ratio (%)	ξ_1	ξ_2	2.0
Poisson's ratio	0.48	0.48	0.40

6.1. Model calibration

A numerical model was developed to predict the effectiveness of the stabilisation used at Max IV as a vibration reduction measure. Green-field measurements were conducted in situ in order to obtain realistic material parameters for the soil and bedrock. During the Max IV project, extensive geotechnical and geophysical measurements were carried out in order to assess reliable material parameters: soil sampling, vertical soil profiling tests, surface seismic tests, and falling weight deflectometer (FWD) tests [24]. The interval for each material parameter was determined on the basis of those measurements.

Numerical simulations were performed to determine the best estimated value of each material parameter in the FE model through calibration of the simulation results to the measurement data. Based on the uncertainty interval obtained from the measurements, the material parameters with the largest influence on the simulation results were the elastic modulus and the damping parameter. Note that Poisson's ratio may have had a marked effect on the dynamic response of the soils, but its uncertainty interval was narrow for the soil at the site. Hence, the elastic modulus and damping were calibrated for the soil layers. Table 3 presents the material parameters used in the calibration. Because the load in the FWD tests was measured (see Fig. 17), the tests could be used in conjunction with the FE models through an iterative process in which each of the selected material parameters was varied while the others were kept constant.
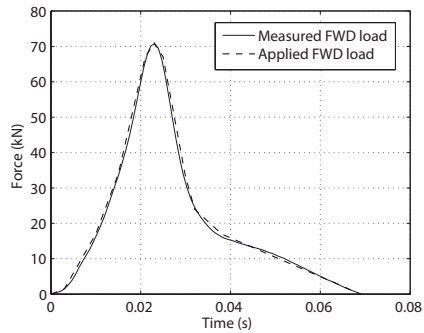
Figure 17: A photograph of the FWD machine is shown in (a) [24]. The machine generates an impulse load on the ground surface as shown in (b).

19

(a) Evaluation 20 m from the source.   (b) Evaluation 80 m from the source.
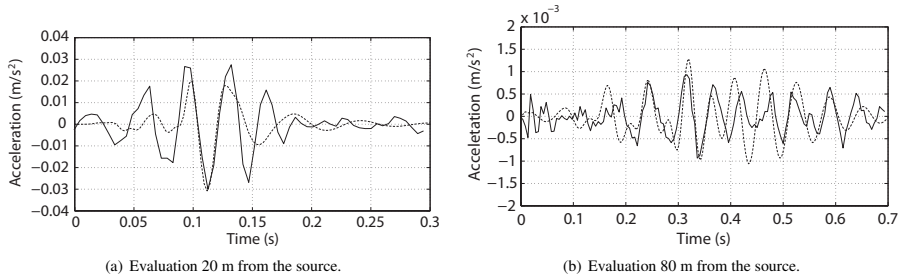
Figure 18: Accelerations evaluated at 20 and 80 m from the vibration source. The measured accelerations are shown by a solid line, whereas the numerically predicted accelerations are shown with a dashed line.

Table 4: Values of the calibrated model.

Value	Measurem. 20 m	Simul. 20 m	Measurem. 80 m	Simul. 80 m
Maximum acceleration (m/s$^2 \cdot 10^{-3}$)	30	31	0.93	1.27
Period time at max acc (s)	0.034	0.035	0.050	0.043
RMS (m/s$^2 \cdot 10^{-3}$)	11	7.4	0.36	0.45

In the FWD tests, an impulse load is created. Fig. 17(b) shows the load spectra. Two accelerometers were placed on the ground surface to record the vertical accelerations along a straight line from the FWD at 20 and 80 m from the source. Wilcoxon 731A/P31 seismic accelerometers and power amplifier system were used for the measurements. The time signals for the transducer and accelerometers were not synchronised. Fig. 18 shows the measurement data obtained by the accelerometers.

For the calibration, an axisymmetric FE model was used for simulations in the time domain. An implicit solver using Hilber-Huges-Taylor time integration [29] was employed with fixed time steps of 0.0015 s. The calibration was aimed at minimising the difference between the simulation results and measurement data in terms of the maximum acceleration and period time at the maximum acceleration. Table 4 presents the obtained values and RMS values of the accelerations shown in Fig. 18.

The FE model generated output that resemble the measurement data to an adequate extent, thus, it can be concluded that the calibrated model is sufficiently accurate for predicting the vibration reduction effect of the stabilised soil. There can be several explanations for the minor differences of the calibrated model relative to the measurement data, for example: simplifications in the numerical model such as completely horizontal layering and homogeneous and isotropic materials, as well as background noise and crude resolution in the measurement data.

The calibration resulted in the values of the material parameters presented in Table 5. Because the calibration was conducted with a transient load, Rayleigh damping was applied. The achieved reduction as presented in Section 6.2 was evaluated in the frequency domain. Here, the loss factor was in relation to the calibrated damping ratio according to Eq. 3.

A 3D FE model was used with dimensions of $360 \times 260 \times 90$ m^3 (length (x) $\times$ width (y) $\times$ height (z)). Fig. 16 shows the model. In the z-direction, the geometry was 14 m of soil and 75 m of bedrock. Quadrilateral 20-node

Table 5: Validated material properties.

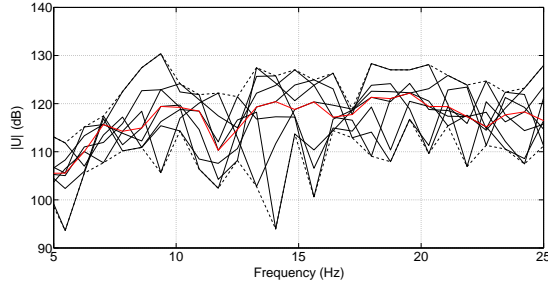| Property	Soil, top layer	Soil, bottom layer
Elastic modulus (MPa)	E_1=500	E_2=2000
Damping ratio (%)	ξ_1 =3.5	ξ_2=3.0

Figure 19: Magnitude spectrum of displacements U(t) obtained from measurements. The 95% and 5% quantile curves are shown as dashed lines. The median value (50% quantile) was used in the numerical analyses and is shown as a red solid line. A reference displacement of 10^{-8} m was used.

hexahedron solid elements obtained by quadric approximation were employed. The FE model contained about approximately 1.1–1.4 million dofs, depending on the load position used.

6.2. Prediction of reduction level

In the example case, road traffic load at a nearby motorway and pedestrian load inside the building were considered. Since vibrations stemming from road traffic mainly have energy in the lower frequency range and because of the low response of the soil at higher frequencies, the upper frequency limit of the analyses was set to 25 Hz. As stated previously, the lower limit was set to 5 Hz. Because the vibrations with the highest amplitude occurred when the motorway was heavily trafficked, the traffic load was regarded as a line load. A line load assumes that all loads act in-phase. In comparative studies on the effectiveness of the stabilisation, this was assumed to have a negligible influence. Fig 19 shows the considered frequencies of the traffic load. See [3] for a detailed description of the procedure applied to determining the frequency content of the traffic load. The harmonic load, representing the traffic, was applied 100 m from the closest distance to the concrete slab, and the displacements were evaluated at nodes located along the ring-shaped concrete structure, as shown in Fig. 20. The RMS value (see Eq. 12) denoting the total vibration level stemming from road traffic was found to be reduced by 55%.

Because the vibration requirements are extreme, a walking load containing frequencies of up to 20 Hz was applied [31]. Considering a walking rate of less than 2.5 Hz, the frequency content within the range of interest (5–20 Hz) can be assumed to be constant in amplitude [30, 31]. A harmonic unit load was applied on the concrete slab 8 m from the outer boundary. The displacements were evaluated at the four closest nodes adjacent to the loading point at a distance of approximately 2 m. The reduction in the total vibration level, using the RMS value defined in Eq. 12, was found to be 77%.
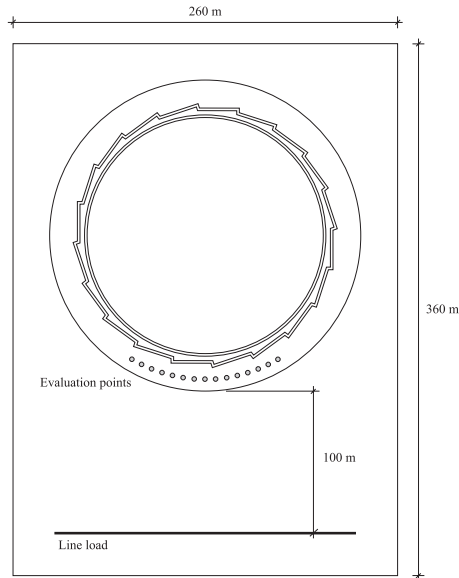
Figure 20: Locations of the evaluation points (grey dots) used when an externally located load (thick black solid line) located 100 m from the closest point of the slab was applied.

7. Concluding remarks

General guidelines were stated from numerical parametric studies that investigate the effects of various parameters of a concrete slab on soil and of stabilised soil underneath the slab on the vibration reduction of external and internal loading. The effects of soil stabilisation at a real-life example case were investigated considering road traffic and walking loads.

In the general design guidelines it is stated that width the slab and the stabilised soil should be 2–4 times the dominant Rayleigh wavelength in order to be most effective in terms of reducing the vibration level of the slab. A high elastic modulus and a large depth of the stabilisation were found to be important parameters in achieving a high degree of vibration reduction. These statements were found to be independently of the applied material properties. The guidelines can be used in the design process of a building requiring a certain level of vibration reduction.

The obtained vibration reduction by using soil stabilisation is strongly dependent on the occurring wavelengths. Thus, it is important to have extensive knowledge of the ground material parameters on-site when designing the stabilisation. Geotechnical and geophysical measurements at the construction site are therefore required. The material parameters given from such measurements often results in intervals for the parameters. It is therefore necessary to calibrate the numerical model to measurement data in order to determine the best estimate of each of the employed material parameters. This can be conducted by employing vibration measurements that measures

22

both the load, as well as, the ground response. Numerical simulations are then needed to avoid resonant behaviour, as well as, to predict the level of reduction obtained by soil stabilisation.

In the example case, the stabilised soil was found to reduce the vibrations from the traffic load by 55%. In comparison, previous work concerning the same example case showed that having a barrier [3] or a shaped landscape [4] between the motorway and building, it is possible to achieve a reduction of approximately 35%. Moreover, stabilising the soil was found to reduce vibrations caused by pedestrians inside the building by almost 80%. Thus, soil stabilisation beneath a slab-on-soil can be concluded to be an effective vibration reduction measure.

The cost involved in stabilising the soil in relation to the cost involved in other vibration reduction measures such as a thickened concrete slab, a wave barrier or a shaped landscape would be interesting to study. The cost-effectiveness of the different vibration reduction measures could then be compared.

[1] Woods RD. Screening of surface waves in soil. J Soil Mech Found Eng (ASCE) 1968;94(4):951-79.

[2] Andersen L, Nielsen SRK. Reduction of ground vibration by means of barriers or soil improvement along a railway track. Soil Dyn Earthq Eng 2005;25(7-10):701–16.

[3] Persson P, Persson K, Sandberg G. Numerical study of reduction in ground vibrations by using barriers, Eng Struct 2016;115:18–27.

[4] Persson P, Persson K, Sandberg G. Reduction in ground vibrations by using shaped landscapes. Soil Dyn Earthq Eng 2014;25:31–43.

[5] Yang YB, Hung HH. A parametric study of wave barriers for reduction of train-induced vibrations. Int J Numer Meth Eng, 1997;40(20):3729–47.

[6] Hung HH, Yang YB, Chang DW. Wave barriers for reduction of train-induced vibrations in soils. J Geotech Geoenviron Eng (ASCE) 2004;130(12):1283–91.

[7] Sanayei M, Kayiparambil AP, Moore JA, Brett CR. Measurement and prediction of train-induced vibrations in a full-scale building, Eng Struct, 77:119–128, 2014.

[8] Sanayei M, Brett CR, Zapfe JA, Ungar EE, Hines EM. Predicting train-induced vibrations in multi-story buildings. In: Proc of the ASCE, Structures Congress 2008, Vancouver, Canada; April 24–26, 2008.

[9] Sanayei M, Maurya P, Zhao N, Moore JA. Impedance modeling: an efficient modeling method for prediction of building floor vibrations. In: Proc of the ASCE, Structures Congress 2012, Chicago, IL; March 29–31, 2012.

[10] Xiong B, Amick H, Gendreau M. The effect of buildings on ground vibration propagation, Proc of Noise-Con 2007, Reno, NV, 22–24 Oct 2007.

[11] Amick H, Xu T, Gendreau M. The role of buildings and slab-on-grade in the suppression of low-amplitude ambient ground vibrations, Proc of 11th ICSDEE & 3rd ICEGE, Berkeley, CA, 7–9 Jan 2004.

[12] Amick H, Wongprasert N, Montgomery J, Haswell P, Lynch D. An experimental study of vibration attenuation performance of several on-grade slab configurations, Proc. SPIE vol. 5933, Bellingham, WA, 2005.

[13] Persson P. Analysis of vibrations in high-tech facility, Report TVSM-5164, Division of Structural Mechanics, Lund University, Lund, Sweden, 2010.

[14] Persson P, Persson K. Analysis of dynamic soil-structure interaction at high-tech facility. In: Eriksson A, Tibert G, editors. Proceedings of NSCM-23: the 23rd Nordic Seminar on Computational Mechanics. Stockholm, Sweden: 2010.

[15] Persson P, Persson K., Sandberg G. Reduction of traffic-induced vibrations at high-tech facility using trenches. In: Freund J, Kouhia R, editors. Proceedings of NSCM-24: the 24rd Nordic Seminar on Computational Mechanics. Helsinki, Finland: 2011.

[16] Bathe KJ. Finite element procedures, Prentice Hall, New York, 2006.

[17] Zienkiewicz OC, Taylor RL. The finite element method, volume 1 and 2, MacGraw-Hill, London, 1994.

[18] Craig Jr RR, Kurdila AJ, 2006. Fundamentals of structural dynamics, John Wiley & Sons, New Jersey.

[19] Chopra A. K., Dynamics of structures, Prentice Hall, Upper Saddle River, 1995.

[20] Das BM, Ramana GV. Principles of soil dynamics, Cengage Learning, Stamford, 2011.

[21] Dassault Systémes SIMULIA. Abaqus 6.12.

[22] Lysmer J, Kuhlemeyer RL. Finite dynamic model for infinite media. J Eng Mech Div (ASCE), 859-877, 1969.

[23] Cohen M, Jennings PC. Silent boundary methods for transient analysis. In: Belytschko T, Hughes TJR, editors. Computational methods for transient analysis, Elsevier, 1983.

[24] Tyréns, Geotechnical investigation report, Reference number 225686G, Helsingborg 2010-12-10.

[25] Richart FE, Hall Jr JR, Woods RD. Vibrations of soils and foundations, Prentice Hall, Englewood Cliffs, 1970.

[26] Massarsch KR. Vibration isolation using gas-filled cushions. Soil Dynamics Symposium in Honour of Prof. Richard D. Woods, Geo-Frontiers 2005, Austin, Texas, 2005.

[27] Fojab arkitekter Malmö, Hallenborgs gata 1A, 211 19 Malmö, Sweden, 2012.

[28] Snøhetta, Akershusstranda 21, N-0150 Oslo, Norway, 2012.

[29] Hilber HM, Hughes TJR, Taylor RL. Improved Numerical Dissipation for Time Integration Algorithms in Structural Dynamics, Earthq Eng Struct Dyn 1977;5:283–292.

[30] International Organisation for Standardisation. Bases for design of structures – Serviceability of buildings and walkways against vibration, ISO 10137:2007.

[31] Brownjohn JMW, Middleton CJ. Procedures for vibration serviceability assessment of high-frequency floors. Eng Struct 2008;30:1548–1559.

Paper D

Reduced order modelling of liquid-filled pipe systems

P. Persson [*,1], K. Persson [1], G. Sandberg [1]

Department of Construction Sciences, Lund University, P.O. Box 118, SE-22100 Lund, Sweden

ARTICLE INFO

ABSTRACT

In the design of vibration-sensitive structures, large three-dimensional numerical models are frequently used, those occasionally being too large to be simulated in a practical manner. More specifically, the analyses of vibrating complex water-pipe systems require efficient model order reduction strategies. In the paper, a numerical procedure for model order reduction of a water-pipe system housed in a vibration-sensitive research facility is presented. The finite element model employed includes a water-pipe system where fluid–structure interaction effects are accounted for. The reduced model is developed using component mode synthesis and a reduction of the interface degrees of freedom, enabling time-efficient dynamic analyses. The model was proven to be time-efficient and to generate output of high accuracy.

© 2015 Elsevier Ltd. All rights reserved.

1. Introduction

Occasionally, very strict vibrational requirements are specified for sensitive equipment used in high-tech facilities such as radar towers, large ground telescopes and synchrotron facilities. Various external and internal vibration sources, for example traffic, indoor pumps and human activities, can have appreciable effect on the vibration levels in a facility (Persson, 2010). Vibrations originating from external sources could be markedly reduced by using wave obstacles such as trenches and shaped landscapes; see for example Andersen and Nielsen (2005), Persson et al. (2014). The present paper deals with reduction in vibrations stemming from an internal vibration source, namely liquid-filled pipe systems which require large three-dimensional (3 D) numerical models in order to be analysed in a proper manner. The analyses of those models require an efficient numerical model that results in output of adequate accuracy. The pipe system analysed in the paper pertain to a vibration-sensitive research facility; Section 3.1. Note that the presented numerical procedure may be used for dynamic analysis of any application of liquid-filled pipes, such as in automotive and marine industry.

An extensive literature review on liquid-filled pipe systems is presented in Tijsseling (1996), focusing on the development of mathematical models and validation of models to measurements. He stated that the basic equations of fluid-structure interaction (FSI) analyses were derived already in the 19th century and in the 1950 s, the corresponding analytical solutions were presented. In the 1970 s, the basic FSI equations could be solved numerically and in the 1990 s, commercial finite element (FE) codes for FSI analysis were released. In the following non-exhaustive literature review, some of the important work within this field is presented. Several comprehensive studies have been conducted, such as the review of several FE formulations used for solving FSI problems presented in Everstine (1997). Depending on the problem that is to be analysed, different formulations were concluded to be advantageous. In that paper, formulations for FE, boundary element

---

* Corresponding author.
  E-mail address: peter.persson@construction.lth.se (P. Persson).
  [1] Tel: +46 46 222 8353.

and infinite element modelling of the fluid domain interacting with the FE structural domain are summarised. The formulations presented can be used for a variety of problems such as transient acoustics, acoustic cavity analyses and dynamics of fluid-filled pipes. Studies comparing numerical models with measurement data obtained from test set-ups can be found in the literature for several numerical methods. The influence of considering FSI is presented in, for example, Sreejith et al. (2004) where an FE formulation for FSI analyses of liquid-filled pipes used in nuclear reactors is studied. The response from the numerical simulations was validated by a test set-up and it was concluded that FSI had a marked effect on the dynamical behaviour of the structure. Pipe systems are often constructed by assembled standardised components such as pipe fittings, flanges, joints, supports and pipe segments. For these types of structures, it is suitable to use substructuring techniques in order to reduce the often large required size of the FE models. In Maess and Gaul (2006), a substructuring technique for fluid-filled pipes considering FSI by employing the FE method is presented. The reduced model, using component mode synthesis (CMS), was proven to be well-consistent to a full model as well as to measured data. In Maess and Gaul (2007), further model reduction was obtained by employing modal truncation. The model reduction achieved by CMS can be extended by reducing the number of degrees of freedom (dofs) at the substructure interfaces. This was performed by Herrmann et al. (2010) by incorporating reduction of the substructure interfaces, realised by Ritz vectors, resulting in a time-efficient reduced order model introducing low error levels.

Some general conclusions from the papers referred to above can be drawn. By considering the interaction between the pipe and the liquid, the dynamical behaviour of the system changes, hence, it is often needed to consider the interaction between the pipe and its containing liquid, especially for thin-walled pipes. In order to improve the computationally efficiency of the numerical analyses, reduced order modelling can be employed through the use of CMS. Since the efficiency of CMS depends on the number of interface dofs, the use of interface reduction results in a more time-efficient model. None of the investigations referred to above, however, considered the technique of reducing the number of dofs at the substructure interfaces by using a condensation node. The concept of using a condensation node, in relation to Ritz vectors, for reducing dofs at the interfaces results in a more versatile approach since the substructure interfaces are reduced independent from each other; see Sections 2.4 and 3.2. The study presented here focuses on the development of an efficient numerical procedure using interface reduction in combination with CMS. CPU times for different reduced order models in relation to their introduced error are studied by employing coupled FSI analyses by means of the FE method.

2. Governing equations

In the section, the governing theory of structural dynamics, the interaction between an acoustic fluid and a structure and the basic equations of component mode synthesis and of interface reduction, are presented.

2.1. Structural dynamics

The differential equation of motion for the continuum formulation of a three-dimensional solid is written as

$$\tilde{\nabla}^T \boldsymbol{\sigma}_S + \mathbf{b}_S = \rho_S \frac{\partial^2 \mathbf{u}}{\partial t^2} \tag{1}$$

where $\boldsymbol{\sigma}_S$ is the stress tensor, $\mathbf{b}_S$ is the body force vector, ρ_S is the mass density, $\mathbf{u}$ is the displacement vector, $\tilde{\nabla}$ is a differential operator and t is the time. With use of Galerkin's method, FE formulation for the structural domain becomes (Bathe, 2006; Zienkiewicz and Taylor, 1994)

$$\mathbf{M}_s \ddot{\mathbf{u}} + \mathbf{K}_s \mathbf{u} = \mathbf{f}_s, \tag{2}$$

where $\mathbf{M}_s$ is the mass matrix, $\mathbf{K}_s$ the stiffness matrix, $\mathbf{f}_s$ the load vector and $\mathbf{u}$ the nodal displacement vector. Since damping has to be included in the FE model in order to obtain a realistic response, a rate-independent linear damping was assumed by means of the loss factor, introduced by the structural damping matrix (Craig and Kurdila, 2006).

2.2. Fluid–structure interaction

In the present paper, completely filled pipes are assumed where acoustic pressure is dominant, i.e. sloshing is not considered. Two governing equations can be employed for describing the pressure filed of a homogeneous acoustic fluid, which is assumed to be inviscid, irrotational (curl $\mathbf{u}_f = 0$), compressible and to undergo small pressure changes. The equation of motion, the volumetric drag being neglected here, can be written as

$$\rho_0 \frac{\partial^2 \mathbf{u}_f}{\partial t^2} + \nabla p = 0 \tag{3}$$

where ρ_0 is the static density, $\mathbf{u}_f$ is the fluid displacement vector, t is the time, ∇ is the gradient operator and p is the acoustic fluid pressure (Morand and Ohayon, 1995; Sandberg and Ohayon, 2008). The constitutive equation for a barotropic fluid

with constant density can be written as

$$p = -c_0^2 \rho_0 \nabla \mathbf{u}_f,$$ (4)

where c_0 is the speed of sound. With use of Eqs. (3) and (4), the wave equation for the acoustic fluid, the pressure serving as the field variable, can be written as the Helmholtz equation

$$\frac{\partial^2 p}{\partial t^2} - c^2 \nabla^2 p = 0.$$ (5)

By expressing the pressure as a complex harmonic function

$$p = \hat{p} e^{i\omega t}$$ (6)

the wave equation in the frequency domain becomes

$$\nabla^2 \hat{p} + \frac{\omega^2}{c^2} \hat{p} = 0.$$ (7)

Thus, with use of Galerkin's method, the FE formulation for the acoustic fluid domain can be written as

$$\mathbf{M}_f \ddot{\mathbf{p}} + \mathbf{K}_f \mathbf{p} = \mathbf{f}_f,$$ (8)

where $\mathbf{p}$ the nodal pressure vector.

2.3. Coupling of domains

Continuity in fluid and structural displacements, as well as in pressure, is assumed in the direction normal to the domain's common boundary. By introducing a coupling matrix, $\mathbf{H}$, the complete fluid-structure system of equations can be written as

$$\underbrace{\begin{bmatrix} \mathbf{M}_s & \mathbf{0} \\ \rho_0 \mathbf{H}_{sf}^T & \mathbf{M}_f \end{bmatrix}}_{\mathbf{M}} \underbrace{\begin{bmatrix} \ddot{\mathbf{u}} \\ \ddot{\mathbf{p}} \end{bmatrix}}_{\ddot{\mathbf{x}}} + \underbrace{\begin{bmatrix} \mathbf{K}_s & -\mathbf{H}_{sf} \\ \mathbf{0} & \mathbf{K}_f \end{bmatrix}}_{\mathbf{K}} \underbrace{\begin{bmatrix} \mathbf{u} \\ \mathbf{p} \end{bmatrix}}_{\mathbf{x}} = \underbrace{\begin{bmatrix} \mathbf{f}_s \\ \mathbf{f}_f \end{bmatrix}}_{\mathbf{q}}.$$ (9)

2.4. Component mode synthesis

Various methods for conducting substructuring have been developed over the years, see for example Flodén et al. (2014). The substructuring process used here, CMS by Craig–Bampton, is currently the most common method used for substructuring in structural dynamics problems (de Klerk et al., 2008). In the substructuring process, a structure is divided into smaller parts called substructures, each of them described by the equation of motion (Craig and Kurdila, 2006). Since the damping in the reduced parts is low, it has a negligible influence on the eigenmodes and eigenfrequencies. The damping matrix can therefore be neglected in the reduced system, thus, in the following derivations, the damping matrix is left out. The dofs are separated into boundary dofs (index b) and internal dofs (index i), the internal dofs being reduced in the Craig-Bampton method. Thus, the so-called boundary dofs are retained in the process. The size of a substructure is reduced by introducing a transformation of the field vector, thus partitioning of the equation system in Eq. (9) results in

$$\begin{bmatrix} \mathbf{M}_{bb} & \mathbf{M}_{bi} \\ \mathbf{M}_{ib} & \mathbf{M}_{ii} \end{bmatrix} \begin{bmatrix} \ddot{\mathbf{x}}_b \\ \ddot{\mathbf{x}}_i \end{bmatrix} + \begin{bmatrix} \mathbf{K}_{bb} & \mathbf{K}_{bi} \\ \mathbf{K}_{ib} & \mathbf{K}_{ii} \end{bmatrix} \begin{bmatrix} \mathbf{x}_b \\ \mathbf{x}_i \end{bmatrix} = \begin{bmatrix} \mathbf{q}_b \\ \mathbf{q}_i \end{bmatrix}.$$ (10)

In the Craig–Bampton method, the neglected inertia terms in condensation methods, for example in Guyan reduction (Guyan, 1965), are compensated by considering eigenmodes that are obtained with fixed interface boundary dofs, $\mathbf{u}_b = \mathbf{0}$ (Craig and Kurdila, 2006). Therefore, a set of generalised coordinates $\boldsymbol{\xi}$ which represent the amplitudes of the eigenmodes is introduced. Assuming unloaded internal dofs, $\mathbf{f}_i = \mathbf{0}$, as well as a harmonic solution, the following eigenvalue problem is obtained

$$\mathbf{K}_{ii} \boldsymbol{\Phi} = \omega^2 \mathbf{M}_{ii} \boldsymbol{\Phi}$$ (11)

from which the eigenmodes $\boldsymbol{\Phi}$ and the eigenfrequencies ω can be calculated. Eigenmodes are selected as additional basis vectors to the approximation of the internal dofs as

$$\mathbf{x}_i = -\mathbf{K}_{ii}^{-1} \mathbf{K}_{ib} \mathbf{x}_b + \sum \boldsymbol{\Phi}_j \xi_j = \boldsymbol{\Psi} \mathbf{x}_b + \boldsymbol{\Phi} \boldsymbol{\xi}.$$ (12)

The transformation matrix according to the Craig–Bampton method, $\mathbf{T}$, can then be defined by

$$\begin{bmatrix} \mathbf{x}_b \\ \mathbf{x}_i \end{bmatrix} = \begin{bmatrix} \mathbf{I} & \mathbf{0} \\ \boldsymbol{\Psi} & \boldsymbol{\Phi} \end{bmatrix} \begin{bmatrix} \mathbf{x}_b \\ \boldsymbol{\xi} \end{bmatrix} = \mathbf{T} \overline{\mathbf{x}}.$$ (13)

Thus, the reduced coupled system in Eq. (9) can be obtained as

$$\overline{\mathbf{M}}\ddot{\overline{\mathbf{x}}} + \overline{\mathbf{K}}\overline{\mathbf{x}} = \overline{\mathbf{q}} \tag{14}$$

where $\overline{\mathbf{M}} = \mathbf{T}^T\mathbf{M}\mathbf{T}$, $\overline{\mathbf{K}} = \mathbf{T}^T\mathbf{K}\mathbf{T}$ and $\overline{\mathbf{q}} = \mathbf{T}^T\mathbf{q}$.

2.5. Interface reduction

To increase the computational efficiency of CMS it is advantageous to also reduce the number of retained interface dofs ($\mathbf{u}_b$) already in the substructure generation process. A condensation node (having three translation and three rotational dofs) is then introduced for each interface surface of the substructure with the intention to represent the motion of the interface in question, i.e. the dofs at the interface are coupled to the condensation node. The coupling can be realised in various ways, rigid and distributed coupling being used here. Therefore, only the dofs of the condensation nodes are retained in the substructuring process (instead of all interface dofs). The dofs of the condensation nodes appear as boundary interface boundary dofs, $\mathbf{x}_b$, in the reduced system (cf. Eq. (13)).

2.5.1. Rigid coupling

In rigid coupling, the interface is assumed to undergo rigid body motions which are described by the dofs of the condensation node. The coupling between the interface nodes and the condensation node is given by

$$\mathbf{u}_i = \mathbf{u}_c + \mathbf{\Theta}_c \times \mathbf{r}_{ci} \tag{15}$$

where $\mathbf{u}_i$ is the displacement vector of the ith interface node, $\mathbf{u}_c$ is the displacement vector for the condensation node, $\mathbf{\Theta}_c$ is a vector containing the rotations of the condensation node and the vector $\mathbf{r}_{ci}$ contains the distances from node i to the condensation node.

2.5.2. Distributed coupling

In distributed coupling, a weighted average motion of the interface surface is used to describe the motion of the condensation node. The forces and moments acting on the condensation node are coupled to the interface nodes by (Dassault Systèmes SIMULIA, 2012)

$$\mathbf{f}_i = \hat{v}_i\left(\mathbf{f}_c + \left(\mathbf{P}^{-1}(\mathbf{m}_c + \mathbf{r}_c \times \mathbf{f}_c)\right) \times \mathbf{r}_i\right) \tag{16}$$

where

$$\mathbf{P} = \sum_i \hat{v}_i\left((\mathbf{r}_i^T\mathbf{r}_i)\mathbf{I} - (\mathbf{r}_i\mathbf{r}_i^T)\right). \tag{17}$$

The forces acting on interface node i are denoted $\mathbf{f}_i$, whereas the forces and the moments acting on the condensation node are denoted $\mathbf{f}_c$ and $\mathbf{m}_c$, respectively. Thus, i, spans over the set of interface nodes. The vectors $\mathbf{r}_i$ and $\mathbf{r}_c$ contains the distances from the weighted centre of the interface, $\overline{\mathbf{x}}$, to the condensation node and to node i, respectively. They are given by

$$\mathbf{r}_i = \mathbf{x}_i - \overline{\mathbf{x}}, \quad \mathbf{r}_c = \mathbf{x}_c - \overline{\mathbf{x}} \tag{18}$$

where

$$\overline{\mathbf{x}} = \sum_i \hat{v}_i\mathbf{x}_i, \quad \hat{v}_i = \frac{v_i}{\sum_i v_i}. \tag{19}$$

The vectors $\mathbf{x}_i$ and $\mathbf{x}_c$, contain the coordinates of the interface node i and the condensation node, respectively, and the weight factor assigned to the interface node i is denoted v_i.

This type of coupling results in the displacements of the condensation node being weighted averages of the displacements of the interface according to

$$\mathbf{u}_c = \sum_i \hat{v}_i\mathbf{u}_i, \tag{20}$$

$$\mathbf{\Theta}_c = \sum_i \hat{v}_i\frac{\mathbf{r}_{ci}}{|\mathbf{r}_{ci}|^2} \times \mathbf{u}_i. \tag{21}$$

The weight factors can be chosen arbitrarily, resulting in an infinite number of ways to define the coupling. The simplest way is uniform weighting where the loads are distributed equally to the condensation node as

$$v_i = 1. \tag{22}$$

Other common methods use polynomials to describe the decreasing influence of the interface forces with increasing distance to the condensation node, for example, linearly and quadratically decreasing weighting as

$$v_i = 1 - \frac{|\mathbf{r}_{ci}|}{|\mathbf{r}_{c0}|}, \quad v_i = 1 - \left(\frac{|\mathbf{r}_{ci}|}{|\mathbf{r}_{c0}|}\right)^2. \tag{23}$$

where $\mathbf{r}_{c0}$ is the distance from the condensation node to farthest located interface node.

3. Numerical procedure

In the section, the numerical example case as well as the employed FE model considering FSI are described. Also, the developed reduced order model employing interface reduction as well as CMS, is presented.

3.1. FE model

The MAX IV facility, which was used as an example case in this study, is built in order to improve research possibilities and to address new scientific challenges in research fields such as material science and medicine. In the large ring-shaped building at the MAX IV facility (Fig. 1), electron beams are to be controlled by a large number of magnets that are distributed along that building as well as along beamlines that lead electrons to measurement stations. Since the quality of the measurements depends upon the vibration levels of the magnets, strict requirements are specified for the vibration-sensitive parts of the facility. The vibration requirements regarding vertical displacements of the magnets are especially strict, its being required that these be less than 20–30 nm in RMS per second. Several water-pipe systems used for cooling purposes will be placed near vibration sensitive areas in the facility and thus transmitting vibrations that could exceed the vibration
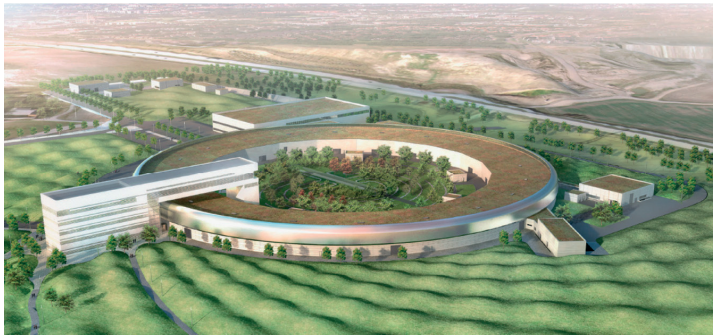

Fig. 1. An architectural sketch of the MAX IV facility as planned (Fojab, 2012; Snøhetta, 2012).
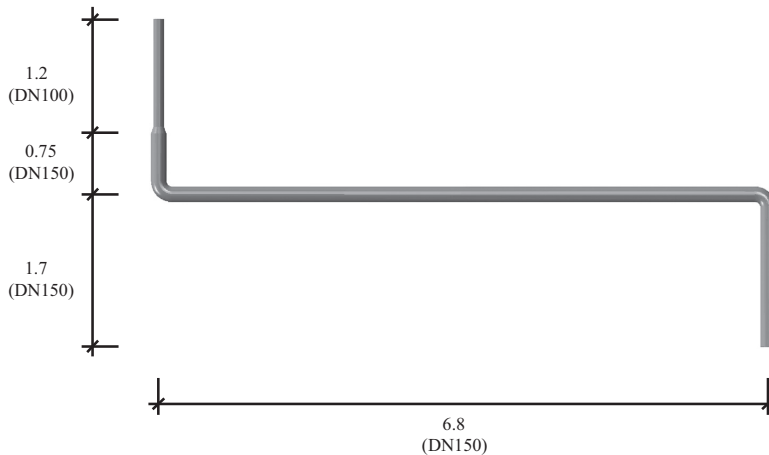

Fig. 2. The modelled pipe system. The dimensions are in units of meters.

requirements. Hence, time-efficient numerical studies needs to be conducted in order to investigate the vibration transmission from those pipe systems.

A water-pipe system constituted by two different pipe cross-sections, DN100 and DN150, which mimics those located in the MAX IV facility was used as a test example here; see Fig. 2. The pipes and their supports were assumed to be made of the stainless steel, having a 5 mm soft elastomer layer in between them (cf. Fig. 5); see Table 1 for the material properties. In the study, the frequency-dependence of the elastomer material properties was assumed to be negligible. A 3D FE model was developed with the use of the FE software package *Abaqus* 6.12 (Dassualt Systèmes 2012). The parts involved in the model were the pipes, including the water contained in them and the supports. Each of the supports has a length of 0.2 m and a squared cross-section with the side length 0.02 m. The supports had fixed displacement boundary conditions at their building interfaces. Considering the contacts between supports–elastomer and pipe–elastomer, the friction was assumed to be strong, hence, full interaction by coupling of the displacement dofs was applied. The employed loss factors include attenuation effects such as the friction in joints. Strains corresponding to displacements at the nano-scale are usually at a level such that the assumption of linear elasticity is applicable for the involved materials. Solid 20-node elements with quadratic approximation, using reduced integration, were employed for the steel supports and for the elastomer layer, whereas quadratic 8-node shell elements were used for to the pipes. The water was assumed to have a temperature of 10 °C, the static density of it, ρ_0, being set to 1000 kg/m^3 and the speed of sound, c_0, to 1450 m/s, resulting in a bulk modulus, K, of 2.10 GPa. In modelling the water, 20-node quadratic acoustic pressure elements were employed.

To compare different ways of modelling the water contained in the pipes, eigenvalue analyses were performed under free-free conditions. Two different models were used for the investigation; one model considering FSI of the pipes and the water contained in them, and the other model considering the water as an added mass modelled by increasing the mass density of the steel pipes, i.e. no interaction between the fluid and the structure was considered in the latter model (Sandberg and Ohayon, 2008). The eigenvalue analyses were performed for eigenfrequencies up to 100 Hz, involving the first 12 eigenmodes (excluding the rigid body modes). The modal assurance criteria (MAC) is used here for comparing eigenmodes (Allemang and Brown, 1982) obtained from different FE models. The criteria provides a measure of the consistency between two eigenmode vectors, were a MAC value of 1 is obtained in the case of two identical vectors. The MAC value for the ith eigenmode of model A, Φ_i^A, as compared with the jth eigenmode of model B, Φ_j^B, is defined as

$$\text{MAC} = \frac{|(\Phi_i^A)^T(\Phi_j^B)|^2}{(\Phi_i^A)^T(\Phi_i^A)(\Phi_j^B)^T(\Phi_j^B)}. \tag{24}$$

In Fig. 3(a), the MAC values for the FSI model compared to itself are shown, used here as the reference plot. Since the eigenmodes are non-orthogonal in the dot-product, the off-diagonal terms are generally non-zero. In this particular case, the off-diagonal terms are less than 0.2 for the eigenmodes considered. In Fig. 3(b), the eigenmodes of the FSI model are compared to the added mass model. As can be seen, the two sets of eigenmode vectors are not consistent. Especially, mode number 1 and 2 are shifted. Moreover, modes 6, 8–10 and 12 have very low MAC values, especially modes 9, 10 and 12

Table 1
Properties of the solid materials.

Property	Stainless steel	Elastomer
Elastic modulus (MPa)	200,000	1
Loss factor	0.02	0.1
Mass density ($\cdot 10^3$ kg/m^3)	7.9	1
Poisson's ratio	0.30	0.45
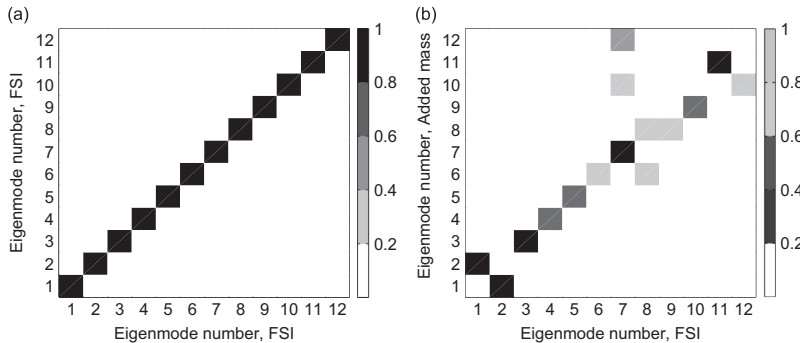
Fig. 3. MAC values for the first 12 eigenmodes for the FSI model (a) compared to itself and (b) compared to the added mass model.

where the cross-sections of the pipe are much more deformed in the added mass model. The normalised relative frequency difference (NRFD) was used to compare eigenfrequencies from different models to each other. It is defined, in percent, for the ith eigenmode as

$$\text{NRFD} = 100\frac{|f_i^A - f_i^B|}{f_i^B}, \tag{25}$$

where f_i^A is the ith eigenfrequency of model A and f_i^B is the ith eigenfrequency of model B. As can be seen in Fig. 4, those modes do not necessarily need to have large NRFD values. The ninth mode, for example, has a very low NRFD value, approximately 1%, but the eigenmodes are, however, not consistent. Due to the low correlation between the FSI model and the added mass model, FSI was used here where the water was modelled as an acoustic fluid, using acoustic pressure as the field variable.

3.2. Interface reduction

Different methods for reducing the dofs at the interfaces between the pipe and its supports retained in a substructuring process were investigated here. The complete modelled pipe system is shown in Fig. 5. Also, the support and the pipe are separated in order to show the coupling of the interface nodes to the condensation node. Different interface reduction methods, all using a condensation node, were applied to the interface between the elastomer and the attaching part of the pipe. All possible combinations of rigid coupling and distributed coupling using uniform-, linear- and quadratic weighting were employed for the interface of both the pipe and of the elastomer. As shown in the figure, the condensation node is located in the centre of the coupling.

The pipe has one element in the width of the support. Since quadratic interpolation was used, this results in three nodes in the support width. The elastomer layer, however, has two elements, and thereby five nodes, in the width of the support. Considering the interface reduction of the pipe interface, the normalised weighting factors, defined Section 2.5.2, will have
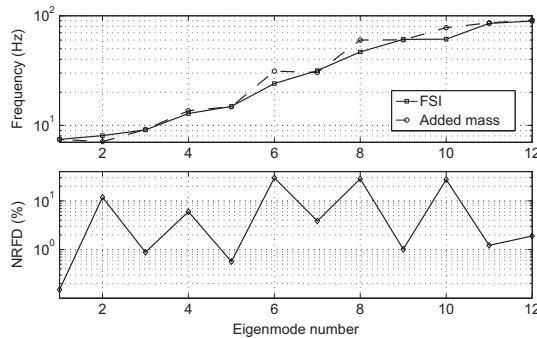

Fig. 4. Eigenfrequency versus eigenmode number, considering the FSI model and the added mass model, as well as NRFD values versus eigenmode number.
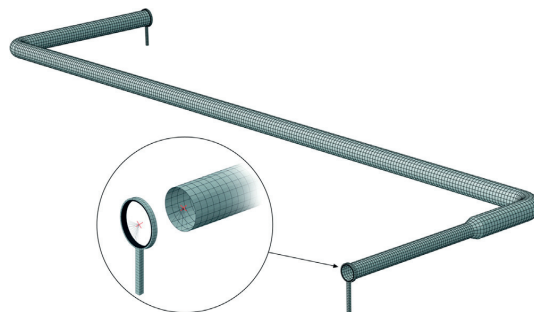

Fig. 5. FE mesh of the modelled pipe system, excluding the contained water. The elastomer is shown in black colour and the steel in grey colour. The condensation node is marked with a cross in red colour. The coupling constraints are schematically shown as dashed black lines for a quarter of the interface. Note that only the corner nodes of the elements are involved in the illustration for the sake of visibility.
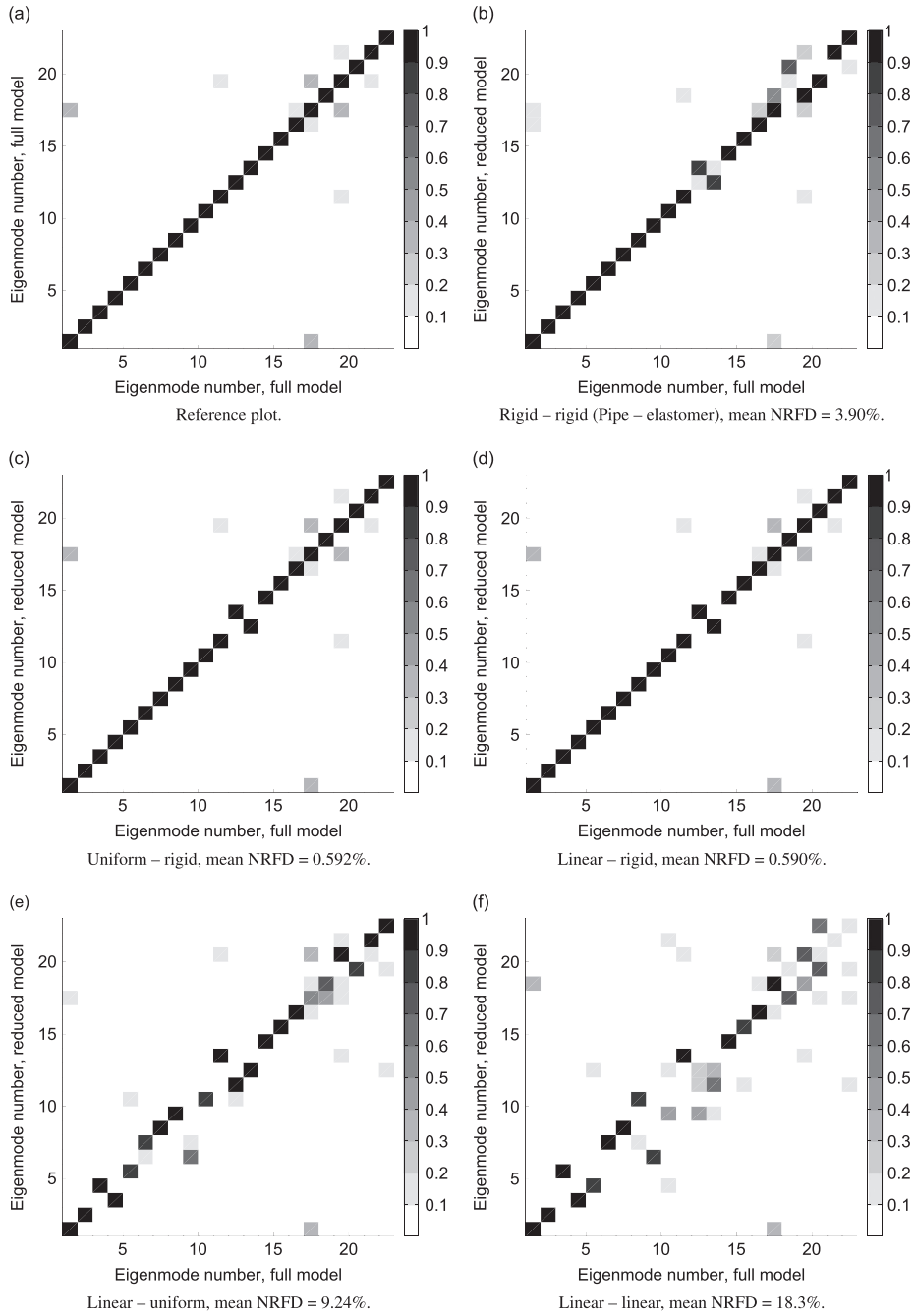
Fig. 6. MAC values for the first 22 eigenmodes for the reduced interface models as compared to the full model, using different weighting methods for the interfaces between the pipe and the supports.

the same value for linearly and quadratically distributions since the weighting factor used for the farthest nodes will be zero (cf. Eq. (23)). Having an uniform coupling constraint for the pipe resulting in practically the same eigenfrequencies and eigenmodes as for the other types of distributed coupling even though the two outer rings of element nodes have a weight factor in the uniform coupling. By using uniform distributed coupling type for the elastomer interface, as compared to the linear- and quadratic coupling type, however, results in a different response since the linear and quadratic coupling types yield spurious modes of the elastomer. In difference to the pipe interface, the elastomer interface is constituted of five (instead of three) rings of nodes, resulting in that the difference between linear interpolation and quadratic interpolation comes into play (only the farthest nodes having a weighting factor of zero).

MAC values for different coupling types compared to the full model are shown in Fig. 6. In subplot (a) the full model is compared to itself, used here as a reference plot. By comparing MAC values in the subplots (b)–(f) with MAC values in the reference one (a), the consistency between the modes can be evaluated. Considering rigid coupling for both interfaces (b), a fairly good resemblance to the reference plot is depicted up to mode number 16, with the exception that mode 12 and 13 are shifted. The 12th mode in the full model is slightly shifted up in frequency, resulting in that mode appearing as the 13th mode in the reduced models instead. Mode numbers 18-20 in the full model involve breathing modes of the pipe, which rigid coupling cannot resolve. The shift of modes 12 and 13 is also seen in (c) and (d), where distributed coupling is used for the pipe and rigid coupling for the elastomer. Except that shift, (c) and (d) are identical to the reference plot. As seen in subplot (e), by changing the coupling of the elastomer interface from rigid to uniform, a marked effect on the eigenmodes is found where only about one third of the eigenmodes were consistent. As stated earlier, using linear or quadratic coupling for the elastomer appreciably influence the eigenmodes, due to spurious modes, as portrayed in subplot (f).

In Fig. 7(a) it is seen that using rigid coupling on both the pipe and the elastomer interface, respectively, results in consistently stiffer coupling than in the full model. This is explained by the fact that additional stiffness is being imposed by using rigid coupling. By employing distributing coupling (uniform, linear, quadratic) for both interfaces, uniform being shown here, a consistently weaker coupling is introduced since relative motion of the interfaces is allowed. For the models considering rigid coupling on one of the interfaces and distributed coupling on the other, alternating stiffer and softer behaviour is found for the different eigenmodes. In Fig. 7(b), the NRFD values for the coupling types presented in Fig. 7 (a) are shown. Considering those four types, it is seen that uniform coupling of the pipe interface and rigid coupling of the elastomer result in the lowest mean NRFD value.

Since full interaction is assumed and because the elastomer strip is very soft, as compared to the steel pipe, the motion of the elastomer surface at the pipe interface follows the motion of the pipe. Hence, the soft interface surface shows a rigid
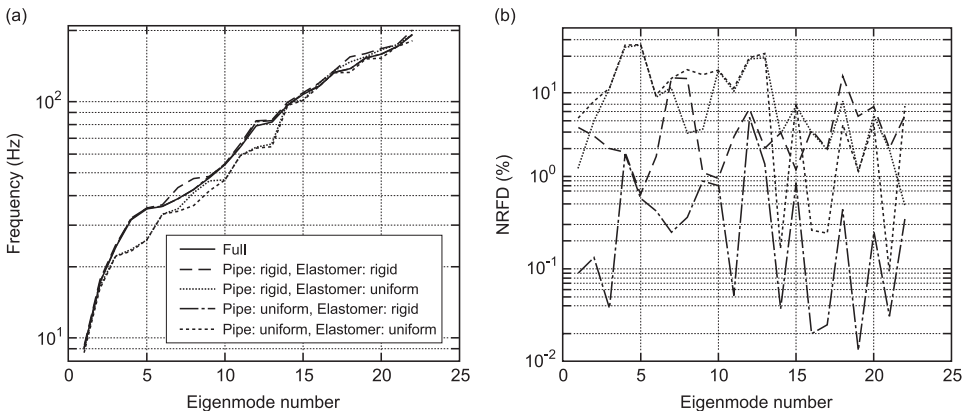

Fig. 7. Eigenfrequency (a) and NRFD values (b), respectively, versus eigenmode number, considering different weighting methods for the interface reduction. The legend shown in (a) is valid for both plots.

Table 2
Mean NRFD values, in percent, for all combinations of the different coupling types. Maximum NRFD values within brackets.

Pipe	Elastomer			
	Rigid	Uniform	Linear	Quadratic
Rigid	3.90 (12.20)	8.01 (26.36)	16.56 (39.55)	16.55 (39.54)
Uniform	0.592 (4.37)	9.23 (26.41)	18.26 (40.62)	18.25 (40.62)
Linear/quadratic	0.590 (4.36)	9.24 (26.40)	18.26 (40.62)	18.25 (40.62)
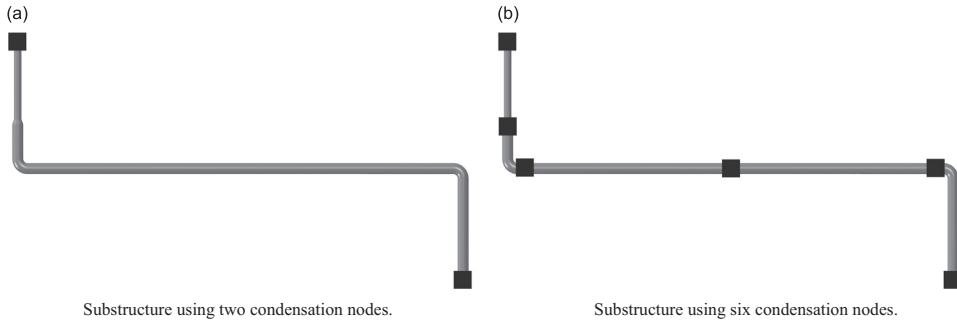
Fig. 8. The placement of the retained condensation nodes, illustrated by black coloured squares: (a) substructure using two condensation nodes and (b) substructure using six condensation nodes.
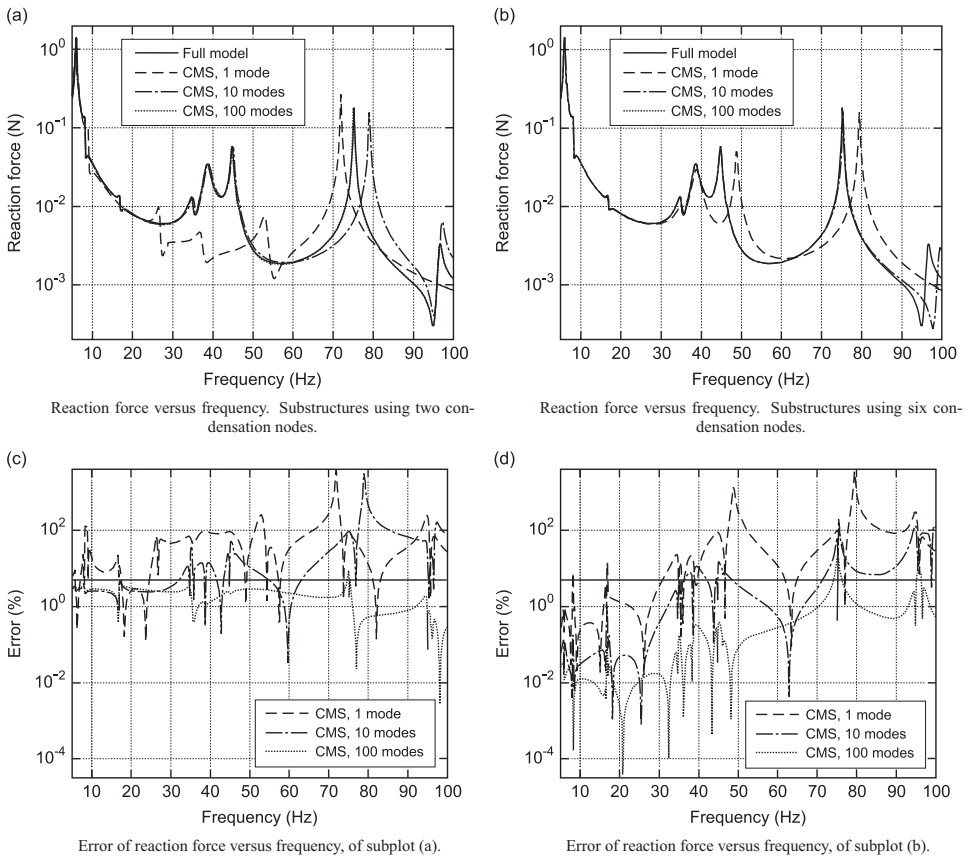
Fig. 9. Reaction force evaluated at one pipe support. In subplot (c) and (d), the horizontal solid line in black colour represents an error level of 5%. (Note that in subplots (a) and (b), the lines representing the full model and the CMS model retaining 100 modes coincides (a) Reaction force versus frequency. Substructures using two condensation nodes (b) Reaction force versus frequency Substructures using six condensation nodes (c) Error of reaction force versus frequency, of subplot (a) (d) Error of reaction force versus frequency, of subplot (b).

behaviour (as compared to the interior of the part with the soft material), thus rigid coupling being the most accurate interface reduction type for the elastomer. Since the distances between the node rings of the elastomer interface are small in the FE model employed here, the descending effect of linear and quadratic coupling is negligible. As breathing modes of the pipe are of great importance for its dynamic behaviour, distributed coupling for the pipe yielding the lowest errors since the coupling type allows radial movement of the interface nodes, which is not the case for rigid coupling. In Table 2, the NRFD values for all different coupling types are shown. It is portrayed that using distributed coupling for the pipe, with either linear or quadratic weighting, in combination with rigid coupling of the elastomer resulted in the lowest error, i.e. the lowest NRFD values.

3.3. Component mode synthesis

In order to further reduce the models, investigation of the effect of the number of retained modes as well as various number retained dofs on CMS by Craig–Bampton (here denoted as CMS) was conducted. Note that in the example case used here, the number of interface nodes (that has to be retained if interface reduction is not used) being very large. It results in that it was not possible, at the computer used, to set up the system matrices with using interface reduction. Hence, since it was not possible to run those simulations, it was not discussed in the paper.

Steady-state analyses were carried out here in order to study the time-efficiency achieved, as well as the errors introduced. A harmonically varying acoustic unit pressure (1 Pa) was applied to the free end of the DN150 pipe-section. At the other end of the water-pipe system, the gradient of the water pressure was prescribed to zero, thus, representing a stiff boundary surface. Throughout this section, two supports were used for the pipe system in the FE model, one in each end; see Fig. 5. In order to investigate the accuracy of the reduced order models, the reaction force at the support located at the opposite end of the pipe in relation to where the acoustic pressure was applied, was evaluated. Since the numerical efficiency of the models reduced by employing CMS depends on the number of retained interface dofs, interface reduction, as described Section 3.2, was employed. The elastomer interfaces were, hence, rigidly attached to their corresponding condensation nodes, whilst the coupling of the pipe to the condensation nodes was realised by using linear distributed coupling.

Substructures using two condensation nodes (cf. Fig. 8(a)), as well as six condensation nodes (cf. Fig. 8(b)) were investigated. In the substructures based on two retained condensations nodes, 12 (2×6) retained dofs were used, whereas the substructures with six condensation contained 36 (6×6) retained dofs. The computational cost increases with increasing number of retained dofs, however, the frequency of the highest retained eigenmode is higher, generally resulting in lower errors for the same number of retained eigenmodes.

To evaluate the number of retained eigenmodes needed to obtain a reduced order model that generates output of adequate accuracy, both the mean and the maximum errors introduced by the CMS models with various number of retained eigenmodes were studied. The size of the substructure model is given by the number of retained eigenmodes and the number of retained dofs. By using a reduced order model of the pipes and its contained water, the number of unknowns is drastically reduced, which decreases the computational time and the needed memory capacity required for dynamic analyses of the water-pipe system. The system matrices will not be entirely banded in the reduced order models due to the

Mean error versus number of retained modes.
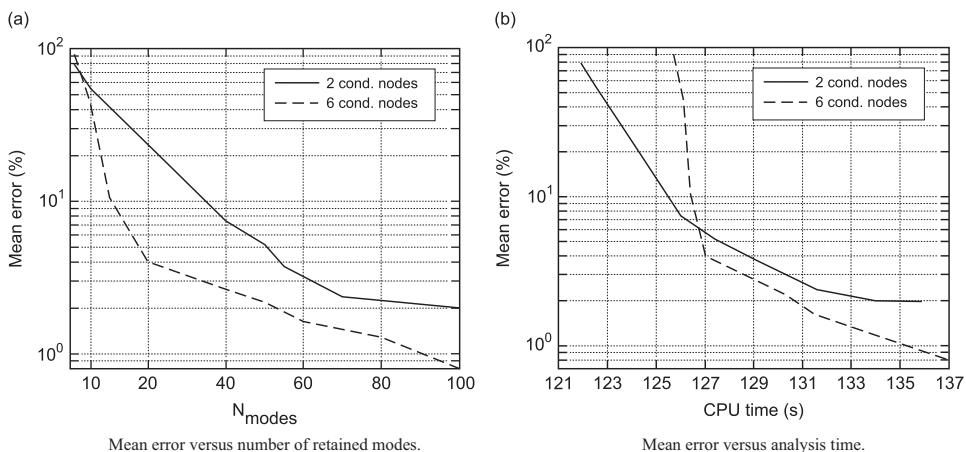
Mean error versus analysis time.

Fig. 10. Mean error of reaction force versus number of retained eigenmodes and analysis time, respectively: (a) mean error versus number of retained modes and (b) mean error versus analysis time.

full matrices corresponding to the retained dofs, i.e. the total number of unknowns is not a sufficient measure of the computational efficiency of a reduced order model, hence, the analysis time was evaluated.

In Fig. 9, the reaction force versus frequency is plotted in subplot (a), the corresponding error is plotted in the subplot (c), for substructures using two condensation nodes; see subplots (b) and (d) for six condensation node substructures. As seen in Fig. 9b, by retaining only one mode for the substructure using two condensation nodes resulted in errors frequently exceeding 5% at about 8 Hz and higher frequencies. By using the substructure involving six condensation nodes, however, errors frequently exceeding the same limit (5%) occur first at approximately 30 Hz. When 100 modes are retained, the investigated substructures introduced an error, generally, lower than 5%, only at the frequency peak of 75 Hz the error exceeded that limit.

The analysis times presented in the paper are the actual CPU time used in executing a steady-state analysis of 100 frequency steps, using one core of an Intel i7-2640 M of 2.80 GHz with 5 GB of RAM available.

In order to achieve a mean error of the reaction forces of less than 5%, 55 modes were needed to be retained in the case with two retained condensation nodes, whereas in the case of six retained condensation nodes, 11 modes were needed. The analysis time for the steady-state analyses performed for the two different models ended up in 129.1 s for the two condensation node model and 126.5 s for the six condensation node model, thus the six node substructure being preferable. In considering a lower limit for the accuracy, for example a mean error of less than 2%, 110 retained modes were required for the two condensation node model, whereas the six condensation node model required 54 modes. The analysis time ended up at 134.6 s for the two node model and at 130.6 s for the six node one. It is therefore advantageous, also in this case, to use the six condensation node substructure. Moreover, the substructure using six condensation nodes has six different locations to place the supports, which is a great advantage over the two node model that, obviously, only has two possibilities. By using the six node substructure, the same substructure can be used throughout an investigation of the influence of varying the support locations, thus the modelling time decreases.

In Fig. 10(a), it is portrayed that the mean errors introduced by the substructures using six condensation nodes decreases more rapid with number of retained modes as compared to the two condensation node substructures. Further, it is possible to achieve a lower mean error with the six condensation node substructures than with the two node ones, which reaches a threshold at a mean error of approximately 2%. In Fig. 10(b), it is depicted that in case of allowing large mean errors, larger than approximately 6%, the substructures using two condensation nodes contributes to faster simulations than the substructures using six nodes does. At lower mean errors, however, use of six condensation node substructures results in shorter analysis times.

4. Concluding remarks

In the paper, a numerical procedure for reducing large three-dimensional numerical models of vibrating complex water-pipe systems, was presented. The FE model employed includes a water-pipe system, considering FSI as well as the use of CMS involving interface reduction, to enable time-efficient dynamic analyses. The use of the developed reduced order model was proven to be time-efficient as well as to generate output of high accuracy, using full FE model as reference.

Applying interface reduction for a soft interface, as compared to the surrounding structure, rigid coupling will preferably be used since the interface surface is exposed to small strains compared to the interior of the part. Since breathing modes are important for the dynamical behaviour of a liquid-filled pipe, distributed coupling is advantageous for the pipe interface. Which of the different distributed coupling methods to use in calculating the weighting factors depends on the interface stiffness of the application at hand. In the paper, the breaking point where the substructure model using six retained condensation nodes and the two node model have the same computation time, occurs at a mean error of 6%. Thus, the substructures using six condensation nodes are preferably used when lower errors are required. It is also possible to achieve lower mean errors by using the six node substructure than the two node one. By retaining more condensation nodes in the substructure generation process, additional possibilities for support locations are allowed. CMS in combination with interface reduction results in time-efficient numerical models, generating output of high accuracy as compared to the full model, while at the same time reducing the analysis times markedly. The obtained reduced order model from the developed numerical procedure presented here, may be well-suited for dynamic analyses in various application, such as vibration reduction in buildings and in vehicles.

References

Andersen, L., Nielsen, S.R.K., 2005. Reduction of ground vibration by means of barriers or soil improvement along a railway track. Soil Dynamics and Earthquake Engineering 25 (7–10), 701–716.
Allemang, R.J., Brown, D.L., 1982. A Correlation Coefficient for Modal Vector Analysis, In: Proceedings of International Modal Analysis Conference, pp. 110–116.
Bathe, K.J., 2006. Finite Element Procedures. Prentice Hall, New York.
Craig Jr., R.R., Kurdila, A.J., 2006. Fundamentals of Structural Dynamics. John Wiley& Sons, New Jersey.
Dassault Systèmes SIMULIA, 2012. Abaqus documentation 6.12.

de Klerk, D., Rixen, D.J., Voormeeren, S.N., 2008. General framework for dynamic substructuring: history, review, and classification of techniques. AIAA Journal 46 (5), 1169–1181.

Everstine, G.C., 1997. Finite element formulations of structural acoustics problems. Computers and Structures 65 (3), 307–321.

Fojab, Hallenborgsgata, 2012 1A, 21119 Malmö, Sweden.

Flodén, O., Persson, K., Sandberg, G., 2014. Reduction methods for the dynamic analysis of substructure models of lightweight building structures. Computers and Structures 138, 49–61.

Guyan, R.J., 1965. Reduction of stiffness and mass matrices. AIAA Journal 3, 380.

Maess, M.K., Gaul, L., 2006. Substructuring and model reduction of pipe components interacting with acoustic fluids. Mechanical Systems and Signal Processing 20, 45–64.

Maess, M.K., Gaul, L., 2007. Simulation of structural deformations of flexible piping systems by acoustic excitation. Journal of Pressure and Vessel Transactions (ASME) 129, 363–371.

Herrmann, J., Maess, M.K., Gaul, L., 2010. Substructuring including interface reduction for the efficient vibro-acoustic simulation of fluid-filled piping systems. Mechanical Systems and Signal Processing 24, 153–163.

Morand, H., Ohayon, R., 1995. Fluid-Structure Interaction. Wiley, Chichester.

Persson, P., 2010. Analysis of vibrations in high-tech facility,. Lund University Division of Structural Mechanics, TVSM-5164.

Persson, P., Persson, K., Sandberg, G., 2014. Reduction in ground vibrations by using shaped landscapes. Soil Dynamics and Earthquake Engineering 60, 31–43.

Sandberg, G., Ohayon, R. (Eds.), 2008. Computational Aspects of Structural Acoustics and Vibration, CISM Courses and Lectures, vol. 505, Springer Wien, New York.

Snøhetta, Akershusstranda, 2012 21, 0150 Oslo, Norway.

Sreejith, B., Jayaraj, K., Ganesan, N., Padmanabhan, C., Chellapandi, P., Selvaraj, P., 2004. Finite element analysis of fluid-structure interaction in pipeline systems. Nuclear Engineering Design 227, 313–322.

Tijsseling, A.S., 1996. Fluid-structure interaction in liquid-filled pipe systems: a review. Journal of Fluids and Structure 10, 109–146.

Zienkiewicz, O.C., Taylor, R.L., 1994. The Finite Element Method, Volume 1 and 2, MacGraw-Hill, London.